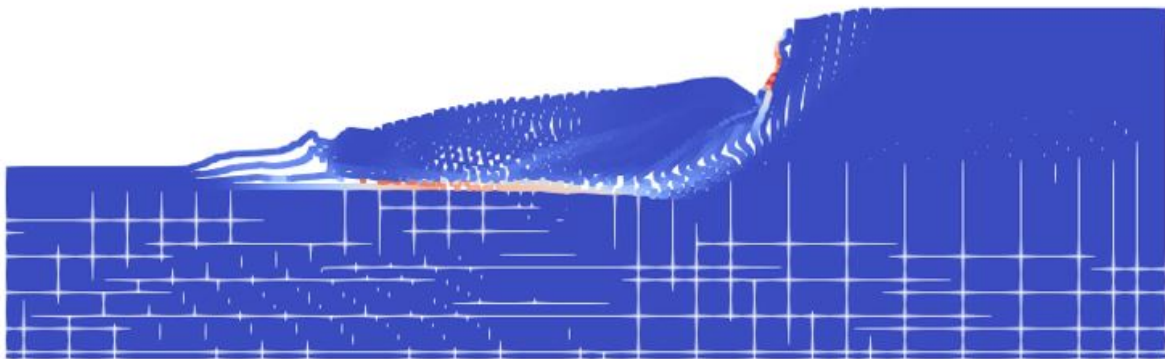


Residual strength and profile of the Eemdijk full-scale test

V.J.F. Leclercq



Residual strength and profile of the Eemdijk full-scale test

by

V.J.F. Leclercq

to obtain the degree of Master of Science
at the Delft University of Technology,
to be defended publicly on Friday January 31st, 2020 at 15:30 PM.

Student number: 4283732
Project duration: February 4, 2019 – Januari, 2020
Thesis committee: Prof. dr. ir. M. Hicks, TU Delft
Ir. H.J. Lengkeek, Witteveen + Bos & TU Delft
Dr. ir. C. Zwanenburg, Deltares & TU Delft
Dr. ir. R. Lanzafame, TU Delft

An electronic version of this thesis is available at <http://repository.tudelft.nl/>.

Preface

This thesis was written as finalisation of my Master's degree in Geotechnical Engineering at the TU Delft. I decided to pursue this Master mainly because I enjoyed the uncertainties involved in the design of soil-structures. I hope that this thesis will provide helpful insights to at least solve a small amount of them.

First, I would like to express my deepest gratitude towards my supervisor's, especially Ir. Arny Lengkeek and Dr. ir. Cor Zwanenburg, for allowing me to contribute to the Eemdijk full-scale test project. They have always provided very helpful support, and it was a pleasure to work with them.

This thesis would not have been possible without the help of Dr.ir. Mario Martinelli at Deltares, who provided indispensable help for the MPM part of my thesis. I am extremely grateful to him.

I would also like to thank Joost van der Meer and his group at Witteveen+Bos Rotterdam, for providing an enjoyable work space and helping me when I needed it.

Finally I would like to thank and apologise to Esther, to my friends, and to my family, or anyone else who had to endure my rambling about clay.

*Vincent Leclercq
Delft, January 2020*

Contents

Abstract	vii
List of Symbols	ix
List of Abbreviations	xi
1 Introduction	1
1.1 Problem description	1
1.2 Problem statement	1
1.3 Research questions	2
2 Research Method	3
2.1 Introduction	3
2.2 Back-analysis of mobilized strength.	3
2.3 Material Point Method modelling.	4
3 Experiment Description	5
3.1 Location	5
3.2 Dyke geometry	8
3.3 Phasing of the experiment	11
3.4 Failure description	13
4 Residual Strength	17
4.1 Residual Strength in literature.	17
4.2 Residual Strength and profile from case histories	22
4.3 Residual strength of Eemdijk soil: laboratory experiments	23
4.4 Summary residual strength hypotheses	24
5 Strength properties back calculations	25
5.1 Discretization in LEM.	25
5.2 Residual strength hypotheses in LEM	31
5.3 Green dyke strength back calculation	33
5.4 Blue dyke recommendations	38
6 Material Point Method	39
6.1 Material Point Method concept	39
6.2 MPM Benchmarks	43
6.3 Eemdijk experiment MPM discretization	54
6.4 Strength conversion.	55
6.5 Strength summary	56
6.6 Modeling steps	57
6.7 Failure phase results	60
6.8 Variation: Mohr-Coulomb sand core	63
7 Discussion	65
8 Conclusions	67
9 Recommendations	69
A Pore pressure development	71
B Staggered sheet pile wall schematization	73
C Final Design	75

D	Experiment Phasing	76
E	As failed pictures	80
F	Limit Equilibrium Method discretizations	81
G	3D Effect calculation	85
H	Blue dyke LEM analysis	89
I	Benchmark material properties	92
J	MPM strength conversion	93
K	MPM failure phase snapshots	96
	Bibliography	99

Abstract

To reduce the flood risk of the Netherlands, the national standard was updated. Due to this 1100 km of levees need to be reinforced by 2028. Including a sheet pile wall in a levee permits to build higher, less wide levees, thus increasing the macro-stability. They can therefore be a design solution for urbanised areas. The Eemdijk experiment was setup to gain more insights into the pre and post failure strength of a dyke with sheet pile wall. During this experiment two full scale dykes were brought to failure, one with a sheet pile wall built in and one without.

The water turning capacity of a dyke with sheet pile wall is dependent on the strength of soils after a large amount of strain has been mobilized. This is known as the residual strength. During laboratory testing on the subsurface clay layers of the experiment, the residual strength measured was not in accordance with what could be expected from the literature. This raises the question whether the Dutch organic clays behave differently as the predominantly mineral clays described in the literature, or whether the testing methods proved inadequate for the measurement of residual strength of organic clays.

This thesis tried to quantify the strength reduction of the soft soil layers of the experiment through a back analysis of the failure of the dyke without sheet pile wall. Residual strength hypotheses were formulated based on a literature study and the current design norm of dyke design on soft soil layers in the Netherlands. A Limit Equilibrium Method analysis of the pre and post failure geometry served as a basis to determine the peak and residual strength of the soft soil layers following the residual strength hypotheses. The 3D effect was taken into account in these analyses, and determined to be around 20%. A Material Point Method model of the experiment without sheet pile wall was then created to test the different residual strength hypotheses. Factors were applied on the strength properties calculated from the LEM model to match the MPM model. A factor of 1.23 was applied to account for 3D-effect and 1.16 to correct for water on passive side being absent from MPM discretization.

The Material Point Method model showed that during failure the behaviour of the clay layers could be expressed with an Undrained SHANSEP formulation. In this formulation the residual strength of clays was found to be independent of the Over-Consolidation Ratio. In a Mohr-Coulomb formulation this results in a complete loss of cohesion. Leaving the OCR out of the strength formulation of clayey layers resulted in horizontal displacement of 4.5 m, which is close to the 6 to 8 m found during the experiment. Further decrease in S-ratio of 30% resulted in horizontal displacement going up to 7.5m in the MPM model. A reduction of 0 to 30% of the S-ratio could therefore be concluded to be a range of friction softening. This was concluded to be in accordance with what was found in literature. Laboratory testing and correlations based on index properties effectuated prior to the experiment showed residual friction angle around 30°. The residual strength back-calculated are much lower, and therefore in contradiction with the laboratory testing results effectuated. The use of cyDSS and LDSS tests was therefore deemed inappropriate for the determination of residual strength.

The Limit Equilibrium Method analysis of the dyke with sheet pile wall was deemed inappropriate for the back analysis of the soft soil layers. The horizontal forces induced by the soil-structure interaction cannot be disregarded. It is recommended to back calculate the peak and residual strength of the peat layer using a Finite Element Method analysis. The displacement measurements of the failing dyke with sheetpile wall in the peat layer showed similarities with strain localisation in a DSS test.

List of Symbols

Symbol	Unit	Description
A	[m^2]	Surface area
b	[-]	Body force vector
B	[m]	Width of slide
bx	[-]	Compressibility coefficient
c'	[kPa]	cohesion
C	[-]	Courant number
$c_{eq;a}$	[kPa]	Equivalent associative cohesion
$c_{eq;na}$	[kPa]	Equivalent non associative non dilative cohesion
c_p	[kPa]	Peak cohesion
c_r	[kPa]	Residual cohesion
$C1$	[-]	Stress normalisation exponent
d	[m]	Radius difference
DR	[-]	Relative Density
e	[-]	Void ratio
E_c	[kPa]	Constrained modulus solid
E_d	[-]	Plastic strain matrix
F	[kN]	Mobilized force
$F_{1,2,3}$	[-]	Yield function
K_a	[-]	Active earth pressure coefficient
K_L	[kPa]	Liquid Bulk Modulus
L	[m]	Length of sliplane
m	[-]	SHANSEP strength increase exponent
n	[-]	Porosity
p_a	[kPa]	Atmospheric pressure
p'	[kPa]	Mean effective stress
$P_{1,2,3}$	[-]	Plastic Potential function
q	[kPa]	Deviatoric stress
Qc	[-]	Compressibility coefficient
S	[-]	SHANSEP strength ratio
S_u	[kPa]	Undrained shear strength
S_p	[-]	Peak strength SHANSEP S -ratio
S_r	[-]	Residual strength SHANSEP S -ratio
t	[s]	time
t_s	[m]	Prescribed solid traction
u_s	[m / s]	Prescribed solid velocity
v_s	[-]	solid particle speed
ϕ'	[°]	Effective friction angle
ϕ_r	[°]	Residual friction angle
ϕ_{cv}	[°]	Constant volume friction angle
ϕ_{tc}	[°]	Triaxial friction angle
$\phi_{eq;a}$	[°]	Equivalent associative friction angle
$\phi_{eq;na}$	[°]	Equivalent non associative non dilative friction angle
ϕ_p	[°]	Peak friction angle
η	[-]	Softening parameter
σ'_h	[kPa]	Horizontal effective stress
σ'_v	[kPa]	Vertical effective stress
$\sigma'_{v,0}$	[kPa]	Vertical effective stress before failure
$\sigma'_{v,i}$	[kPa]	Vertical effective stress at any given time

σ'_n	[kPa]	Normal effective stress on a plane
σ_y	[kPa]	Highest historical stress
σ_s	[kPa]	Cauchy stress tensor
ν	[-]	Interparticle friction
τ	[kPa]	Mobilized shear strength
ψ	[°]	Dilation angle
ψ_p	[°]	Peak dilation angle
ψ_r	[°]	Residual dilation angle
δ	[°]	Interface friction coefficient
ρ	[kg/m ³]	Density
ρ_S	[kg/m ³]	Solid density
ρ_L	[kg/m ³]	Liquid density
ϵ_{vol}	[-]	Volumetric strains
γ_{corr}	[-]	Strength correction factor
γ	[kPa]	Unit weight

List of Abbreviations

Abreviation	Explanation
CPS	Damping type
CPT	Cone Penetration Test
cyDSS	cyclic Direct Simple Shear
DSS	Direct Simple Shear
FEM	Finite Element Method
FoS	Factor of Safet
HWBP	Hoogwaterbeschermingsprogramma
LDSS	Large Direct Simple Shear
LEM	Limit Equilibrium Method
MPM	Material Point Method
NAP	Nieuw Amsterdams Peil
OCR	Over-consolidation Ratio
PoP	Pre-Overburden Pressure
POVM	Projectovertijgende Verkenning Macrostablieit
SAAF	Shape Accel Array Field
SPW	Sheet pile wall
SSC	Soft Soil Creep
MC	Mohr-Coulomb
MCSS	Mohr-Coulomb Strain Softening

Introduction

1.1. Problem description

The Netherlands have a growing demand for higher levees due to the increase in sea water level in combination with land subsidence. The national standard on levee design was updated in 2017. Due to this more than 1,100 km of levees need to be strengthened by 2028. Including a sheet pile wall in a levee increases the macro-stability. This allows less wide, higher levees to be built. Up to this day no validated design method is available for the design of sheet pile walls in levees. The lack of knowledge on the soil-structure interaction of a dyke with sheet pile wall often results in over-dimensioning of sheet pile walls, and therefore to an uneconomic design. It is therefore necessary to get better insights into the actual behaviour of failing levees.

It is in this context that Projectovertijgende Verkenning Macrostabieliteit (POVM) was created by "hoogwaterbeschermingsprogramma" (HWBP). HWBP is a cooperation of the Dutch government through Rijkswaterstaat and the Waterschappen (political organ responsible for the maintenance of the dutch dyke system). Deltares and Witteveen+Bos cooperated with the Projectovertijgende Verkenning Macrostabieliteit in the realization of a full scale-dike experiment at the Eemdijk location. During this experiment two full scale dikes were brought to failure, one with a sheet pile wall built in and one without. A high amount of data was gathered during these experiments, which can be used to acquire a better understanding of the strength and deformation properties of a failed dyke with sheet pile wall.

1.2. Problem statement

During the experiment the sheet pile wall remained upright even after failure of the dyke (Breedeveld, 2018) [13]. Even though buckled, it still fulfilled a water retaining function. This raises questions on the supportive strength the failed soil can still offer to the sheet pile wall. The residual strength of a failed dyke with sheet pile wall is strongly dependent on the post failure strength and geometry of the soil. In the current Dutch norm a dyke with sheet pile wall should be designed based on a passive side slope having failed, therefore a deformed geometry. The failed slope is to be taken as 1/3 of the height of the original slope. In the design the strength of the failed slope should not be reduced, and kept at peak strength. Literature however shows that soft soils show a loss of strength, or softening, when exposed to large displacements. If the residual strength of a dyke with sheet pile wall is to be predicted, better insights are required on the magnitude of possible strength loss and deformations cohesive soils undergo during failure of a dyke with sheet pile wall.

1.3. Research questions

The main research question of this thesis is:

- What is the post failure strength and profile of the Eemdijk full-scale test, and how can these best be modelled?

Secondary questions that will be investigated are:

- Do the clay and peat layers behave in a drained or undrained fashion when subjected to large displacements?
- Does the Overconsolidation Ratio still play a role in the slip plane strength after remoulding due to large shear strain?
- What is the magnitude of the strain softening of different soil layers?
- How is the failure mode of a dyke influenced by the presence of a sheet pile wall?
- Can MPM be used in practice to predict the post failure geometry?



Figure 1.1: Picture of the failed dyke with sheet pile wall

2

Research Method

2.1. Introduction

The goal of this thesis is to get better insight into the strength reduction of cohesive layers in relation to the post failure geometry of the Eemdijk full-scale tests, and on the best way to model these. The strength reduction behaviour will be investigated by focusing the analysis on the dyke without sheet pile wall. Ultimately the objective of this thesis is to serve as recommendations on the current Dutch design norm regarding the strength and shape of a failed dyke with sheet pile wall.

The first part of this thesis will present an overview of the different theories regarding the residual strength of clay and peat through a literature study. More insights into the residual behaviour of soft soils will be acquired by analysing previous case histories where residual strength was a factor of attention. Finally an overview of the laboratory experiments on the clay and peat of the Eemdijk experiment will be presented. This literature study will serve as basis for the formulated hypothesis regarding the residual behaviour of clay.

The second part of this thesis will be to back calculate the strength properties of the soil of the Eemdijk full-scale test through a Limit Equilibrium Method analysis. The peak strength of different layers will be determined based on the geometry right before failure. The hypothesis describing the residual strength of the clay will be formulated into different scenario's. In combination with the measured residual profile a range of possible residual strength will be concluded from this analysis.

The final part of this thesis will deal with the modelling of the displacements of the failing dyke without sheet pile wall from the Eemdijk full-scale test in a Material Point Method model. The different residual strength scenario's determined from the literature study and backcalculated in the LEM analysis will be translated to a MPM model. The displacements obtained for each scenario will be compared to the displacement measurements of the Eemdijk full-scale test, and conclusions will be drawn on the most probable way to express strength reduction of clays in a macro-stability problem.

2.2. Back-analysis of mobilized strength

The first part of this thesis deals with investigating the magnitude of the strength loss cohesive layers undergo during a dyke macro-stability failure. The mobilized strength parameters of the soil therefore needs to be assessed. Limit equilibrium calculations such as the Bishop, Spencer or Morgenstern-Price methods provide robust solutions to investigate the macro stability of a slope. These analyses can be performed in D-Geo Stability software. The shape of the failed slope can be drawn based on the post failure excavation analysis, the displacement monitoring with the SAAF's (Shape Accel Array Field) and the prisms measurements. Comparison between the measured displacements of the dyke with and without sheet pile wall will investigate the influence of a sheet pile wall on the failure mode of the soil on the passive side.

For each dyke an analysis of the peak and residual strength will be provided. By carrying out an analysis of the geometry right before failure, the peak strength properties can be found. With the information about

the location of the slip surface (width and depth), the 3D effect can be calculated. Similarly the post failure geometry can be analyzed to determine the residual strength properties of the soil layers. These values will be compared to expected values from literature and to the laboratory test results executed by Deltares (Breedeveld, 2018) [14].

This part will answer the following questions:

- What is the magnitude of the strain softening of different soil layers?
- How is the failure mode of a dyke influenced by the presence of a sheet pile wall?

2.3. Material Point Method modelling

The different strength scenario's presented in the Limit Equilibrium Analysis need to be tested. Material Point Method is a numerical method that has an arbitrary Lagrangian-Eulerian formulation, which offers the ability to model large displacements without losing mesh integrity. This theoretically makes MPM a perfect candidate to model the failure phase of the Eemdijk experiment. The code used "Simon_2D_DP_20191101_1652" is provided by Deltares, and close in resemblance to Anura3D. Anura3D is a MPM software developed by a community of universities and research institutions. Different constitutive soil models are available in the most recent update of Anura3D v2019.1. These are: linear elasticity, Mohr-Coulomb (linear elastic-perfectly plastic), Mohr-Coulomb strain softening (with shear strain dependent decrease of cohesion, friction and dilation), and Modified CamClay.

The Mohr-Coulomb with Strain Softening model seems to be the most appropriate to describe a shear induced strength loss. Implementing the different scenarios determined in the Limit Equilibrium Analysis chapters into the Material Point Method analysis will provide a base to compare the displacements measured during the experiment. This will enable conclusions to be drawn on the most probable way to describe the strength loss of the soft soil layers of the Eemdijk experiment. This will hopefully serve as advice for engineers who want to determine the post failure strength of a dyke with sheet pile wall.

This part will answer the following question:

- Does the Overconsolidation Ratio still play a role in the slip plane strength after remoulding due to large shear strain?
- Do the clay and peat layers behave in a drained or undrained fashion when subjected to large displacements?
- Can MPM be used in practice to predict the post failure geometry?

3

Experiment Description

3.1. Location

3.1.1. Decision making

The goal of the Eemdijk experiment was to get better insights into the deformations and strength of failing levees on soft soil reinforced by an unanchored sheet pile wall. In this experiment two levees were brought to failure: one with a sheet-pile wall (further referred to as Blue dyke) and one without (further referred to as Green dyke). The Green dyke serves as reference case for the Blue dyke. It was therefore required to choose a location that would fit a number of criteria:

- Homogeneity of the subsurface;
- Thickness of soft layers;
- Dimensions of the location;
- Possibility to create an uplift failure;
- Strength of the soft layers.

Homogeneity of the subsurface was of great importance to the experiment. The main objective of the construction of the Green dyke was to serve as reference for the Blue dyke. This could only be achieved if the soil layers are homogeneous. If a large difference between weak and strong zones were present at the location, no good conclusions could be drawn with regard to the mobilized strength of each layer. The thickness of the soft layers was also of importance. In the ideal situation the prediction of the behaviour of the soil during the experiment would be close to the actual behaviour. To reduce the uncertainty as to the location of a failure surface it was important to choose a location with soft layers that were neither too thick nor too thin. Thin soft layers would lead to difficulties predicting the strength of the layers, while a thick layer reduces the certainty as to where in the layer the slip surface would pass. Thin layers also increases the probability of a weak zone in the soft soil, which is difficult to predict from laboratory testing. Furthermore, uplift failure can be the dominant failure mode for a high number of Dutch dykes. The possibility to conduct testing for the Uplift failure type was also considered. The area of the experiment needs to be wide enough to limit the 3D effect to the maximum. A wide slip surface reduces the mobilized stress of sides compared to the mobilized strength of the bottom, thereby reducing the 3D effect. Finally, the strength of the soft layers was one of the most important factors in the location making. Premature failure needed to be avoided so not to ruin the conclusions of the experiment.

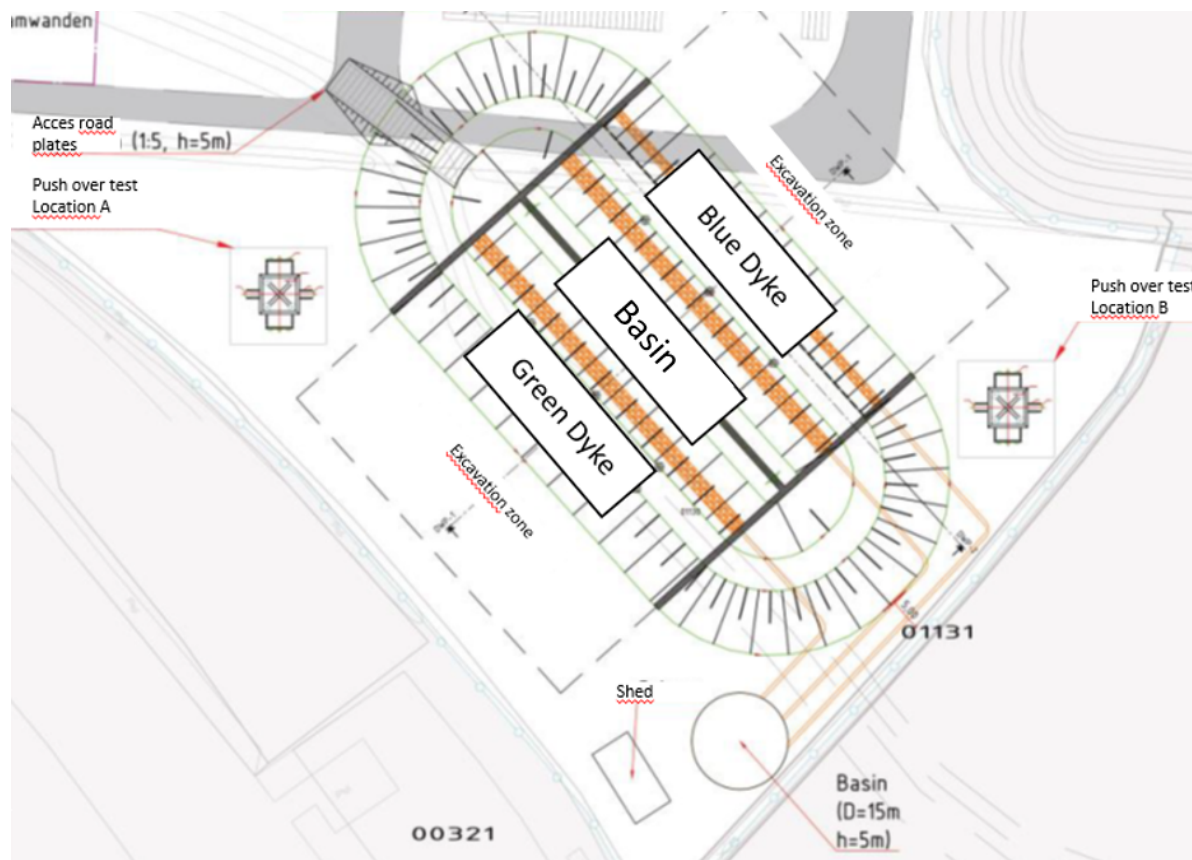


Figure 3.1: Aerial schematisation of the experiment (Analysis report) [13]

The final location that was chosen for the experiment was the Gronddepot Eemdijk. An old summer dyke was present at this location. This led to slight overconsolidation of some layers, and could have changed the local thickness of soil layers. Further soil investigations did not show these changes in layer thickness. It was further concluded that the first loading step induced by the staged dyke construction already surpassed the historical loading. In the rest of the experiment this old dyke was therefore neglected. An aerial schematisation of the experiment location is shown in Figure 3.1.

3.1.2. Soil stratigraphy

As described previously, the Eemdijk location was mainly chosen based on the low variability of the subsoil composition from the green to the blue dyke. A variation in the subsurface was however noted. A small layer (0.5 m thickness) of soft clay (Layer 3a) was found at the location of the green dyke. This soft layer proved to be critical in the overall stability, as the slip plane of the Green dyke passed through that layer. An overview of the soil stratigraphy at the Eemdijk experiment location is presented in Table 3.1. It can further be noted that layer 2 was originally unsaturated. Due to the settlement induced by the construction of the dykes this layer ended up under the groundwater table, and is therefore assumed to be saturated in the rest of the analysis. As layer 2 is comprised of the same clay as layer 3, they will be modeled as a single soil layer in the stability and deformation analysis.

Further research into the exact location of the 3a layer was carried out with infrared satellite imagery. Figure 3.2 shows the results of this imagery. A wet zone (green area circled with a blue dotted line) might be attributed to the presence of this soft layer. The rest of the analysis will therefore be based on the assumption that layer 3a is present in the area of the wet zone. The 3a layer will be modelled as reaching up until half the width of the slope.

Table 3.1: Soil stratigraphy

Layer number	Soil Layer	Soil Description	Level top layer [m NAP]
1	Top layer	Sandy Clay	0.0
2	Cohesive layer	Clay, Unsaturated	-0.2
3	Cohesive layer	Clay, Saturated	-0.8
3a (only under green)	Cohesive layer	Soft Organic Clay, Saturated	-1.5
4	Cohesive layer	Peat, Saturated	-2.0
5	Granular layer	Sand, Saturated	-4.2
6	Cohesive layer	Stiff Clay, Saturated	-9.5
7	Granular layer	Sand, Saturated	-11.0

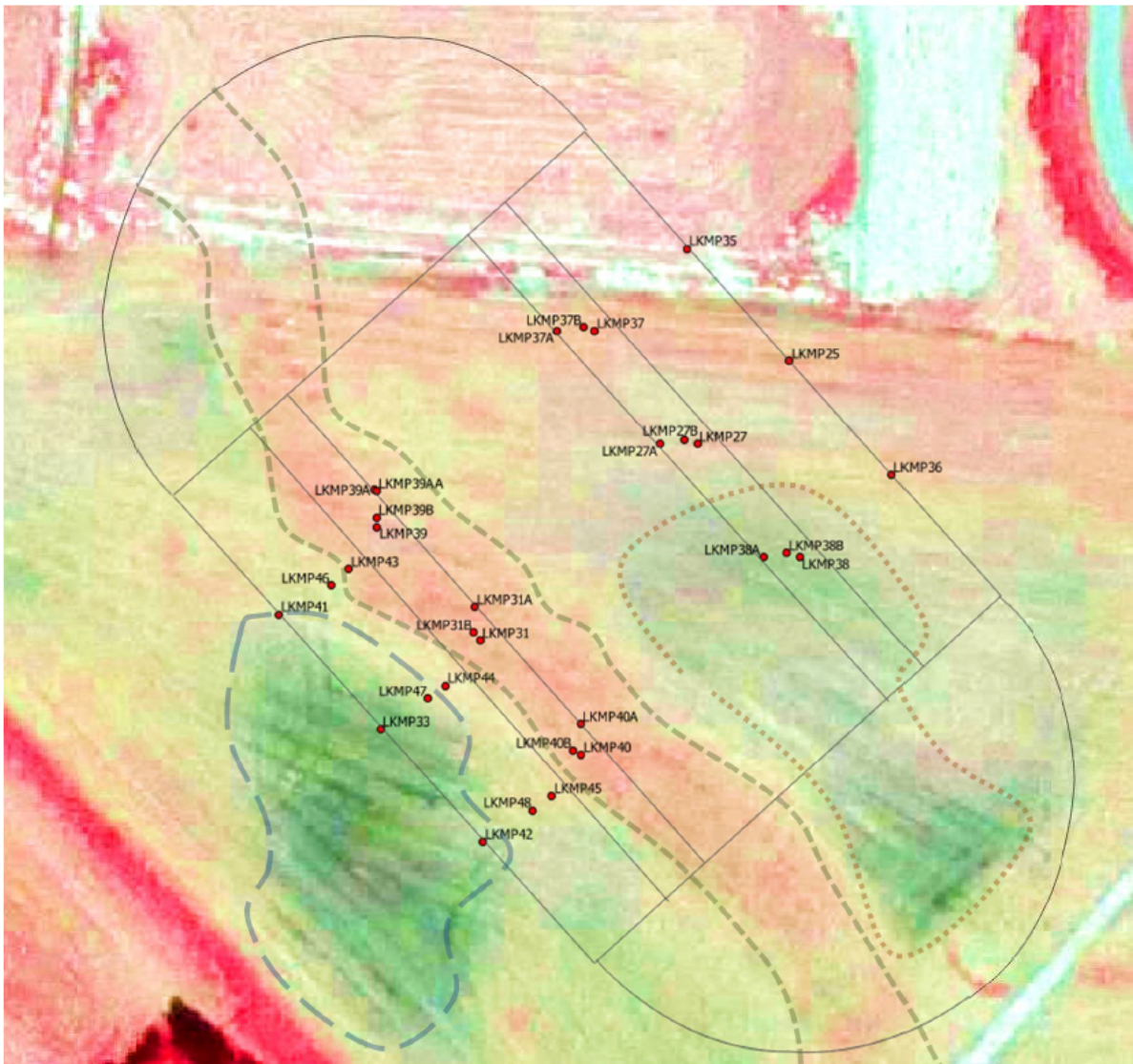


Figure 3.2: Infrared satellite of the experiment location [13]. The wet zone is shown in green under the green dyke by a blue dotted line. The old summer dyke is shown in red circled by a brown dotted line

3.1.3. Groundwater conditions

The phreatic conditions are of high importance for the accuracy of the analysis (Agam et al, 2016) [1], and were therefore assessed prior to the experiment. The groundwater table was found to be at -0.5 m NAP at the start of the Green dyke experiment, while it was found to be at -0.8 m NAP at the start of the Blue dyke experiment. The hydraulic head in the first sand layer (layer 5) was found to be at -0.4 m NAP. It was shown that the seasonal variations of the water level of the nearby river was of little influence on the hydraulic head of the layer 5 aquifer, and could therefore be disregarded.

Excess pore pressures were generated during construction as shown in Appendix A. At the end of the construction phase excess pore pressure equivalent to 3.5 m water head are still present in both the shallow and deep layers below the dyke crest. The shallow layers present somehow more excess pressures than the deeper layers. This is due to the fact that more pressure is generated in the top layers than in the deeper layers, as a result of stress distribution with depth, or that the peat layer is less responsive than clay, with faster consolidation time. Loading by heightening of the water table in the core also results in generation of pore pressures.

3.2. Dyke geometry

3.2.1. Levee material

The dyke core was made of medium to fine sand, with a small percentage silt. The cover was made of clay, and built thick enough to prevent seepage from water out of the core during the experiment. It should be noted that no laboratory testing was carried out on the dyke material. CPT's and boreholes carried out after construction provide the only quantitative basis for the determination of the strength properties of the sand core. The clay cover strength properties were solely based on engineering judgement in the Back analysis report [13]. As no new information was acquired, the same assumptions will be handled.

3.2.2. Measurement equipment

The different types of measuring apparatus used during the experiment are described below. The location area has been split in 3 cross sections: North, Middle and South. In each cross section measuring apparatus have been placed in the subsurface at the toe and crest of both the blue and green dyke, as shown in Figure 3.3. A schematisation of the dyke cross section with location of measurement equipment is shown in Figure 3.4.

Displacement measurement

Monitoring of displacements during the construction phase was required to determine the magnitude of settlements. To this end, settlement plates were installed to monitor settlement during construction. Settlement over the profile cross section were monitored by 3 settlement hoses. The results from the settlement hose installed in the middle of the setup were discarded after 10 m from the toe of the green dyke, due to a faulty measuring equipment. Three inclinometers were installed on each dyke to monitor the displacements inside the soil mass. 42 Prisma's on the Green dyke and 50 prisma's on the blue dyke were installed on the outer slopes to monitor the displacements automatically through a total station system for the loading phases.

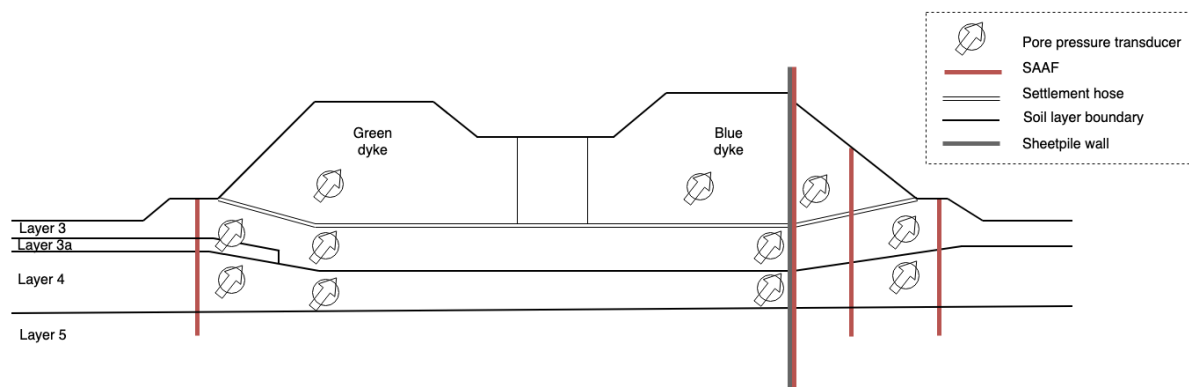


Figure 3.4: Schematization of the measurement equipment setup in the experiment

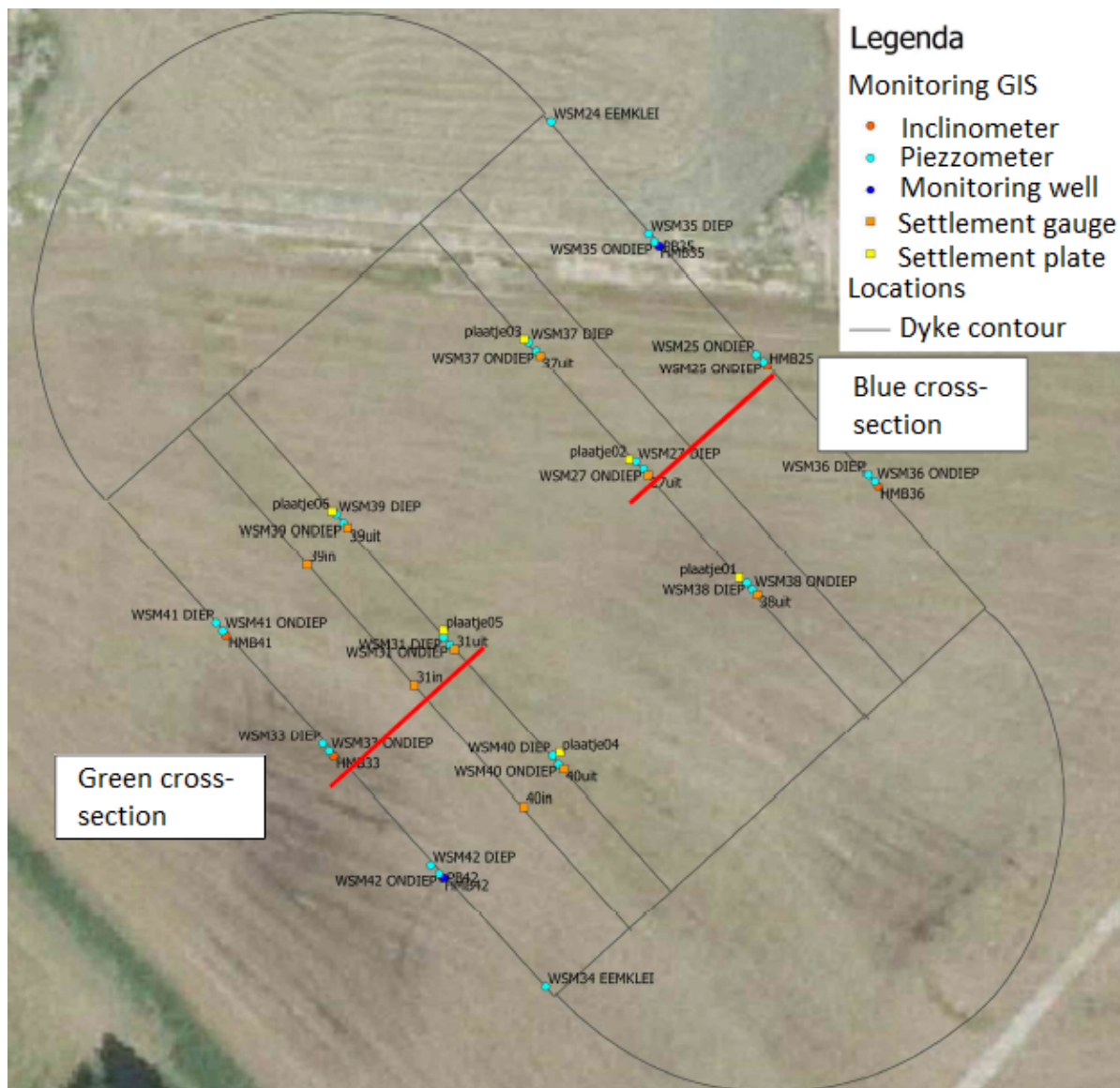


Figure 3.3: Top view of location of the monitoring system

Displacements also needed to be monitored during the failure phase. Three SAAF's were placed in the toe of the Green dyke. Three SAAF's were placed in the toe of the Blue dyke, 3 were placed in its outer slope while 4 were installed on the sheet pile wall. These monitored the horizontal and vertical displacements during the tests. Glass fibre strain gauges were also installed on the sheet pile wall to closely monitor the displacements of the wall during loading. During the test however most of these measuring instruments failed.

Pore Pressures meters

Pore pressure transducers were installed on different locations and depth in the Green and Blue dyke during the construction and testing phase. In each cross section pore pressure transducers were installed in the crest and toe subsurface to monitor the development of excess pore pressures during construction. At these locations the water pressures were measured at a depth of -1.5 m NAP and -3.0 m NAP. These levels coincide with the depths of the clay and peat layers respectively. They therefore offer a clear view of the degree of consolidation of these layers. The development of pore pressures throughout the construction phase is shown in Appendix A. A piezzometer was also installed in the passive side excavation of each dyke to monitor the water level in the excavation. Finally a piezzometer was installed further away from the experiment to monitor the location of the groundwater table in relation to the water level of the river Eem.

3.2.3. Sheet pile wall

A choice on the sheet pile wall type was made based on the goal to let the blue dyke fail. The available options were Z, U or H profiles. Z-profiles are generally used in practice. The choice of a double AZ-13 profile was weighed, however the thinnest profile were still anticipated to be too strong to induce plastic failure during the test. Difficulties also arose when trying to reduce the quality of the steel to S240GP. A triple GU8N profile was therefore chosen, as schematized in Figure 3.5. This option was deemed most safe for the success of the test.

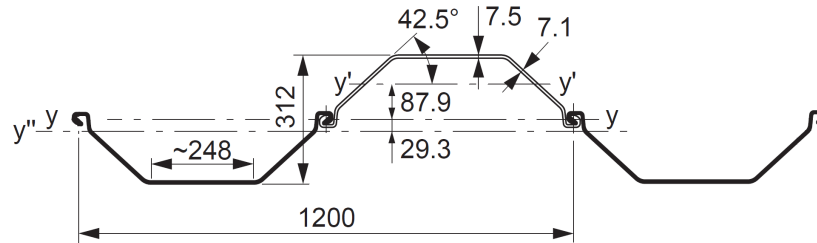


Figure 3.5: Triple GU8N Sheet pile wall profile systematization (ArcelorMittal)

Joining of the profiles beforehand by the manufacturer is done by punching or intermittent welding. This results in a stiffer profile (reduction of loss in moment of inertia and section modulus due to oblique bending). To ensure that the test would result in plastic failure of the sheet pile wall, a staggered installation was chosen. The final sheet pile wall consists of alternating 8.5 m and 18.0 m triple GU8N profiles. The bottom of the short profiles is embedded in the peat layer, while the bottom of the long profiles is embedded in the deep sand layer. A representation of the staggered sheet pile wall is given shown in Appendix B. This modelling fell out of the scope for this thesis.

3.2.4. Final geometry

The final geometry design is shown in Appendix C. The input geometry that was used as input for the modelling part are described below.

Green dyke geometry

Based on the Factual report of the construction (De Bruin, 2018) [18] the green dyke geometry at the end of the construction phase was:

- Level toe inner slope (after excavation): NAP 0 m
- Angle inner slope (after excavation): V:H = 1 : 1.7
- Crest height: NAP +5.4 m
- Crest width: 5.8 m
- Angle outer slope V:H = 1 : 2
- Water basin height: NAP +3.5 m
- Thickness basin clay cover : Not taken into the model
- Thickness inner toe clay cover (horizontal): 4.5 m
- Thickness crest inner slope clay cover (horizontal): 1 m
- Thickness crest inner slope clay cover (horizontal): Not taken into the model

Blue dyke geometry

Based on the Factual report of the construction (De Bruin, 2018) [18] the blue dyke geometry at the end of the construction phase was:

- Level toe inner slope (after excavation): NAP 0 m
- Angle inner slope (after excavation): V:H = 1 : 1.7
- Crest height in front of the sheet pile wall: NAP +4.8 m
- Distance of center of sheet pile wall to inner slope: 0.7 m
- Crest height behind the sheet pile wall: NAP +5.5 m
- Crest width behind the sheet pile wall: 5.5 m
- Angle outer slope V:H = 1 : 1
- Level clay cover outer slope: NAP +4.2 m
- Water basin height: NAP +3.3 m
- Thickness inner toe clay cover (horizontal): 1.5 m
- Thickness crest inner slope clay cover (horizontal): 2 m
- Thickness crest outer slope clay cover (horizontal): 1 m

3.3. Phasing of the experiment

3.3.1. Construction procedure

A phased construction with time to consolidate between each phase was executed. Construction started on the 12th of June 2017. This date is set as reference start date of the project for the rest of the analysis. The final goal of the full-scale test was to be able to bring 2 dykes to failure under approximately the same soil conditions. Similar consolidation times were therefore handled between construction and failure phase of the two dyke experiments. This way excess pore pressures still present in the subsurface are almost identical from one experiment until the other.

Special attention was paid to the creation of compartments. Strength of soil is dependent on the loading history. Since the two experiments were not conducted simultaneously it was important that the effect of one failure was not felt by the other dyke. Compartments were therefore created with clay separations. The basin and inner dyke slopes were fully covered with 0.5 m clay (to be able to heighten the water level in the sand core), and the two dyke bodies were separated by a 1 m thick clay coffin. These dimensions were chosen based on experience, and were (successfully) deemed thick enough to prevent seepage from one compartment to another. The three compartments are:

- Core of Green dyke;
- Core of Blue dyke (basin side of the sheet pile wall);
- Core of Blue dyke (outer slope side of the sheet pile wall).

Care was also taken to install a drainage system in each compartment to control the phreatic level of each core separately. After the experiment on the Green dyke was conducted, time was also taken to reconstruct the basin properly, as the basin was required to bring the Blue dyke to failure. An overview of the different phases of the construction of the Green and Blue Dyke are shown in Tables D.1 and D.2 in Appendix D.

3.3.2. Loading procedure

Green dyke loading

The experiment phase of the green dyke started on the 24th of January. The first part of the experiment phase consisted on excavating a trench at the toe of the dyke. The excavation was carried out wet, and in different phases. First the top part of the trench on the slope toe side was excavated in stages to the levels -0.25, -0.90 and -1.5 m NAP. The trench was then widened in two different phases. This excavation phasing is shown in Figure D.1 in Appendix D. The water level of the passive side trench was lowered to -0.5 m NAP. Finally to bring the dyke to failure the water level was raised in the dyke core to reduce the effective stress. This was done in total of 3 stages: + 1.0, + 2.0 and +2.9 m NAP. In the last phase failure was induced on the 30th of January around 10h30 and complete around 16:30. An overview of the experiment phase loading steps is presented in Table D.3 in Appendix D.

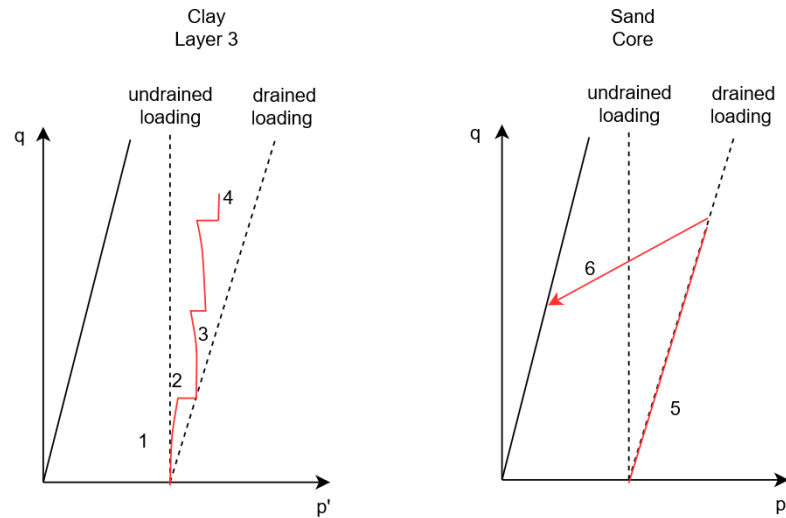


Figure 3.6: Qualitative representation of the stress path in the clay during construction (left) and in the sand core during construction and loading (right)

The stress path during construction in the clay has been represented in Figure 3.6. For each construction step the clay behaves in an undrained fashion. In an undrained compression test the stress path follows a vertical line (assuming all extra load is taken on by pore pressures, and no pore pressures are generated by shearing). In reality the clay is overconsolidated, resulting in the generation of negative pore pressures (dilative behaviour when sheared). The stress path during deviatoric loading will therefore curve to the right in p' - q space loading step 1. Consolidation time results in dissipation of pore pressures, therefore increase in mean effective stress without change in deviatoric stress. This is represented by trajectory 2. Shearing of normally consolidated clays results in the generation of negative pore pressures (contractive behaviour). This is represented by trajectory 3. Finally, the filling of the sand core leads to a slight increase in total weight of the sand (from 18 kN/m^3 to 19.5 kN/m^3). This leads again to an undrained loading, which can be seen in step 4.

The stress path during construction and loading at the bottom of the sand core can also be seen in Figure 3.6. The construction phase is represented by the drained loading by path 5. The unloading stage due to the filling of the dyke core is represented by path 6. Due to the reduction during unloading in vertical stress, the horizontal component will also decrease. An upper boundary of this strength reduction is therefore the active earth pressure coefficient K_a , expressed in Equation 3.1. In Chapter 6, this value will be used to determine an equivalent unloading poisson ratio.

$$K_a = \frac{1 - \sin(\phi)}{1 + \sin(\phi)} \quad (3.1)$$

This loading path leads to increased reduction of vertical versus horizontal effective stress, and can be described as unloading extension. The slope inclination of the stress path in sand can be calculated quite simply, and can be visualised by trajectory 5 in Figure 3.6.

$$\Delta\sigma'_h = Ka * \Delta\sigma'_v \quad (3.2)$$

$$\Delta p' = \frac{(2 * \Delta\sigma'_h + \Delta\sigma'_v)}{3} \quad (3.3)$$

$$\Delta q = \Delta\sigma'_v - \Delta\sigma'_h \quad (3.4)$$

$$\frac{\Delta p'}{\Delta q} = \frac{2 * Ka + 1/3}{1 - Ka} \quad (3.5)$$

Blue dyke loading

The experiment phasing of the Blue dyke also started with the excavation of the passive side. In this case it was carried out in 4 phases. First, the removal of the top layer (to -0.25 m NAP), then the staged excavation to -1 than -2 m NAP, and finally horizontal expansion of excavation as shown in Appendix D, Figure D.2 were executed. The core of the dyke was then filled in stages to +2, +3 and +4.2 m NAP. Load was added on top of the crest by filling the water containers with 2 m of water. The containers were spaced by 1.5 m, therefore a correction factor of 0.85 was applied over the load from the containers. Water was then infiltrated in the outer slope side core of the dyke to +1 m NAP, after which the basin was filled to +4.5 m and then to +5.0 m NAP. The outer slope side core of the dyke was then filled with water until +1.5 m NAP, further reducing the effective stress. Failure was triggered by lowering the water table of the passive side excavation to -0.9 m NAP on the 17th of March around 16:00. The description of the different loading phases is presented in Appendix D.

3.4. Failure description

The geometry of the failed dykes was described in the back analysis report [13]. The failure of the dykes will be described in the following paragraph, to serve as reference for the stability back calculation and displacement modeling.

3.4.1. Green dyke failure

Failure of the green dyke was initiated on January 30th at 11:15, on day 233 and completed at 16:30. After the water table on the passive side was lowered to -0.5 m NAP and the water level in the dyke was heightened to +2.9 m NAP, a 20 to 30 m wide failure surface was created. In the rest of the analysis 20 m will be used.

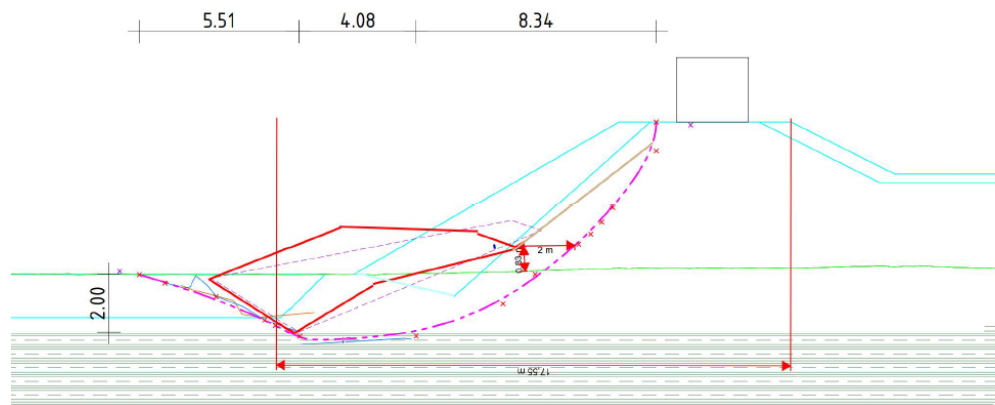


Figure 3.7: Settled failed geometry as described in Back analysis report (Bredeveld, 2018) [13]

After failure was completed the excavation was dried up, and the slip surface was excavated. Pictures of the failure are shown in Appendix E. The locations of the slip surface were measured with GPS. Based on this the shape of the slip surface could be described in the Back analysis report [13] as shown in Figure 3.7. The SAAF measurements at the toe of the Green dyke also provide an indication of the location of the slip surface, as shown in Figure 3.8. It can be noted that at the 11:00 measurement the SAAF buckled at a depth of -2.5 m NAP. This indicates that the slip surface at the toe passes through Layer 3a. This is supported by the strain accumulation shown in Figure 3.9. Strains were defined by the horizontal displacements over the

height of a single SAAF element of 0.5 m, as done by Murano (2019) [40]. It can be noted that the strains first accumulate before failure evenly through the peat and clay layers. Right before failure occurs at 10:00, the strains accumulate in clay layer 3a at -2.5m, after which the SAAF fully buckles at the moment of failure.

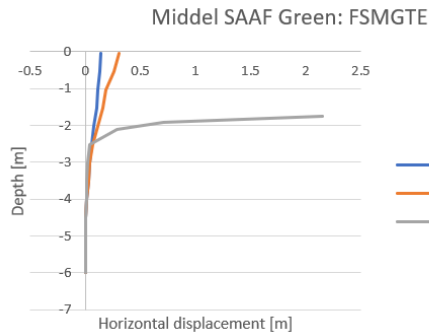


Figure 3.8: Middle SAAF displacement measurements of the green dyke at different time steps

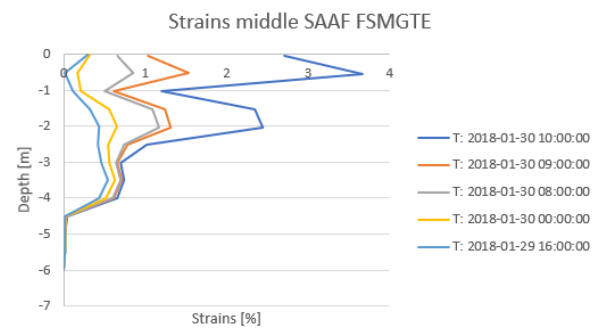


Figure 3.9: Middle SAAF strains of the green dyke at different time steps

The slip surface emerged vertically through the sand at the crest of the dyke approximately halfway between the containers and the inner slope crest, at approximately 1.5m from the initial edge of the slope. A significant portion of the slip surface passes through the sand core. At the level of the toe, the slip surface passes horizontally through the soft clay layer 3a, to emerge in the passive side basin near the edge. It is unclear until which point the slip surface remained through layer 3a. The non circularity around the toe can be explained by the reduced stress level induced by the passive side excavation, forcing the slip surface upwards.

Note should be taken that after failure the sand in the dyke core remained close to vertical near the crest of the dyke for a long period of time. In a cohesionless soil like the sand core the natural slope should be close to φ' . This indicates the presence of suction pore pressures in the unsaturated sand core, resulting in apparent cohesion. These suction pore pressures are dissipated once the peak strength is reached and deformations gain in magnitude. This means that the apparent cohesion should be determined and taken into account when modelling the peak strength of the unsaturated sand in the dyke.

Water table in a dyke has a high influence on the final factor of safety. From the timelapse videos it was noted that failure was finished around 16H30. The water level in the failed core was still at +2.9 m NAP at that time, as indicated by the pore pressure transducer in the core. In the residual geometry LEM discretization the water table in the dyke core will therefore be fixed at +2.9 m NAP.

Reference points can be defined to determine the amount of displacements. The clay cover has been found upon excavation and will serve as reference. Both the top and bottom of the clay cover have moved with 6 to 8 m horizontally. The top of the clay cover dropped by 3.5m vertically. Exact information about the deformations of the subsurface clay could not be found. It seems safe to assume that the clay at the toe of the deformed profile was pushed from under the profile. This also corresponds to deformations in the order of 6 m. These will serve as reference for the modelling of the displacements in MPM.

3.4.2. Blue dyke failure

Failure of the Blue dyke was initiated on the 17th of March at 16:00 on day 278. The failure was finally triggered by heightening the water level in the dyke core to +5m NAP, heightening the level on the inner slope side to +1,5 m NAP, and lowering the water level in the excavation on the passive side to -0.9 m NAP. During failure the water level in the core on the inner slope side was maintained at +1.5m NAP. Pictures of the failure are presented in Appendix E. Contrary to the green dyke, no clear slip surface could be excavated at the blue dyke. This is probably due to the fact that the sheet pile wall pushed the soil mass while failing, making the boundary less visible.

An approximation of the location of the slip surface can nonetheless be made by investigation of the SAAF measurements presented in Figure 3.12. As shown in Appendix C, 3 SAAF's were installed to monitor the horizontal displacements during the experiment: one on the sheet pile wall, one in the middle of the inner slope and one at the toe of the dyke. It can be noted from the sheet pile wall SAAF measurements and from

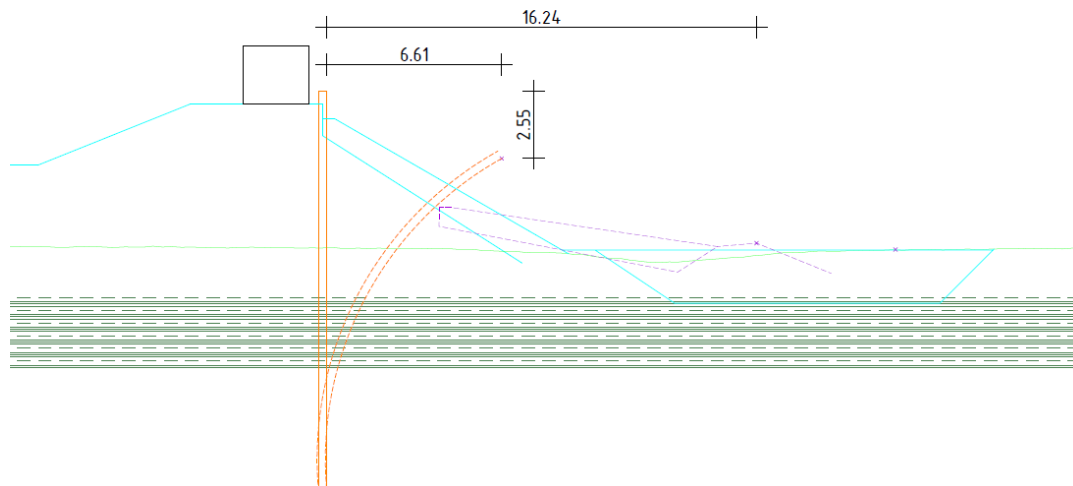


Figure 3.10: Settled failed Blue geometry as described in Analyse rapport

the back analysis report (Bredeveld, 2018)[13] that the sheet pile wall buckled at a depth of around -3.5 m. The slope SAAF shows large horizontal displacements at a depth between -4 m and -3 m, while the toe SAAF buckles between -4.5 m and -4 m. Figures 3.13 and 3.14 show the strain in time during loading before failure in the Blue dyke slope and toe. It can be noticed that at each measurement a higher level of strain was present in the toe than in the middle of the slope. This shows a strain concentration away from the SPW. A schematic representation of the strain localisation is shown in Figure 3.11. The depth of the strain localization confirms that the slip surface either passed through the peat or at the interface with the sand layer. The resemblance with strain localisation in a DSS test can be noted.

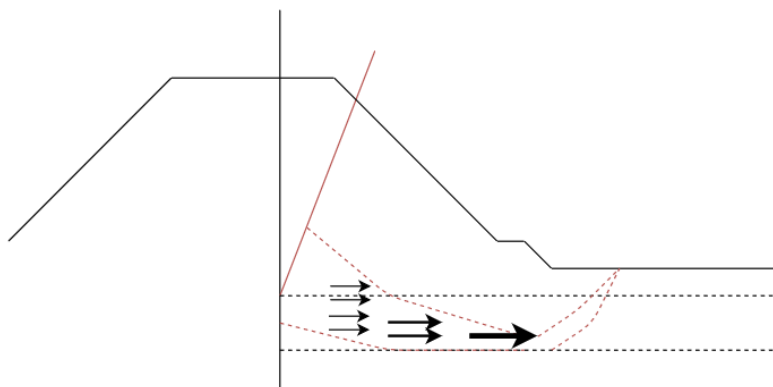


Figure 3.11: Schematisation of the strain localization during Blue dyke failure

The passive side of the slip surface emerged halfway through excavation, meaning the peat layer was pushed up by 1m. A crack appeared at the place where the peat layer got pushed up. The peat was pushed out with a slope of 1:1 to a level of -1.5 m NAP, which tells us the inclination of the slip surface at the emerging surface. Little information is known on the exact layering of the soil after failure. The deformed profile was measured, schematized in the back-analysis report [13], and can be seen in Figure 3.10. It can note from 3.10 that the sheet pile wall and clay cover both showed horizontal displacements in the order of 5 to 6 m.

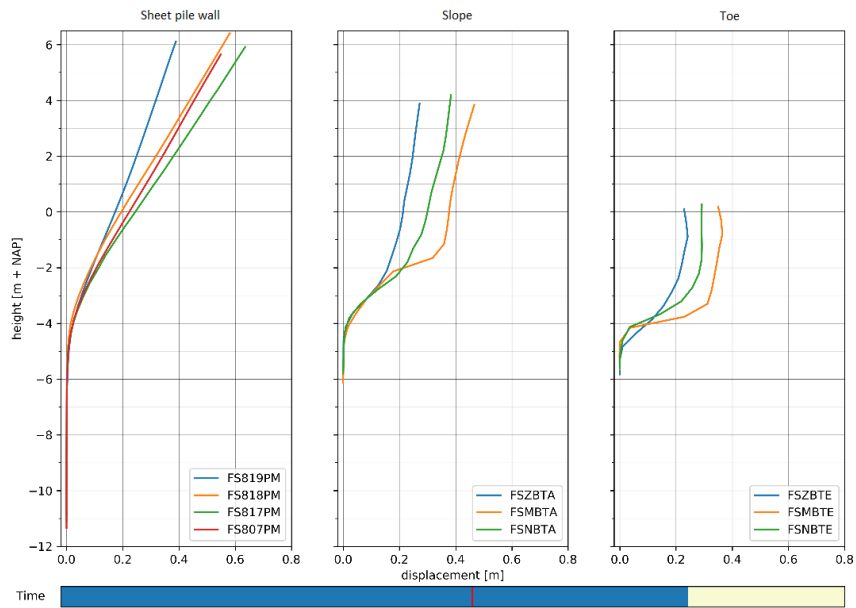


Figure 3.12: SAAF measurements at different location in Blue Dyke at 15:50

Strain vs depth Blue dyke middle slope

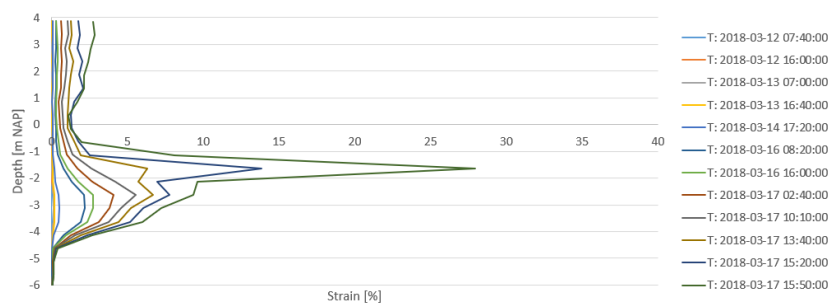


Figure 3.13: Strains measurements from middle SAAF in the slope

Strain vs depth Blue dyke toe

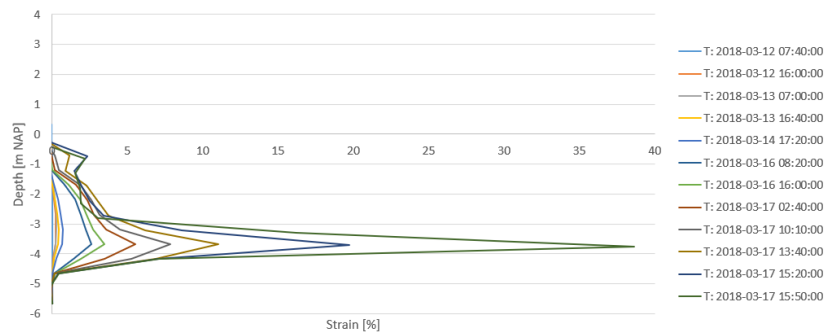


Figure 3.14: Strains measurements from middle SAAF in the toe

4

Residual Strength

In this Chapter a literature study will provide a summary of the current theories regarding the strength behaviour of soils under large displacements. The different theories will be translated to hypotheses, which will form the basis on which the strength properties of the soil layers in the slip surface of the Eemdijk experiment will be back calculated.

4.1. Residual Strength in literature

4.1.1. Strain dependency of strength

In the context of this thesis, it is important to understand that the shear strength of a soil is strongly dependent on the degree of interlocking of particles in a soil. The strength of a soil is therefore a function of the packing state. Consequently, soil shear strength is dependent on the amount of shear mobilized. This is the central idea of the Critical State Theory. The strain induced strength loss is known as strain softening.

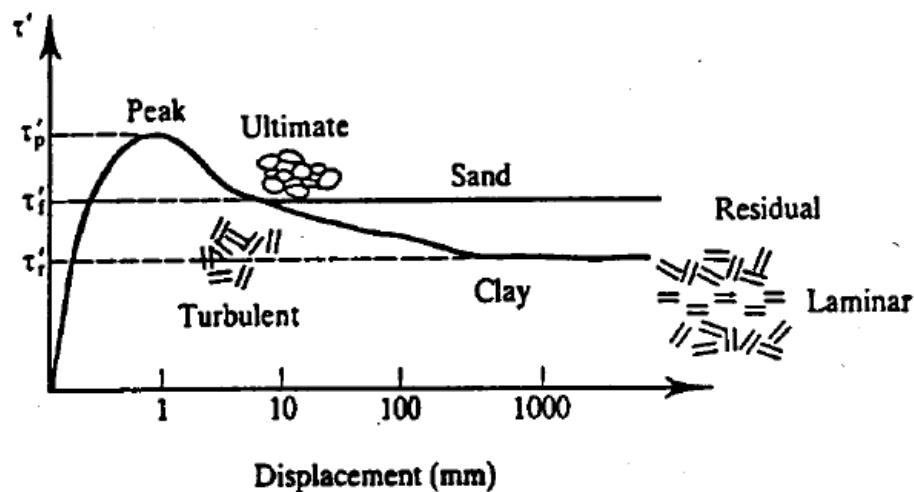


Figure 4.1: Schematization of the drained strain-dependent strength reduction in soil (Atkinson, 1993)[3]

The idealized behaviour of a soil in a drained shear test, as shown in Figure 4.1 gives a good overview of the strength reduction a soft soil or loose sand undergoes when exposed to different levels of shear. Peak strength is classically reached around 1 % of strain (Atkinson, 1993) [3]. Further shearing leads to the particles rolling over each other, without further volume change. This state, reached between 10% and 50 % strain (Atkinson, 1993) [3] is known as the critical state (or constant volume). Soft soils like clay can exhibit a strength loss when imposed displacements become even larger, like during a slope failure for example. This strength, known as residual strength, can be significantly lower than the critical State strength. The strength loss is due to the rearrangement of platy grains in the orientation of the slipplane, and was studied extensively by

(Skempton, 1985) [47]. Sand do not exhibit this further strength loss beyond critical state due to the larger, round particle composing it.

Peak Strength

Soils obtain their peak strength by the interlocking of particles. As stated previously, the peak strength is reached at small strains. In over-consolidated soils the peak strength is the strength required to overcome this particle interlocking during shearing. The peak strength is reached at maximum dilation angle ψ (Atkinson, 1993) [3]. Normally consolidated soils therefore do not exhibit such a peak strength, since they have not been compacted like the over-consolidated soils. In the case of normally-consolidated soils the peak strength will therefore be equal to the critical state strength.

Critical state strength

The critical state of a soil is defined as the state at which no more volume change is induced upon shearing (Roscoe, 1958) [42]. It represents a unique relationship between shear stress, normal stress and void ratio. The critical state line is therefore often represented in a p', q, e space (Atkinson, 1993) [3]. It is can also be seen as the packing state of the soil (Schofield, 1968) [43] in relation to a confining pressure. If a soil is in a looser state than the critical state, it will contract under shearing which will reduce the water content. It can therefore be defined as being on the wet side, as shearing will generate positive pore pressures that will seep out of the soil. In that case particles do not need to overcome interlocking resulting in a similar critical state strength as peak strength. If on the other hand the soil is in a denser state than the critical state it will dilate upon shearing and inversely as for the loose soil absorb water. The soil can therefore be referred to as being on the dry side. This is shown in Figure 4.3.

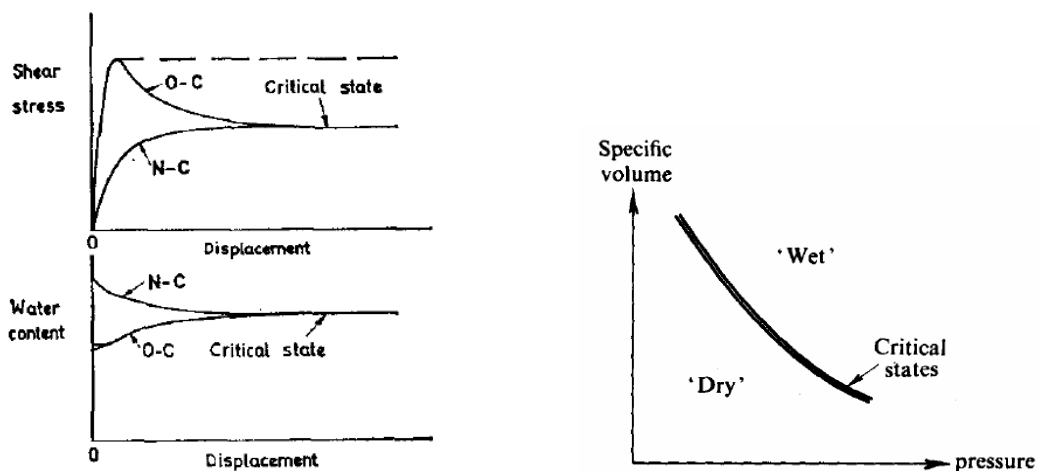


Figure 4.2: Representation of the critical state stress-strain behaviour for an ideal clay from (Skempton, 1970) [46]

The critical state of a soil also defines its failing point (Budhu, 2011) [16]. In p', q space it is represented by a line of slope M , which is often an input parameter for different soil models. The inclination of this slope is dependent on the stress path followed to bring the soil to failure. Physically the critical state line represents the point at which further shearing does not generate any more volume change in the soil. (Skempton, 1970) [46] showed a representation of the ideal stress-strain response of an ideal clay, which is shown in Figure 4.2.

The uniqueness of the relation between p', q and e is also illustrated by the fact that the undrained and drained test on clay provide the same Critical State line, or as it was called by (Roscoe, 1958) [42], the Constant Void Ratio line.

Residual strength

The residual strength of a soil is defined as the lowest strength a (soft) soil can obtain when sheared without volume change. It is reached when large displacements are imposed on clay. It is therefore usually not required to assess the residual strength of a clay except when investigating an old landslide (Skempton, 1964)

[45]. (Mesri and Shahien, 2003) [37] also showed that strain softening until residual strength levels can be achieved during first time slides. Lupini [35], [34] did some extensive study on the residual soil behaviour. He assessed different modes of residual shear: sliding, transitional and turbulent. The mode of residual shear defines the final strength loss a soil can undergo. The mode of residual shear is dependent on the soil composition. Granular materials will behave under a turbulent mode, while platy materials will tend to slide. A transitional behaviour is encountered in mixture soils.

Lets look deeper into the different modes. Sliding occurs in the case of platy shaped minerals. Strength drop is induced by reorientation of particles. When platy minerals turn in an orientation parallel to a slip plane, less interparticle friction can be mobilized. This results in a strength drop even after critical state has been reached. Soft soils like mineral clays typically exhibit this sliding behaviour, and can therefore have drastically low residual strength values. The residual strength of sliding soils is mostly dependent on the interparticle friction μ , but also on the loading rate, as shown in Equation 4.1

$$\varphi'_{R,clay} = f(\varphi\mu) \quad (4.1)$$

For granular materials, like sand, shearing beyond the critical state does not induce any further loss in strength. This is logical since there is no preferential orientation of the particles. The residual strength of granular material is therefore identical as the critical state strength, as shown in Equation 4.2.

$$\varphi'_{R,sand} = \varphi'_{CV} \quad (4.2)$$

Different factors influence the sensitivity of a soil to exhibit strain softening towards a residual strength level. The percentage clay particles (size <0.002 mm) is the main factor determining the sensitivity of a soil (Lupini, 1980) [35]. No drop beyond critical state strength will be felt unless the amount of clays particles exceeds 20 to 25 % of the soil weight. Confining pressure influences the rate of strength drop, as shown by (Sinclair & Brooker, 1967) [44]. A high confining pressure leads to faster reorganisation of platy particles, resulting in a residual strength reached at lower levels of strain. Displacement rate influence the residual strength as shown by [34] and [48]. They showed an increase in residual strength with increasing shear rates.

4.1.2. Residual strength of clays

Idealized drained strain softening of clays

When describing the residual strength of a failed dyke it is important to distinguish whether the situation should be modelled in a drained or undrained fashion. The failed dyke will behave in a drained fashion if the hydraulic conductivity of the soil through which the landslide passes is large enough to dissipate pore pressures during the remoulding of the soil (Stark et al, 2005) [52]. (Skempton, 1985) [47] showed that after an embankment failure the soil could be in residual strength conditions. (Terzaghi et al, 1996) [54] noted that drained parameters should be applied on the analysis of landslides that have reached residual strength conditions. This leads to the conclusion that an effective stress analysis is applicable to this case.

(Stark et al, 2005) [52] regrouped a number of recommendations on the use of drained parameters in the analysis of landslides. The most important part of their analysis might be about the loss of cohesion. (Skempton, 1985)[47], (Terzaghi,1996) [54] and (Mesri and Abdel-Ghaffar 1993) [36] stipulated that the reorientation of particles induced by the large deformations reduced the cohesion to 0 in a Mohr-Coulomb model. The particles are in a "face to face" orientation after the shearing. This creates an unfavourable situation for bonding, which leads to a low shear strength. This joins the more recent relation of clay strength based on critical state theory indicating that the cohesion of clays is actually a function of the packing state (through the OCR). When a soil is sheared until critical state, the particles are not compacted anymore and therefore do not bond. The residual strength is therefore independent of the loading history, meaning that over-consolidated and normally consolidated will drop to a single identical residual strength level (Skempton, 1964) [45]. This is shown in Figure 4.4.

(Stark and Eid, 1997) [51] research indicates that the strength of landslide clays has dropped to lower strength than the critical state. (Mesri and Shahien, 2003) [37] support this by showing that at least a part of the studied landslide has reached full residual strength.

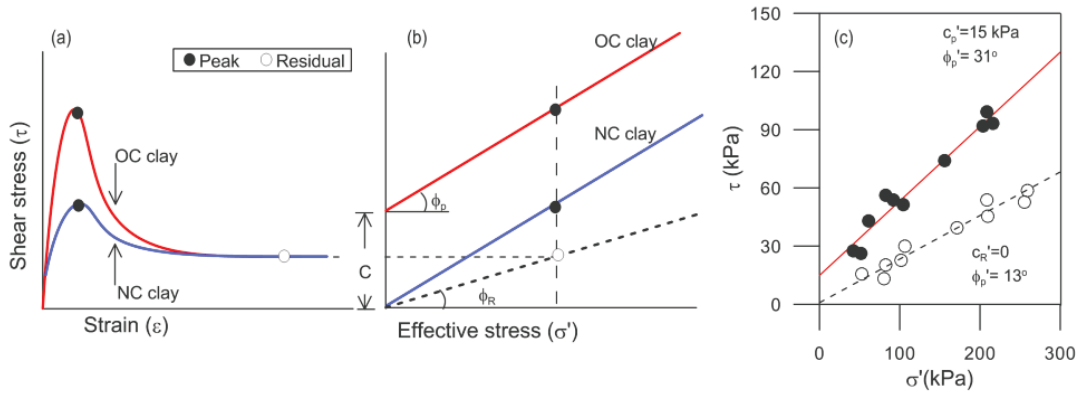


Figure 4.4: Idealised drained response of clays (Skempton 1964)[45]

Idealized undrained strain softening of clays

Another hypothesis is that the critical state strength reduction at around 20 % strain is not induced by a direct reduction of ϕ , but rather an effect of the excess pore pressure generated by a dilative behaviour under undrained conditions. This was first suggested by (Janbu, 1985) [27] and (Bjerrum, 1961) [10]. This is supported by numerous others like ,Jostad et al. (2005) [28], Thakur (2007) [55] and Gylland (2012)[24]. An interesting paper (Thakur et al, 2012) combines a lot of the known information about the undrained strain softening behaviour in soft sensitive clays [56]. Figure 4.5 is extracted from that paper, and shows the expected undrained response for 10-20 % strain.

The paper however does not conclude that the stability of a landslide should be assessed with an undrained analysis, as the critical stability of overconsolidated clays is often the long term stability. They also do not refute that a strength loss in ϕ is present. They only state that for landslides where large strains occur the first part of the strength trajectory towards critical state is induced by the generation of pore pressures. As noted by (Stark and Eid, 1994) [49] and (Stark and Contreas, 1996) [17], the strength drop beyond 20 % strain can still be described in a drained fashion.

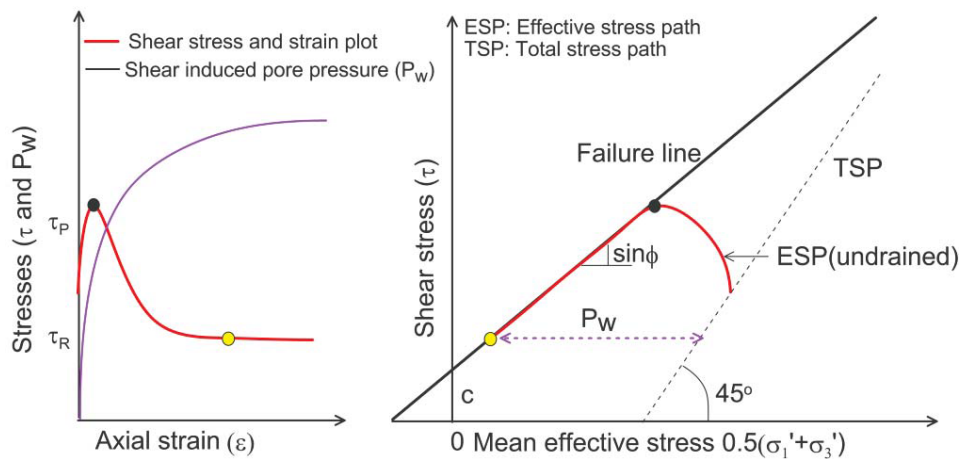


Figure 4.5: Idealized undrained response of clays (Jostad et al, 2012) [56]

4.1.3. Shear strength of peat

To understand the shear strength of peat, one must embrace the deeply anisotropic nature of this soil. Peats are organic soils, with a high content of non decomposed fibres. One of the main factors influencing the strength is therefore the orientation of the loading compared to the orientation of the fibers.

The shear strength of peat is mainly obtained from these fibres, resulting in high friction angles with low cohesion as studied by (Yamaguchi, 1985) [58]. When studying the peats of Japan he found extremely high friction angles, from 35 to 57 °. These values seemed to be unrealistically high. As supported by (Den Haan and Kruse, 2006) [22], the triaxial test seems to overestimate the strength of the peat. It was concluded based on a back analyses of the Booneschans failure (Zwanenburg et al, 2005) [60] that results from a DSS provided better strength estimations.

Little laboratory research has been carried out on the residual strength of peats. Vane tests are often used to assess the remoulded strength, however these often show unreliable results as studied by Landva(1980) [30]and (Boylan 2008) [12]. Some tests were effected in a ring shear test apparatus to try to assess the shear strength of peats. (Landva and La Rochelle,1980) [31] tried to find the residual shear strength properties of Canadian peat. They assumed that the residual strength was equivalent to the matrix friction strength of the peat, and performed ring tests. They noted lower friction angles, from 27 to 32.5 °.

Back calculation of strength properties of peat in full scale experiment in Bergambacht or Uitdam [32] [59] show that in practice crack formation is decisive in the final strength of a peat layer. More on this will be explained in the literature study of historical cases.

4.1.4. Critical state strength of sand

The shear strength of sands is historically difficultly described by the critical state theory. This is due to the difficulty of finding a virgin consolidation line (Been et al, 1991) [7]. More recent studies show that the dilative behaviour in dense sands lead to a strength towards a critical state strength, at which the sand can sustain further shearing without volume change. The behaviour is similar in drained and undrained conditon [11]. A representation of this behaviour is shown in Figure 4.7. This behaviour is however not uniform with stress changes. As stress increase beyond 1 MPa, the critical state line seems to shift, as shown in Figure 4.6. This non-uniqueness of the critical-state line makes it more difficult to couple the theory with practice.

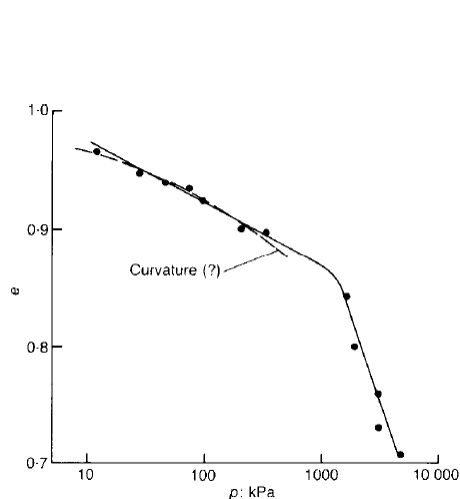


Figure 4.6: Critical state line for sand (Been et al, 1991) [7]

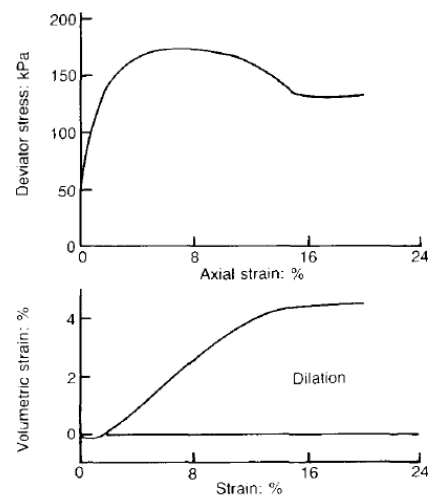


Figure 4.7: Typical drained strain-dependent strength reduction in sand (Been et al, 1991)[7]

(Bolton,1986) [11] came up with a number of easily implement correlation to estimate the magnitude of the drop towards critical state. These correlations with the constant volume friction angle are presented in Equation 4.3.

$$\phi_{cv} = 36 + \Delta\phi1 + \Delta\phi2 + \Delta\phi3 + \Delta\phi4 + \Delta\phi5 \quad (4.3)$$

Where:

- $\Delta\phi1$ = correction for particle shape
- $\Delta\phi2$ = correction for particle size
- $\Delta\phi3$ = correction for gradation
- $\Delta\phi4$ = correction for relative density
- $\Delta\phi5$ = correction for type of mineral

It should be noted that within this context (Bolton 1986) [11] found that for quartz sands a value of $\phi_{cv} = 33^\circ$ can be expected. However this is for pure sands. As sands are usually comprised of a silt fraction, this value can be expected to drop to values as low as 30° .

4.1.5. Principal stress rotation

A note can be added on principle stress rotation. In anisotropic soils the rotation of principle stress can lead to significant strength drop. Principle stress rotation can lead to significant drop of strength of soils due to their inherent anisotropy. (Broms and Casbarian, 1965) studied the effect of loading direction on the strength of remoulded clay [15]. They found a difference in 7° friction angle with a principal stress rotation of 45° . A similar study was carried out on the undrained analysis of saturated by (Symes et al, 1984) [25]. It was shown that the original anisotropy could have great effects on the generation of pore pressures, hence the final intersect with the critical state line.

As a concluding remark, principal stress rotation have strong influence on the measured strength of anisotropic soils. For the case of back calculation of strength from the Eemdijk experiment it will however be difficult to assess which part of strength reduction is induced by strain softening and how much can be credited to principal stress rotation.

4.2. Residual Strength and profile from case histories

Different full scale dyke failure experiments have already been carried out in the past. The goal of this paragraph is to regroup information on the shear strength encountered in practice.

The first case that will briefly be mentioned is the back analysis of the dyke failure at Streefkerk [5]. This failure was induced during the staged heightening of the dyke by uplift due to the high water table in the Pleistocene sand. The main conclusion applicable to our case is that conversion of strength parameters from one model to another should be effectuated with care and can easily lead to errors.

The next case that will be considered is the Ijkdijk experiment, analysed by (Zwanenburg et al, 2012) [60]. A trial embankment built on peat was brought to failure to test different monitoring methods. The goal was to check whether a dyke failure can be anticipated based on monitoring data. A number of conclusions could be drawn from this experiment that could also be of influence in the Eemdijk experiment. The first interesting conclusion was the difficulty to assess the strength properties of peat based on laboratory experiments. As stated previously, the global shear strength of a peat body is difficult to assess due to the extremely strong anisotropy and fibrous content. It was concluded that results from a DSS test provided the best results to what was back calculated from the experiment. The values from the DSS tests of the Eemdijk will therefore probably provide the best comparison.

Another important consideration from this experiment was the presence of cracks in the peat. Large vertical cracks had formed during failure, which were filled up with sand. At these points the peat did not contribute anymore to the mobilized strength. These cracks might also have contributed to the consolidation of the peat. Some excess pore pressure was still present at the time of failure. After failure the strength measured in the peat was higher than before failure. The hypothesis to explain this is that the cracks might have helped

excess pore pressures to dissipate. In the LEM analysis of the Eemdijk experiment we can therefore expect the excess pore pressures to have dissipated after failure occurred.

Finally an interesting observation from the Ijkdijk experiment dealt with the location of the slip surface. It was noted that the slip surface mostly passed at the interface of the peat and the sand. After effectuating vane test a higher strength was found in the peat than at the interface with the sand. The most critical strength might therefore actually be an interface strength rather than that of a single peat layer.

The next case history that will be discussed is the Bergambacht case [32]. This experiment had as main goal to model the actual strength of a dyke failing in an uplift mode. An interesting part of the work carried out was the determination of the 3d effect based on the failed geometry. This work will serve as basis in our LEM analysis.

Finally the Dijken op Veen project [59], with the Uitdam test showed great coupling with the Ijkdijk experiment concerning the role of vertical cracks in the strength of peat. Similar conclusions were also drawn regarding the inability of in situ method to correctly estimate the strength properties. DSS also provided good results when trying to estimate the shear strength of peat. It was also concluded that the undrained analysis in terms of S ratio and OCR provided better results than with a $c'-\varphi$ analysis.

Important conclusions were also made regarding the role of cracks in the shear strength of peats. Vertical cracks were found in the active, reducing the strength to 0. In the horizontal part of the slip surface the peat was deemed to have a similar shear strength as at peak.

4.3. Residual strength of Eemdijk soil: laboratory experiments

Extensive laboratory experimentation was carried out prior to the Eemdijk experiment to try to assess the residual strength of clay and peat. To this goal cyclic undrained DSS and LDSS (Large Direct Simple Shear) up to 40 % strain. The results of this research are presented in the Geotechnical base report [14].

4.3.1. Laboratory experiments on clay

cyDSS tests

Conclusions from the cyclic Direct Simple Shear (cyDSS) tests were that the residual behaviour of clay expected could not be reproduced in the laboratory. Strains up to 50 % were applied, where strains beyond 40 % produced unreliable results due to the influence of the membrane. Under constant loading a strength drop of 17 % was noted, which is way lower than the 50 % (Skempton, 1985) [47] found.

Another bad coupling between literature and experiments was found on the role of the overconsolidation. As stated previously it is expected that the residual strength of overconsolidated samples drops to an identical value as for normally consolidated samples. This was not measured.

Two hypotheses were presented by Deltares to explain these discrepancies. The first hypothesis is that the clay encountered at the Eemdijk location behaves differently from the clay studied by Skempton due to the presence of organic matter. The second hypothesis is that the residual strength was not reached by the samples due to the cyclic loading of the DSS. Residual strength is reached when particles are oriented parallel to the slip surface orientation. By reversing the orientation of strains at each cycle it is possible that the particles could not fully reorient on a single plane orientation, hence the residual strength could not be reached. This point will be further discussed in the LEM analysis.

Index property correlations

Index property correlations with residual strength have been carried out by numerous authors. The clay content and Atterberg limits were shown to be in relation with the residual strength of clay. These correlations were therefore used by Deltares to compare to the values obtained from the cyDSS tests. All the results presented are extracted from the Geotechnical Base Report [14].

The first relation that were tested were based on the clay content of the clays. Authors like Skempton (1964)[45] showed a relation between the percent clay particles in a soil and its sensitivity. Results of these correlations showed residual friction angles around 30 °for the clays used in the cyDSS tests.

Stark and Eid (1994) [50] showed a correlations between the Liquid limit, clay content and tangent residual friction angle. The Liquid Limit of the clays used in DSS tests were therefore also assessed. Again a drained

friction angle of approximately 30 ° was found. The results are presented in Figure 4.8 and 4.9

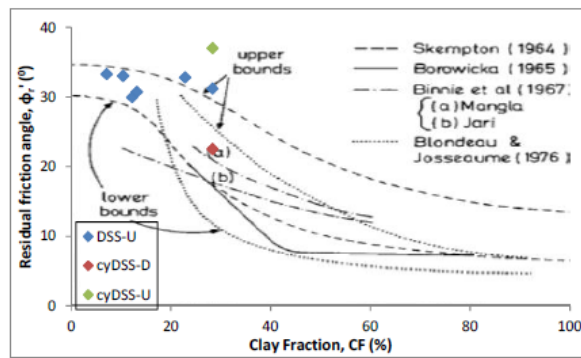


Figure 4.8: Clay fraction correlation with residual strength laboratory results

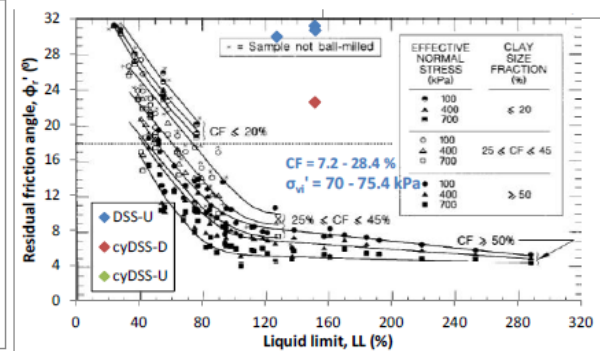


Figure 4.9: Liquid limit correlation with residual strength laboratory results

4.3.2. Laboratory experiments on peat

The laboratory experiment on the peat of the Eemdijk experiment reproduce well what has been encountered in previous case histories like the Uitdam experiment [59] and [60]. The mobilized shear strength originates from the mobilization of specific fibers. This induces that the strength of a peat should not be assessed based on strains, but rather on absolute deformations. The mobilized strength actually increases with deformations, until failure. This occurred after 15 % strain equivalent to 12 cm displacements. After this a jump in deviatoric stress was noted until 20 % strain (eq, 16 cm displacements) in the DSS tests. At failure vertical cracks form, reducing the strength to 0.

The residual strength after failure can be describes as an interface friction, and is therefore dependent on the contact length. [59]. The role of the formation of cracks is therefore decisive in the final strength assessment for peat.

4.4. Summary residual strength hypotheses

In this literature study different points of view are presented regarding the best way to express the strength drop of clay. The first point of view defended by Stark, Skempton and Terzaghi is that the residual strength of landslides should be assessed based on a drained friction angle. The second point of view defended by Janbu and Bjerrum states that the shear induced strength loss in clays should be viewed as undrained, where the strength loss is actually induced by a loss of OCR, and that the further drop of undrained friction angle originates from the generation of pore pressures.

From these points of view 3 hypotheses can be formulated, and tested with MPM.

- Hypothesis 1 : Clay behaves drained when sheared until residual strength level. An apparent cohesion drop to 0 should be considered.
- Hypothesis 2: Clay behaves undrained when sheared until residual strength level, and strength loss is related to a drop in S ratio, as well as the loss of OCR.
- Hypothesis 3: Clay behaves undrained during shearing until residual strength levels, and strength loss solely related to a loss of OCR and generation of pore pressures.

5

Strength properties back calculations

The first goal is to get insights into the actual strength property of the slope before and after failure. This can be done by using a Limit Equilibrium Method (referred to as LEM in the rest of this report). LEM is a robust way of finding the factor of safety for a slope. In this context it will however be used to try and estimate the strength mobilized at and after failure of the slope. First the discretization of the experiment will be presented, after which the methodology to back calculate the strength of the different layers will be explained. This will form the geometrical base to back calculate the peak and residual strength of the different soil layers of the Eemdijk full-scale test.

5.1. Discretization in LEM

5.1.1. Settlement calculation

In order to model the failure phase of the experiment properly it is necessary to determine the post construction stratigraphy. To achieve this goal a 2-D settlement calculation was carried out in D-Settlement. The results from the settlement calculations were compared to the measurement cables results.

Different parameter sets from the back analysis report [13] were compared to settlement plates fit option the D-settlement software offers. The parameters from the back analysis report [13] originated from the post analysis of the experiment in different phases with a SSC model. Parameters from the SSC model are closely related to the isotach a-b-c method. The isotach model will therefore be used in the prediction of the settled profile. The analysis include a postdiction, Best-fit and FEM parameter sets. The postdiction was used after the buildup of the experiment, the best fit was determined post failure, and the FEM was used as a reference to validate the Finite Element Method design approach proposed by Deltares.

Two measurement plates in the central axis of the experiment (at location 27 and 31) were used with the Settlement Plates fit option of the D-settlement software to try to fit the final geometry prediction to the measurements. The results of the settlement analysis are shown in Figure 5.1.

It can be concluded from this analysis that the measurement plate 31 fit analysis produced results that were closest to the settlements measured by the settlement cables. Less settlements were found under the green dyke than under the Blue dyke. This is due to the overconsolidation induced by the weight of the old summer dyke. The fit in the middle of the construction (between the two dykes) was not extremely good. Settlements in this area were overestimated. The goal of this settlement analysis was to get the right magnitude of displacements in the area of the slip surface, therefore around the toe of the two dykes. In this context it is concluded that the settlements were predicted well enough for the scope of this study, therefore the final geometry of the settled subsurface exported to the stability analysis phase is issued from the settlement plate 31 fit. A graphical representation of the settled profile is shown in Appendix F Figure F.1.

5.1.2. Degree of consolidation

The degree of consolidation in the subsurface is required to provide a stress dependent strength of the clay layers. Defining the degree of consolidation as the fraction of pore pressures dissipated over the total load

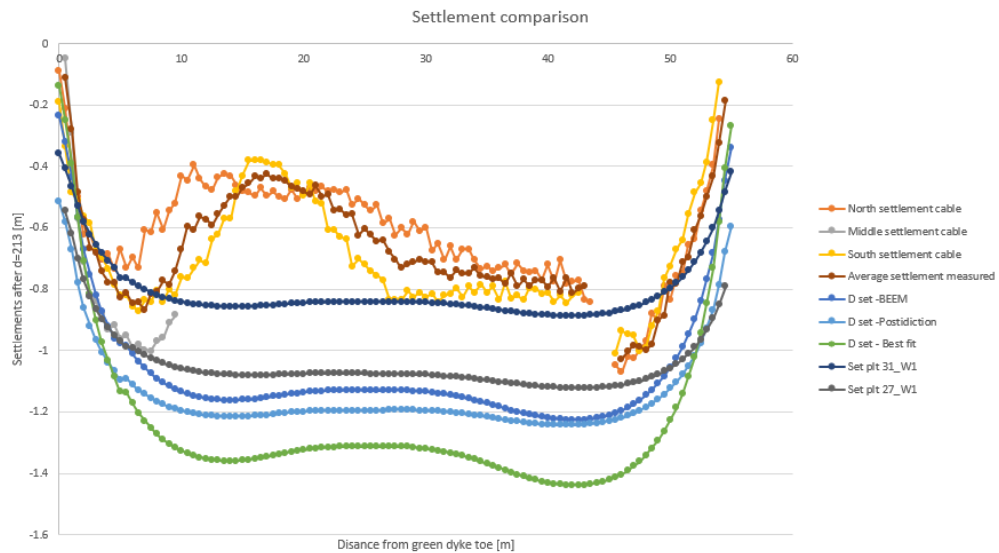


Figure 5.1: Comparison of the settlement analysis of the construction phase

added, the degree of consolidation can be determined based on the water pressure data. Due to the inability of D-Geo Stability to model phases, it was chosen to model the excess pore pressures with the use of PI-lines. Simplifying the consolidation process by assuming constant dissipation through the layer, we can define the excess pore as also being constant inside a soft layer. A representation of the PI-lines discretization in D-Geo Stability is presented in Figure 5.2.

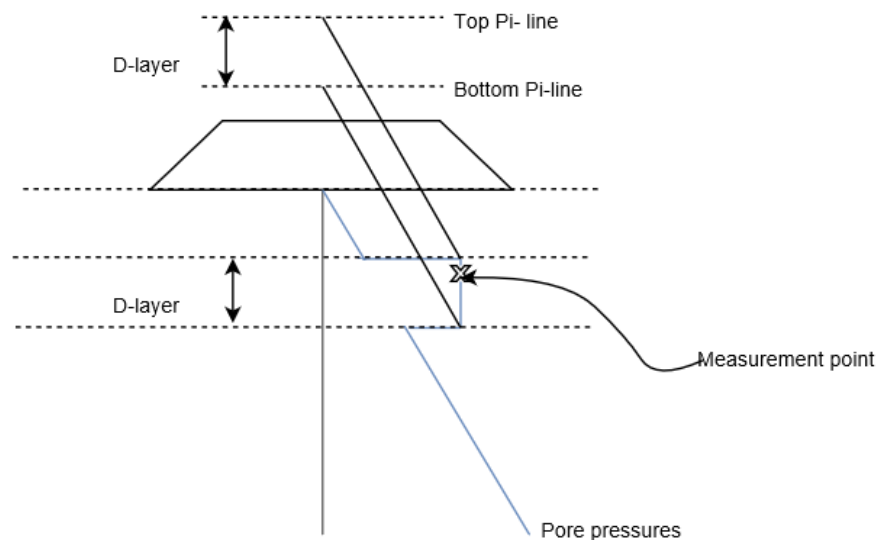


Figure 5.2: Schematisation of the method used to model excess pore pressures in D-Geo Stability

The water pressures development in the subsurface is shown in Appendix A in Figures A.1 A.2. A summary of the pore pressures at the moment of failure are presented in Appendix A Table A.1 and A.2. It was noted that transducers 31o and 40o at the Green dyke, and 27d, 27o and 38d at the Blue dyke showed faulty measurements. These transducer measurements were therefore ignored in the rest of the analysis. In the clay of the Green dyke an average water pressure before failure was found of 16 kPa under the toe and 58 kPa under the crest. In the peat under the Green dyke a water pressure was found of 31 kPa under the toe and 63 kPa under the crest. In the clay of the Blue dyke a water pressure was found of 15 kPa under the toe and 71 kPa under the crest. In the peat of the Blue dyke a water pressure was found of 33 kPa under the toe and 74

kPa under the crest. The Blue dyke showed to have slightly more excess pore pressures than the Green dyke, probably due to the extra height put on top and the extra overconsolidation at the green location.

5.1.3. 3-D effect

In a 2D slope analysis, a plane strain situation is considered. In that situation the stability is only assessed based on the mobilized shear strength at the bottom of a slip surface. When a slope failure is narrow, or when it occurs in cohesive soils, significant strength can be mobilized by the sides with so called "end effects" (Azzouz and Baligh, 1975) [4]. These are 3D effects.

3D effects can be defined as the strength mobilized by a slip surface edge over the mobilized strength by the base of the slipsurface. It is therefore the percentage of the shear strength acting on the side over a classical 2D plane strain analysis. In a 2D analysis no edges are modelled, reducing the problem to a plane strain situation. In reality the side of a slip surface also contribute to the total macrostability. The narrower the slip surface compared to the geometry of the dyke, the higher the 3D effects will become. In a LEM analysis this effect results in an overestimation of the factor of safety in a 2D analysis compared to a 3D situation. Post failure analysis showed that these 3D-effects could not be neglected. It was however not yet managed to quantify these effects. During the Dijken op Veen experiment [59] the magnitude of this effect was determined to be around 10 to 20 %, with a high boundary at 45 % .

In the Bergambacht experiment [32] a geometrical approach was presented to determine the 3D effect. The magnitude of 3D effects can be expressed as the fraction between the mobilized strength over the base (ie the 2D plain strain analysis) over the shear strength mobilized in the sides of the slip surface. Although inaccurate due to simplifications in the geometry, it is a robust way of finding a strength independent analysis of the magnitude of the 3D effects. By assuming a constant value of strength and weight for the entire dyke, we can simplify the 3D effect as the fraction of average slide depth over slide width. In order to quantify the

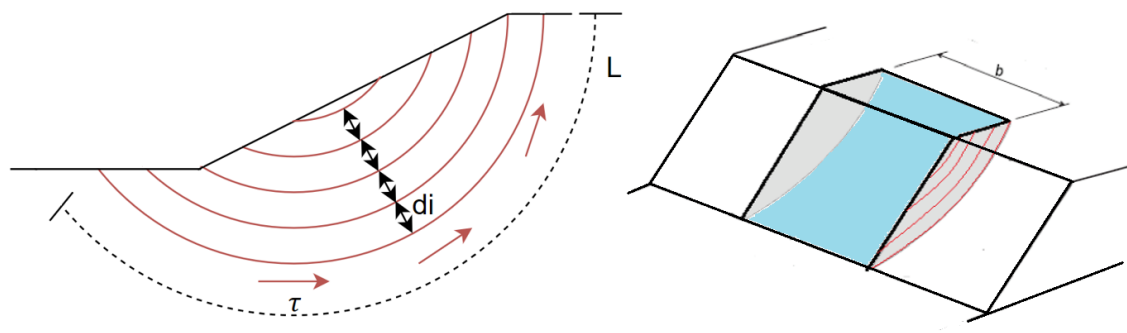


Figure 5.3: Representation of the cylindrical slip surface envelope model used for the 3D effect calculation. In blue the mobilized strength along the bottom, and grey along the sides of the slip surface

3D effects the mobilized shear strength along the sides need to be calculated. A cylindrical slipping volume was assumed, as shown in Figure 5.3. (Michalowski, 2010) [38] developed a model with a more complex shape, taking into account curvature along the sides. However as the slip surface was shallow it was assumed that the added side friction would be small compared to the situation with straight edges. A Bishop analysis with 1 m varying radius can be applied on the profile to determine the average mobilized stress along the sides, following Equation 5.1. By determining the mobilized strength per unit radius the mobilized strength by the sides can be found. The mobilized shear strength at the bottom (or real) slip plane investigated in a 2D plane strain analysis, expressed with Equation 5.2 can be combined with Equation 5.1 to find the 3D effect magnitude in Equation 5.3. A full calculation of the 3D effect is presented in Appendix G

$$F_{sides} = \sum_{n=1}^n \tau_i \cdot L_i \cdot d_i \quad (5.1)$$

$$F_{bot} = \tau_{bot} \cdot L_{bot} \cdot B_{slide} \quad (5.2)$$

$$3D-effect = \frac{2F_{sides}}{F_{bot}} \quad (5.3)$$

A first estimation of the 3D effect can be taken as the fraction of the average depth over the width of the slipplane. In the Green dyke the slip surface was approximately 20 m wide and had an average depth of 3.22 m. This indicates a 3D effect of around 20 %. In the LEM analysis of the green dyke the first target FOS to back calculate the mobilized strength will therefore be 0.8. In the Blue dyke the slip surface was as wide as 5 containers as can be seen from the timelapse video. The containers being placed at 1.5 m distance from one another, the slip surface was concluded to be 40 m wide. The slip surface had an average depth of 3.8 m according to the SAAF measurements. This indicates a 3D effect around 10 %. In the LEM analysis of the Blue dyke a first target FOS to back calculate the mobilized shear strength will therefore be 0.9.

Figure 5.4 shows the flowchart used to determine the 3D-effect and the unknown strength of the soil layer. This iteration process was used to back-calculate the strength of Layer 3 and 3a, and to find the 3D-effect of the Green dyke.

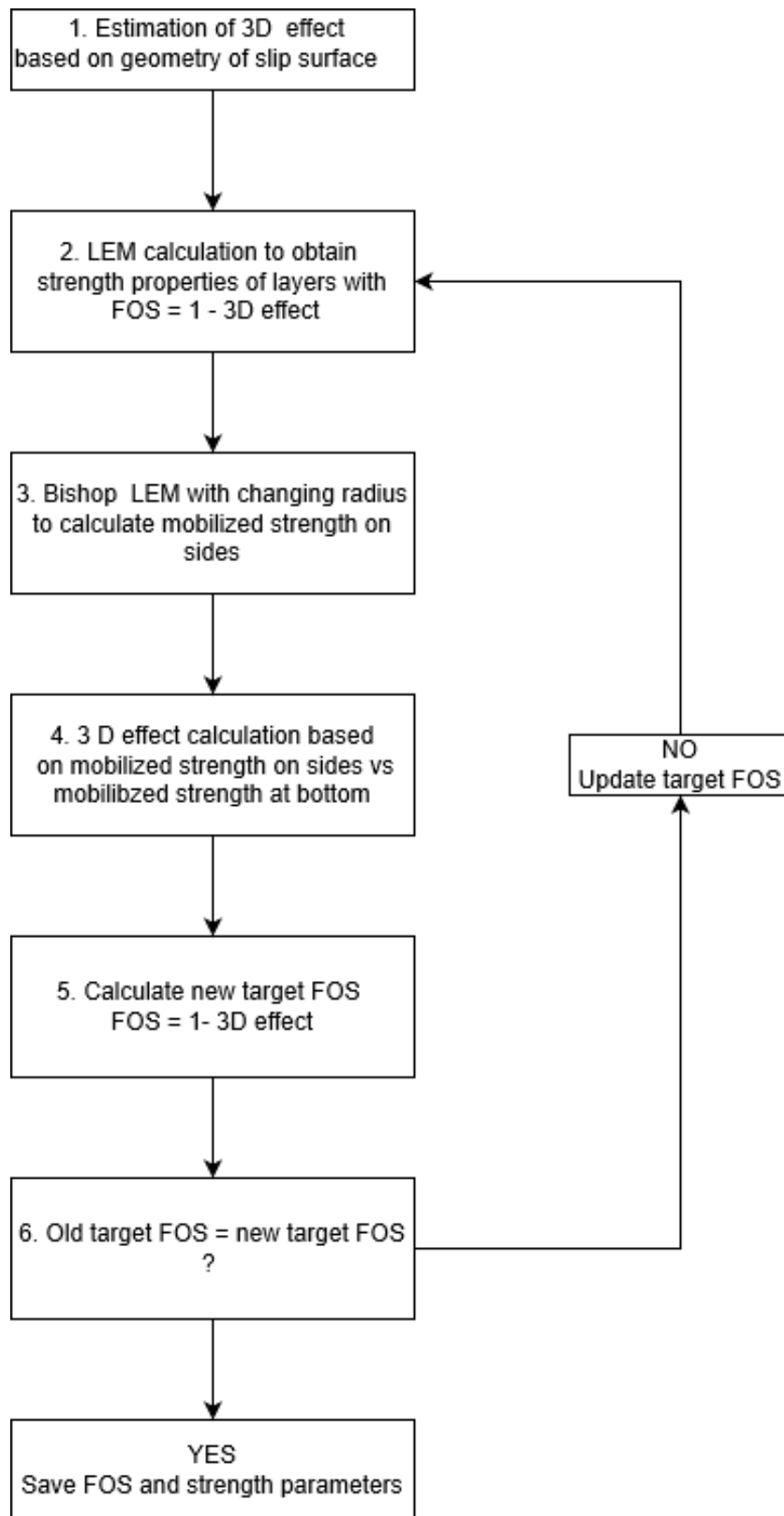


Figure 5.4: Flowchart to back calculate the 3D effect and the soil strength parameters

5.1.4. Shear strength models LEM

A few words need to be used to express the shear strength of the different layers in the LEM formulation of D-Geo Stability [20].

Drained

In D-Geo Stability, the strength of drained layers, for example the sand core, are expressed with a $c-\varphi'$ model with dilatancy in Equation 5.4.

$$\tau_i = c_i \cdot \frac{\cos\psi_i \cdot \cos\varphi_i}{1 - \sin\psi_i \cdot \sin\varphi_i} + \sigma'_{n;i} \cdot \frac{\cos\psi_i \cdot \sin\varphi_i}{1 - \sin\psi_i \cdot \sin\varphi_i} \quad (5.4)$$

With:

- c_i [kN/m³] = Cohesion at the bottom of the slice
- φ_i [deg] = Friction angle at the bottom of the slice
- ψ_i [deg] = Dilatancy at the bottom of the slice
- $\sigma'_{n;i}$ [kN/m²] = Normal effective stress along the bottom of the slice

In practice, a common choice following the old Dutch design norm used to be to assume associative behaviour, meaning $\psi = \varphi'$. In that case, the expression simplifies to the well known Mohr-Coulomb failure line, expressed in Equation 5.5.

$$\tau = c + \sigma'_n \cdot \tan\varphi \quad (5.5)$$

The dilation angle of soils reduces to 0 quickly after the peak stress has been reached upon further shearing. A non-associative formulation is therefore required to formulate strength lower than Critical State strength. When using $\psi = 0$, the shear strength simplifies to equation 5.6.

$$\tau = c \cdot \cos\varphi + \sigma'_n \cdot \sin\varphi \quad (5.6)$$

Undrained

The shear strength of undrained layers are expressed in D-Geo Stability with a SHANSEP formulation through a S_u -calculated with yield shear stress formulation, following the 2017 Dutch norm (WBI). The undrained shear strength formulation is given in Equations 5.7 and 5.8.

$$\tau = \sigma'_v \cdot S \cdot OCR^m \quad (5.7)$$

$$OCR = \frac{\sigma'_y}{\sigma'_v} = \frac{\sigma'_v + POP}{\sigma'_v} \quad (5.8)$$

With:

- S [-] = Strength ratio
- m [-] = Strength increase exponent
- POP [kPa] = Pre-overburden pressure

5.2. Residual strength hypotheses in LEM

As stated in the summary of the literature study on the residual strength of soft soil layers, different hypothesis have been formulated regarding the best way to describe the strength drop. Each hypothesis will now be described, and assumptions to permit the backcalculation of residual strength values with a LEM will be presented.

5.2.1. Hypothesis 1: Drained analysis

The first hypothesis is centered around the idea that the strength of a landslide can best be described with a drained residual friction. In this hypothesis a drained situation will therefore be considered. Distinction can be made in the different types of pore pressures.

Three types of pore pressures can be distinguished: excess pore pressures still present in the soft soil layers from the construction, pore pressures generated during shearing in an undrained failure, and finally pore pressures generated in the layers loaded by the deformed geometry, around the new toe. For this analysis all pore pressures will be deemed to be dissipated from the residual geometry. As stated in literature, (see Chapter 4, the residual strength should be expressed solely as a residual friction angle. Every cohesion will therefore be discarded. A representation of the strength loss has been presented in Figure 4.4.

5.2.2. Hypothesis 2: Undrained analysis, no OCR, friction angle softening

The second hypothesis is centered around the idea that the residual strength of clay should be assessed with an undrained analysis. The strength loss is hypothesized to be induced mainly by the loss of OCR (in Mohr-Coulomb terms therefore by a loss of cohesion), and by the generation of pore pressure due to the undrained failure mechanism. A further drop in strength might still be present. In this hypothesis an S-ratio will be sought for which the residual profile is in equilibrium.

Like in Hypothesis 1, the role of the OCR in this hypothesis is assumed to be completely lost due to the heavy remoulding the particles in the slipplane underwent. This results in a purely frictional soil. Following the works from (Jostad et al, 2012) [56], the cohesion drop is much more brittle than the friction angle drop. This hypothesis defers from the previous one in the treatment of the pore pressures. It is here assumed that the first part of the strength reduction up to levels of 20 % strain is actually induced by the undrained generation of pore pressures. A representation of this strength drop is given in Figure 4.5. At higher levels of strains a friction angle drop can still be expected in a constant volume ring shear apparatus from the work of (Stark and Contreas, 1996) [17]. This hypothesis will be tested by backcalculating the S-ratio required to maintain a stable situation without OCR influence.

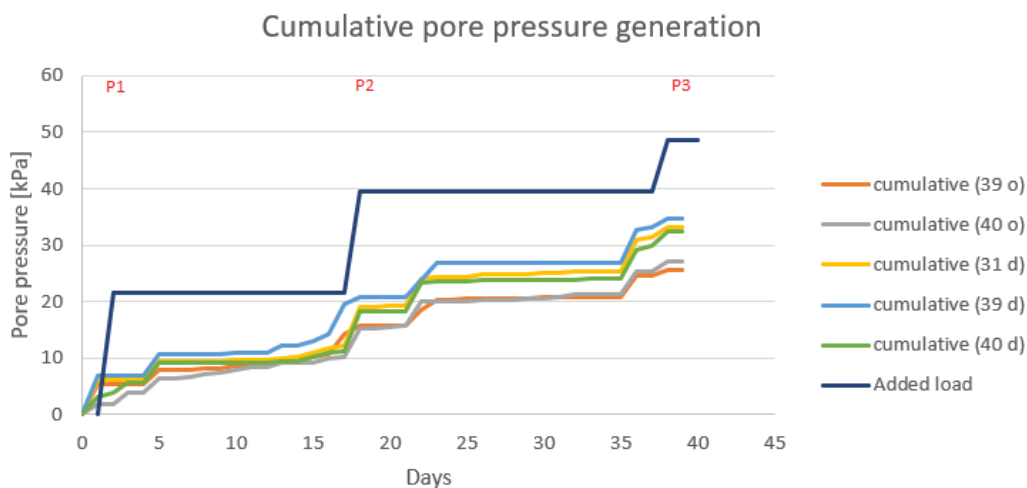


Figure 5.5: Accumulation of pore pressures in the subsurface for the 3 first loading stages

Looking back onto the three different types of pore pressures that can be taken into consideration as-

assumptions can be made for this analysis. The situation will be modelled in an undrained fashion, therefore the pore pressures still present in the subsurface from the construction will be maintained. The pore pressures generated during undrained shearing are related to the dilative behaviour of the soil. These types of pore pressures will be neglected as the large levels of strain make this behaviour difficult to quantify. The final source of pore pressures that needs to be considered are induced by the shift in geometry under undrained conditions. Unloading under these conditions results in the generation of positive pore pressures, while loading results in the generation of negative pore pressures. These pore pressures have a significant magnitude, and will therefore influence the back calculated residual strength.

When loading a soil in an undrained fashion it is never fully known how much of the load will be taken on by the pore pressures and how much by the soil skeleton, or by gasses still present in the pores. As it is known what the applied load is in that case an estimation of the percentage of the load being taken on by the pore pressures for primary loading can be provided. The cumulative positive changes in pore pressures is compared in Figure 5.5 to the added load for the first 3 construction steps. It can be noted that the difference between the added load and pore pressure generation per load step gets smaller. The first step results in a 37 % of the load being taken by pore pressures, while this increases to 54 % in the second step and 58 % in the third step.

The influence of this pore pressure generation can be taken into the residual LEM model through the incorporation of a % Consolidation term in D-Stab. A value of 60 % consolidation was chosen to be induced by the failed clay cover over the underlying clay layers 3 and 3a.

5.2.3. Hypothesis 3: Undrained analysis, no OCR, no friction angle softening

The third hypothesis is an extension of the second hypothesis. It has previously been stated that the largest part of the strength drop is probably due to the loss of OCR, and therewith cohesion, but that a further drop in strength can also be expected (through a φ or S-ratio reduction). This hypothesis will test whether a stable situation can be obtained based solely on an OCR loss. The same pore pressure distribution will be handled as in Hypothesis 2.

5.3. Green dyke strength back calculation

The strength of the different layers of the Green dyke can now be determined. The focus of this thesis lies on the strength evolution of the clay layers under the Green dyke. To do this assumptions need to be made regarding the strength of the sand core. After this the peak strength of the different clay layer can be calculated. Based on the different hypothesis presented in Chapter 4 different scenarios will be elaborated regarding the residual strength of the clay layers.

5.3.1. Peak strength of sand core

After investigation of the shape of the Green dyke slip surface it was noted that a large fraction of the surface passed through sand. At the level of the toe, the slip surface passed through the soft clay Layer 3a. This indicates that a significant portion of the mobilized shear strength on the slip surface was provided by the sand core. The first part of the strength property back calculation will therefore deal with the strength of the sand core. First a LEM model will be used to investigate the apparent cohesion of the unsaturated sand. Empirical correlations between CPT results and relative density will then be used to assess the peak friction angle of the sand core.

Apparent cohesion

After the failure of the Green dyke a sand slope close to vertical remained stable for a period of more than a week until the last construction phase for the blue dyke was completed. This would be impossible in a cohesionless sand, which would settle at an angle close to the internal friction angle. This apparent cohesion can be explained by suction pore pressures in the the unsaturated sand. The magnitude of the cohesion required to keep the slope stable will be determined in this paragraph with a LEM analysis.

Cohesion and friction angle were set as variable in the LEM analysis of the failed green dyke. The model was adapted slightly as the model for the failed green dyke was based on measurements taken a month after failure. The top part of the failed sand core was elongated and made slightly steeper based on the timelapse videos from the failure. The Bishop method was used in D-Geo Stability to find to most critical slip circle, and assess which $\varphi - c$ combination resulted in a stable situation (i.e. with a FOS > 1). The final model can be found in Appendix F, Figure E2. Note should be taken that in this case the target FOS is 1, as opposed to further analysis where 3D effect was taken into account. Since failure did not occur, the situation can still be seen as a in plane strain conditions. The water table was set back to initial groundwater table level, and the simplification was made of assuming a constant degree of saturation through the whole dyke core (resulting in a single cohesion for the whole core). The situation was modelled with the load from the empty containers on top. Following the information from the Back analysis report (Breedeveld, 2018) [13], the weight of the empty containers was assumed to be 4 tons, resulting in an equivalent load of 2.5 kPa.

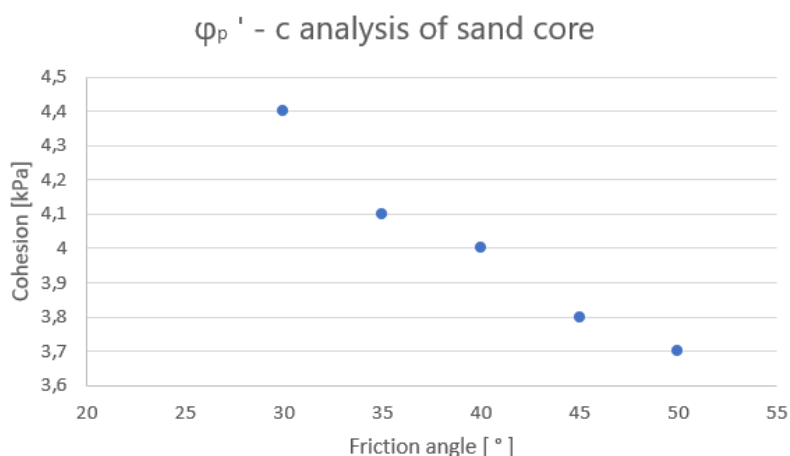


Figure 5.6: $c - \varphi'$ required in unsaturated sand core to maintain stable situation

The combination of cohesion vs friction angle required to reach a FOS = 1 is plotted in Figure 5.6. It can be seen that for a friction angle varying between 30 °and 45 °a cohesion of at least 3.5 kPa is required to main-

tain a stable situation. In the back analysis report [13], a value of 5 kPa was assumed based on engineering judgment. This seems to be a slight overestimation of the apparent cohesion.

Friction angle

A decision now needs to be made concerning the peak friction angle of the sand in the dyke core. A correlation between the relative density and the mean effective stress at failure is proposed by (Bolton, 1986) [11]. Different methods were used to estimate the relative density out of CPT cone resistance and vertical effective stress. (Lunne and Christoffersen, 1983) [33] proposed a generally accepted method for quartz sands, presented in Equation 5.9. It was compared to methods proposed by (Kulhawy and Mayne, 1990) [29], presented in Equation 5.10 and (Jamiolkowski et. al, 2003)[26] presented in Equation 5.11. In the (Kulhawy and Mayne, 1990) [29] equation the term Q_c refers to a compressibility coefficient, equal to Q_c is 0.91, 1.00, and 1.09 for high, medium, and low compressibility sands. The same accounts for the (Jamiolkowski et al, 2003) [26] equations, in which the term accounting for the compressibility is bx ($bx = 52.5, 67.5, 82.5$ for high, medium, and low compressibility sands). The term $C1$ refers to a stress normalization exponent, taken as 0.5. Quartz sands are considered incompressible, a Q_c value of 1.09 can therefore be taken.

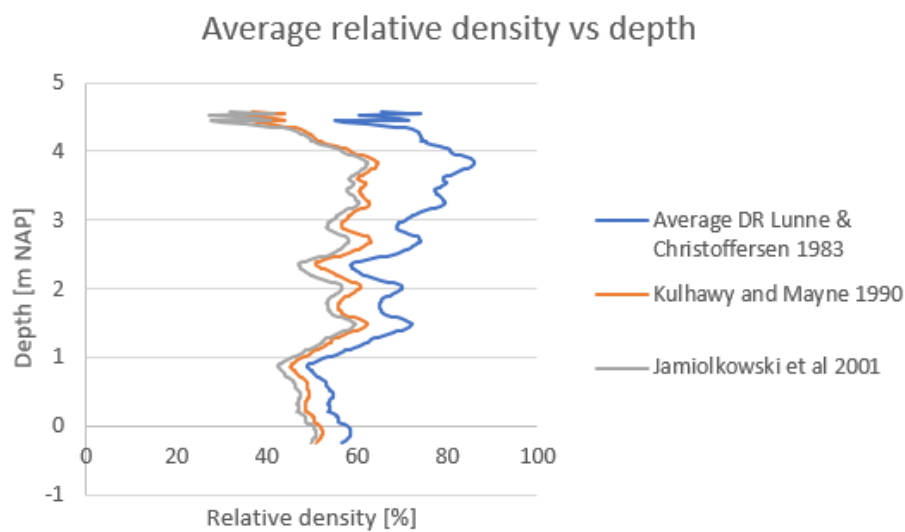


Figure 5.7: Relative density vs depth based on CPT data

The relative density was computed based on the CPT's taken at location 31, 39 and 40. The results were averaged, and presented in Figure 5.7. (Biryaltseva et al, 2016) [9] argues that (Jamiolokowski et al, 2001) underestimates the relative density. Lunne and Christoffersen based their study for the offshore industry. In offshore stress levels are often higher than when considering an embankment. For the rest of the analysis it will be concluded that results by (Kulhawy and Mayne, 1990) [29] seem to provide the most accurate results. It can be concluded from the different methods that the relative density of the sand in the core is varying between 50 and 80 %.

$$DR = \frac{1}{2.91} \ln \frac{q_c}{61\sigma_v^{0.71}} \cdot 100 \quad (5.9)$$

$$DR = 100 * \sqrt{\frac{1}{305Q_c} \cdot \frac{qc/pa}{(\sigma'_{vc}/pa)^{0.5}}} \quad (5.10)$$

$$DR = 26.8 \ln \left(\frac{qc/pa}{(\sigma'_{vc}/pa)^{C1}} \right) - bx \quad (5.11)$$

The average relative density can be used to compute the difference between peak and critical state friction angle based on Equation 5.12, from (Bolton, 1986) [11]. Combining Equations 5.9, 5.10, 5.11 with 5.12, a friction angle drop of 7 to 10 ° can be expected. For further calculations the (Mayne and Kulhawy, 1990) [29] was used. This leads to a drop in friction angle of 8 °.

$$\varphi_{tc} - \varphi_{cv} = 3Dr[10 - \ln(100 \frac{p'}{pa})] - 1 \quad (5.12)$$

With:

- p' [kPa] = mean effective stress
- pa [kPa] = atmospheric pressure

(Bolton, 1986) [11] and (Been & Jefferies, 1985) [6] studied the typical critical state friction angle of sands. Bolton showed that the critical state friction angle was dependent on the particle shape, size, gradation and type of mineral. For quartz sands he concluded that a friction angle of 33 ° was representative. However he also stated that this value could be lowered by a high degree of silt present, towards a friction angle as low as 27 °. (Been & Jefferies, 1985) [6] settled on a range of 30 - 32 °, except for fine sands. The boreholes taken at the CPT locations show that the sand in the core is fine, but not strongly silty. A value of φ_{cv} 30 ° therefore seems to be a good estimation.

The choice of the dilation angle influences the shear strength in the LEM Mohr-Coulomb model as seen in Equation 5.4. (Bolton, 1986) [11] showed a relation between the critical state and peak friction angle as expressed in Equation 5.13. The dilation angle to be input in the peak strength analysis was therefore found to be 10 °.

$$\varphi = \varphi_{cv} + 0.8 \cdot \psi \quad (5.13)$$

Based on this we can conclude that the peak strength of the sand core was around 38 °, with a dilation angle of 10 °. From Figure 5.6, it can be noted that a peak friction angle of 38 ° requires a cohesion of 4 kPa in the unsaturated zone.

5.3.2. Peak strength of clay layers

The mobilized peak strength of the green dyke can now be determined with a Spencer LEM analysis. The discretization of the experiment in D-Geo Stability is presented in Appendix F.3. In the previous paragraphs it was concluded that the sand peak friction angle was round 38 °, with an apparent cohesion of 4 kPa induced by suction water pressures.

The back analysis of the strength properties of clay layer 3 and 3a now has 4 unknowns: The peak strength ratio's S_3 and S_{3a} , and the strength exponents m_3 and m_{3a} . The soil laboratory experiments shown in the Geotechnical base report [14] showed that the strength exponent m to be constant in Layer 3 and Layer 3a. This will therefore be maintained at 0.9 throughout the analysis. In order to solve the 2 remaining unknowns with one model it has been chosen to express the strength of Layer 3a as a fraction of the strength of Layer 3. From the Geotechnical base report [14] the lab test results showed $S_{p,layer3} = 0.47/0.37 * S_{p,layer3a}$. Following the flowchart presented in in Figure 5.4, the strength of the clay layers and the equivalent target Factor of Safety were computed. The results are presented in Table 5.1.

Table 5.1: Results of the peak LEM analysis of the Green Dyke layers

φ_{sand}	c_{sand}	S_{layer3}	$S_{layer3a}$	Target FOS
30	4.4	0.52	0.41	0.79
33	4.2	0.49	0.39	0.79
35	4.1	0.47	0.37	0.79
37	4	0.46	0.36	0.79
38	4	0.45	0.35	0.79
40	4	0.42	0.33	0.79
43	3.9	0.39	0.31	0.78
45	3.8	0.37	0.29	0.78
47	3.8	0.35	0.28	0.78
50	3.7	0.33	0.26	0.77

It can be noted from these results that for $\varphi_{sand} = 38^\circ$ convergence of the FOS was obtained with $S_{Peak,layer3} = 0.45$ and $S_{Peak,layer3a} = 0.35$. The 3D effect was found to be 21 %.

It can also be concluded that the 3D effect becomes higher as the strength of the sand enhances, as most of the mobilized strength of the sides originates from the strength of the sand. A higher strength sand results in a higher mobilized strength of the sides, while the bottom mobilized strength over the whole slipplane remains constant. This effect is however marginal considering the range of possible sand friction angles presented. The magnitude of the 3D effect, and therefore accuracy of the backcalculation, is mostly dependent on the chosen width of the slipsurface.

5.3.3. Residual strength of the sand core

As described previously, the critical state strength of quartz sand is typically around 32 degrees (Bolton, 1986) [11]. Large strain tests by Deltares [14] show results of 31 degrees after 25 % strain. In the determination of the residual strength properties of the clay the friction angle of sand will be set at 30° . It was noted that changing this value in the range of $27 - 32^\circ$ did not have a significant influence on the strength of the clay. Since the apparent cohesion was induced by suction pore pressure it was assumed that the cohesion would drop to 0 during the traject from peak to residual. The definition of critical state being that shearing no longer induces volume loss leads to a choice of 0° dilation angle in the residual strength LEM analysis.

5.3.4. Residual strength of clay layers

Three residual strength hypotheses were formulated in Chapter 4. The residual strength of the clay layers can be determined based on these hypotheses. To this end the post failure geometry was redrawn in D-Geo Stability, and presented in Appendix F. In the first hypothesis all pore pressures still present in the layer are considered to be dissipated, and the residual strength will be expressed as a residual friction angle. The discretization of the residual strength Hypothesis 1 is presented in Figure F4. In the second hypothesis the pore pressures are maintained as in the peak model, and the strength reduction will be presented as a loss in OCR and S-ratio. In the third analysis the influence of the S-ratio reduction will be investigated by discarding it from the strength reduction. The discretization of the residual strength Hypothesis 2 and 3 is presented in Appendix F Figure F5.

The residual strength of the clay layers 3 and 3a can now be determined based on the post-failure geometry. The failed geometry was drawn in D-Geo Stability, and the mobilized strength on the slip could be assessed with a Spencer analysis. An approximation needs to be made regarding the magnitude of strength loss. It was decided to maintain the relation between the strength of layers 3 and 3a presented in Equation 5.14.

$$\frac{S_{p,3}}{S_{p,3a}} = \frac{S_{r,3}}{S_{r,3a}} = \frac{\tan(\varphi_{r,3})}{\tan(\varphi_{r,3a})} = \frac{0.47}{0.37} \quad (5.14)$$

Residual strength: Hypothesis 1

In the first hypothesis the residual strength is expressed as a residual friction angle. It was chosen to set the dilation angle of the sand core to 0, as the soil is assumed to be at residual state, which is far beyond critical state, hence no further volume change will occur upon further shearing.

Assuming that the percentual strength reduction is equal in layer 3 and 3a, ie $\varphi_{r,L3a} = x \cdot \varphi_{r,L3}$ as presented in Equation 5.14 it is possible to calculate the drained friction angle of Layer 3a based on the friction angle of Layer 3. A residual friction angle of 11 ° was found for layer 3, with a residual friction angle of layer 3a of 8.7 °.

A central question of this thesis regards the magnitude of the strain softening of each layer. Preferably, the expression of the residual strength is provided as a percentual drop of strength. In this case however the peak and residual expressions are given as function of different units. An equivalent friction angle can however be attached to the peak strength formulation to at least provide a numerical comparison. $\varphi_{p,eq} = \tan^{-1}(S_p) = 24$ °. Considering this, a friction angle drop of 50 % compared to the equivalent peak friction angle can be described.

$$\varphi_r = 0.5 \cdot \varphi_{p,eq} \quad (5.15)$$

Residual strength: Hypothesis 2

In the second hypothesis the residual strength is expressed with a SHANSEP formulation. As described in the methodology paragraph, this hypothesis is based around the idea that the strength loss can be seen as a loss in OCR, therefore as a cohesion reduction. The residual S-ratio required to maintain a stable situation for the residual profile will now be back calculated.

The parameters for the sand core are maintained identical as for the residual Hypothesis 1 case. The strength ratio's $S_{r,3} = 0.31$ and $S_{r,3a} = 0.24$ were found from the D-Geo Stability model. As opposed to the drained residual friction angle, the SHANSEP formulation is based on the geometry before failure. In D-Geo Stability it is impossible to define the strength as function of original stress distribution σ_{v0} . In D-Geo Stability the strength is expressed as function of the post failure geometry (Equation 5.16). In order to properly define the reduction in strength ratio it is necessary to correct for the stress difference in the slipplane between the peak and residual profile, according to Equation 5.17.

$$Su_r = \sigma_{v,i} \cdot S_{r,DStab} \quad (5.16)$$

$$Su_r = \sigma'_{v,0} \cdot S_r = \sigma_{v,i} \cdot S_{r,DStab} \quad (5.17)$$

The vertical effective stress through the geometry is presented in Figure 5.8. A jump in effective stress for the deformed geometry can be found around -26 m. This is due to the discretization in blocks of layer 3. Since the peak is very narrow it was assessed that its influence on the total strength was restricted, and therefore neglected. The average stress distribution over the slipplane length could then be computed. The average stress prior to failure in the clay layer was found to be 16.8 kPa. After failure a average vertical stress of 17.5 kPa was found. A correction factor of 1.04 therefore need to be applied on the S-ratio to find the actual strength reduction. The corrected residual S ratios are therefore $S_{r,3} = 0.32$ and $S_{r,3a} = 0.25$, which is equivalent to a S-ratio reduction of 29 %.

As a summary of the strength reduction following Hypothesis 2:

$$Su_r = \sigma'_{v,0} \cdot S_p \cdot 0.71 \quad (5.18)$$

Residual strength: Hypothesis 3

Conclusion from the backcalculation of Hypothesis 2 shows that based on a LEM analysis a sole reduction of the m parameter to 0 results in an overestimation of the mobilized strength. IT is however interesting to still compare this case to the two others, therefore the corrected S ratio will be computed. As described above, the SHANSEP formulation is based on the original geometry. An equivalent S-ratio needs to be found and used as input to estimate the difference in FOS.

$$S_{p,corr} * \sigma_{vi} = S_p * \sigma_{v0}$$

A corrected $S_{p3,corr} = 0.43$ was found for clay layer 3 and $S_{p3a,corr} = 0.34$ was found for clay layer 3a. Using these values in the same model as Hypothesis 2 results in a FOS = 1.03. Obviously, this results in a difference of 30 % (note the same percentage difference as the required reduction of strength ratio in Hypothesis 2).

As a summary of the strength reduction following Hypothesis 3:

$$Su_r = \sigma'_{v0} \cdot S_p \quad (5.19)$$

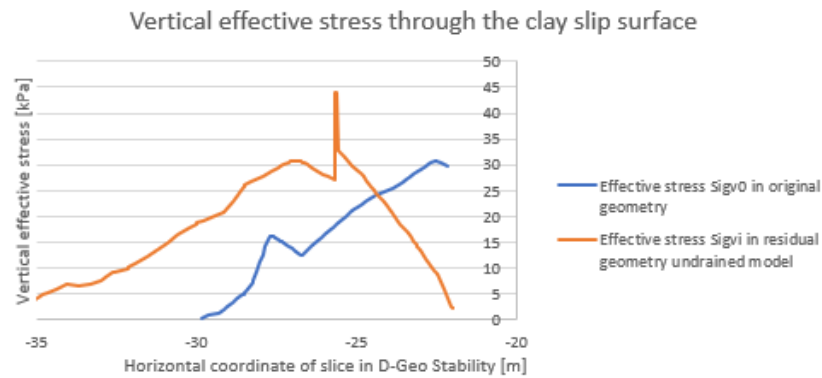


Figure 5.8: Vertical effective stress in the slipplane through clay before and after failure

5.4. Blue dyke recommendations

This thesis originally tried to predict the post failure strength of a dyke with sheet pile wall. These were to be compared with the design recommendations of the new Dutch code WBI 2017. The LEM back-analysis of the Blue dyke proved to be difficult, and results were deemed inconclusive. The LEM analysis is presented in Appendix H. Some conclusions and recommendations could however be formulated on the influence of the sheet pile wall on the failure mode of the soil on the passive side.

In Chapter 3 the strain localisation showed that the failing behaviour of a dyke with SPW showed a similarities with the strain formation in a DSS test. This seems to indicate that the post failure behaviour of a soft soil subsurface can best be described with a LDSS test. The strain localisation's also raise the question whether the failure mode of the passive slope should be seen as a rotational slip surface. It seems indeed that the soil was pushed by the SPW, instead of failing by overturning moment. This might explain the difficulties encountered with the back analysis with a Bishop or Spencer discretization of the slipsurface.

The Dutch design code WBI advises the modeling of a failed dyke with SPW by assigning the peak strength properties of soil to a deformed passive side slope with 1:3 of the original passive slide slope height. This seems close to what was measured in this experiment, as seen in Figure 3.10. The results of this analysis showed that a further loss of strength should probably be assigned to the deformed soil layers.

The Blue dyke back analysis also showed that the slipsurface possibly passed through the interface of sand and peat. Little information in literature is available on this interface strength. It is also difficult to asses this based on laboratory experiments. The residual strength of peats was shown to be dependent on crack formations. Constitutive soil models of the behaviour of peat after large strains used in further analysis should therefore include some form of tension cut-off.

It is therefore recommended to further investigate the peak strength of the blue dyke with a FEM analysis. Considering the pushing behaviour of the sheet pile wall on the passive side soil, it might be interesting to further consider a moving mesh MPM analysis. In this analysis the SPW can be modeled as mesh boundary. This might render the use of a Strain Softening model superfluous.

6

Material Point Method

6.1. Material Point Method concept

This section offers an introduction to the general formulation of an MPM algorithm. It is not the goal of this thesis to implement code refinement. The different aspects will therefore only be briefly mentioned. Every equation was taken from the scientific manual of Anura3d [21].

6.1.1. General framework

MPM is a numerical method created to solve problems involving large deformations. It can be seen as an update on the widely used FEM, and inherits a number of features from this method. FEM relies on Lagrangian elements. Stresses are computed at an integration point, and mapped on a mesh resulting in a mesh deformation. In an Updated FEM, the mesh therefore gets distorted until an equilibrium state has been found. This mesh distortion can cause entanglement of the elements, which can greatly influence the solution for large deformation problems (Sulsky et al, 1994) [53]. A visual example of such a FEM mesh distortion can be seen in Figure 6.1. A meshless method was therefore developed at the Los Alamos National Laboratory, and further developed at the New Mexico University. This method was shown to be successful in the analysis of slope failures with a wide range of failure mechanisms by (Wang et al, 2016) [57]. MPM has also been shown to successfully back analyse a slope failure, as shown by [39]. This makes MPM highly suitable for the back analysis of the Eemdijk experiment.

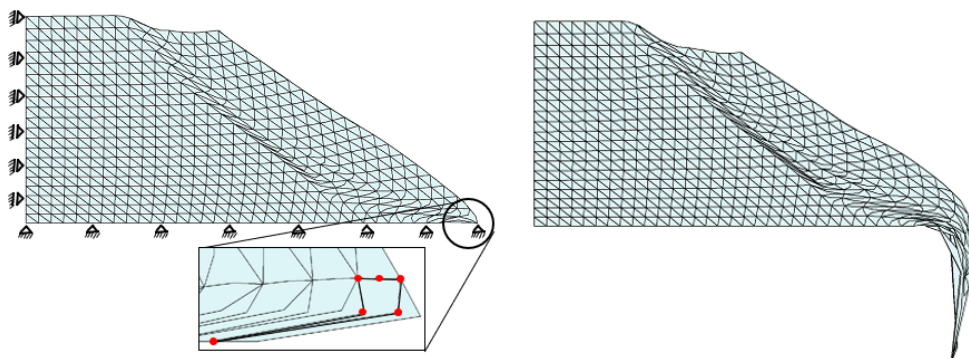


Figure 6.1: Representation of mesh distortion with FEM updated mesh (From Anura3D training course, Tjongi University)

The formulation of MPM is based on an update of the LEM formulation. The main difference is that with MPM the material points are allowed to move freely throughout the mesh, whereas in FEM the integration points are fixed in the element. MPM therefore falls under an Arbitrary Lagrangian-Eulerian formulation within a finite element framework (Beuth et al, 2010) [8].

MPM can be seen in the context of two frameworks: the material points and the computational mesh. The material points carry all the information about the medium. The material points carry information like ma-

terial properties and constitutive models. The material points also initialise and store the different variables computed during an analysis (stresses, strains, velocities...).

The second framework is the computational mesh. This mesh is created in a similar fashion as in FEM. The major difference is that the material points can flow throughout the mesh, therefore leaving some elements empty (referred to as inactive), while other elements will contain more points than after initialisation. This is referred to as an Eulerian mesh.

The mesh equations are solved by mapping the information from the material points onto the mesh through shape functions, like in a FEM analysis. Once the equations are solved the updated information is mapped back onto the material points. The position and solved variables are updated on the material points. This can be iterated for each step in the analysis. A more in depth explanation of this process is provided in the Anura3D scientific manual [21]. The software that will be used to model this experiment was provided by Deltares and to be used only for this thesis: Simon 2D DP.

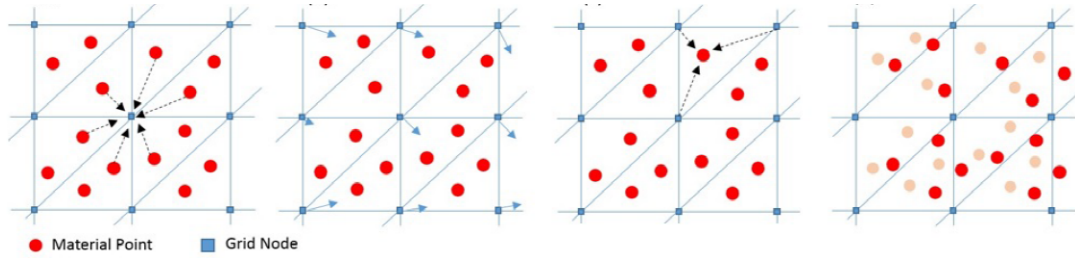


Figure 6.2: Representation of the MPM calculation procedure. Information is first mapped on nodes, equation are solved, variables mapped back on the MP, and displacements are updated in a final step (Anura scientific manual,[21])

MPM offers the advantage of modelling large displacements. However it also presents a number of drawbacks. Numerical errors can become large due to particle crossing boundaries. This can be reduced by the use of damping, where the damping coefficient is equal to the out of balance forces. Numerical errors also grow due to the mapping of information from and to the nodes. As the MP's flow freely through the mesh, their position is not fixed to reduce numerical error like in FEM. This can build up errors. Finally calculation time can become extremely large. Especially coupled analysis with a low permeability results in unmanageable large computation times. Strain softening functions also tend to blow up the computation time.

6.1.2. Governing equations

The general form of the governing equations will be presented below.

Mass conservation

The first governing equation is the conservation of mass. This relation implies that the time derivative of mass in the continuum is always equal to 0. In local form it can be written as Equation 6.1.

$$\frac{d}{dt}\rho + \rho \nabla \cdot v_s = 0 \quad (6.1)$$

Momentum balance

The second governing equation is the momentum balance. The first term (acceleration) is present since the analysis considered is dynamic. σ_s is the Cauchy stress tensor, and b the body force vector.

$$\rho \frac{dv_s}{dt} = \nabla \cdot \sigma_s + \rho \cdot b \quad (6.2)$$

Boundary conditions

Two types of boundary condition can be applied to this formulation: either a prescribed traction (Equation 6.3), or a prescribed velocity (Equation 6.4).

$$\sigma_s(x, t) \cdot n = \hat{t}_s(t) \quad (6.3)$$

$$u_s(x, t) = \hat{u}_s(t) \quad (6.4)$$

6.1.3. Single timestep algorithm

The single timestep algorithm from the Anura 3D manual [21] is presented below.

- Calculate nodal mass with shape function and lumped mass matrix. Evaluate internal and external forces at nodes
- Nodal acceleration are determined by solving the momentum balance (Equation 6.2)
- Update material point velocity
- Update nodal momentum
- Update nodal velocities
- Compute incremental nodal displacement for solid and liquid constituent
- Compute strain increment
- Update stresses based on previously calculated strains and constitutive soil model
- Update volume and density of MP
- Update particle position
- Initialize computational grid, discard nodal values, material points carry all information

6.1.4. 1 vs 2 phase formulation

MPM offers the choice of discretizing the material with a 1 or 2 phase formulation. In a 1 phase formulation the MP carries the information about the liquid and solid. In a 2 phase formulation a coupled analysis is executed to relate the liquid properties to the solid properties. The main variables to be solved in such a calculation are the liquid and solid acceleration.

A note needs to be added regarding the different applications of these formulations. A porous medium is often an interaction between 3 phases (solid, liquid, gas). Modelling these interaction is extremely computational extensive. When possible it is therefore preferred to simplify situations to 1 phase.

Fully saturated drained and undrained conditions can for example be considered as a 1 phase analysis. In a drained analysis the excess pore pressures will always be set to 0. This means that no pressures will influence the stresses in the solid material, which can therefore be simplified to a 1 phase analysis. In the case of an undrained simulation the generation of pore pressures is fixed by the 0 relative movement between solid and liquid phase. The change in pressure is determined by equation 6.5. This means that an undrained analysis will also be simplified to a 1 phase analysis, thereby reducing considerably the computational time. A look into 6.5 shows that a drained analysis can be simulated by choosing a Bulk Modulus of water of 0, while an undrained analysis can be generated with any other value for the Bulk Modulus in a 1 phase analysis. A 2 phase analysis should therefore only be used if the water and solid pressures should be initiated separately, or for a case where pore pressure generation/ dissipation is time dependent (typically a consolidation calculation or a partially drained situation).

$$\Delta p = K_L * \Delta \epsilon_{vol} \quad (6.5)$$

6.1.5. Critical time step

Courant number

Explicit time schemes rely on the Courant-Friedrichs-Levy condition for stability. As it relates a critical time step to a wave propagation speed. For dynamic soil problems a value of 0.9 is advised.

$$C = \frac{u\delta t}{\delta x} \quad (6.6)$$

1-Phase solid critical time step

The critical time step is dependent on the formulation of the problem. For a 1 phase solid problem the critical timestep is dependent on minimal length of an element, the density of the solid and the constrained modulus of the solid, and is presented in Equation 6.7.

$$\Delta t_{cr} = \frac{L_{min}}{c}; c = \sqrt{\frac{E_c}{\rho}} \quad (6.7)$$

2-Phase coupled critical time step

The most critical time step is for a 2-phase coupled analysis. This stability criterion is onerous, therefore simplifications were made. The critical time step is either dependent on the size of the mesh, stiffness, porosity and density of material ($\Delta t_{crit;1}$) or on the permeability, the porosity and the density of the material. The equations are presented in Equation 6.8 to 6.14

$$\Delta t_{cr} = \min[\Delta t_{crit;1}; \Delta t_{crit;2}] \quad (6.8)$$

$$\Delta t_{crit;1} = m \cdot \frac{L_{min}}{c_1} \quad (6.9)$$

$$\Delta t_{crit;2} = m \cdot \frac{2\bar{\rho}k}{\rho Lg} \quad (6.10)$$

$$c_1 = \sqrt{\frac{E_c^u}{\rho}} \quad (6.11)$$

$$E_c^u = E_c + K_L/n \quad (6.12)$$

$$\rho = (1 - n)\rho_s + n \cdot \rho_L \quad (6.13)$$

$$\bar{\rho} = \rho + \left(\frac{1}{n} - 2\right)\rho_L \quad (6.14)$$

6.1.6. Advanced functions

Damping

In a dynamic problem internal forces will lead to energy loss. These forces are however difficult to quantify. In an MPM analysis oscillations are a known problem, which can lead to instabilities in some cases. The use of damping is therefore necessary. Different options are available to introduce damping in MPM.

An efficient way to introduce damping in a dynamic system is through the use of local damping. The damping should be proportional to the out of balance forces of the system, as shown in Equation 6.15. For

quasi-static problems a high value of 0.7-0.8 can be used. For dynamic soil problems a lower value of 0.05 is advised.

$$ma = f + f^{damp} \quad (6.15)$$

De Campos(2016) [19] carried out research on the dynamic behaviour of a debris flow analysis. They concluded soils can be considered as a viscoplastic fluid. Until a failure stress is reached, a soil mass can be considered as having a pseudo-Newtonian behaviour. Post failure, the mass can be considered as a Bingham fluid, with plastic viscosity.

Quasi-static convergence

Quasi static situations can be detected by solving the out of balance forces with the kinematic forces. A quasi static algorithm is implemented and will be used numerous times during the stress initialisation to reach an equilibrium situation faster.

6.2. MPM Benchmarks

Before modeling the Eemdijk experiment in MPM, benchmarks need to be reached. Points of attention for every benchmark are the results of the stress initialisation (pore pressures, vertical and horizontal effective stress) and the strength required to trigger failure. Special attention will be provided to the dilation angle. The goal is to assess what combination of friction angle and dilation angle should be used to match the failure point in D-Geo Stability.

With a LEM the strength required to trigger failure is obvious: when the factor of safety is smaller than 1 the slope is unstable. In MPM this point is harder to define. It could be possible to compare the mobilized strength on the slip surface, but this would be time consuming.

The failure point in MPM for these benchmarks will therefore be defined as the strength for which a full slip surface shows movement. This can be easily visually checked by looking at the displacements or the deviatoric strain. This point will be set as equivalent to a FOS of 1. The difference between the FOS obtained in D-Geo Stability with identical parameters will then be calculated. Conclusions will then be drawn on the closest match in parameters between the failure point in D-Geo Stability and MPM.

6.2.1. Discretization

Geometry

The Benchmark problems will all be tested with the same geometry. A simple 6m wide 4.5m high slope will be tested under different conditions. Liquid fixities are applied in horizontal direction on the surfaces, as during stress initialisation the water pressures are not in equilibrium. Indeed, more water is present on the crest side of the slope in case of a fully saturated slope. Solid and liquid fixities are applied at the borders of the mesh to prevent the material from flowing out. Two surfaces were created, to allow different materials to be defined in the top and bottom of the geometry. A schematisation of the boundary conditions of the benchmark geometry is provided in Figure 6.3. An unstructured triangular quadratic mesh was used, with 3 solid and 3 liquid material points per element. A schematisation of the mesh discretization and particle specification is provided in Figure 6.4.

In the first benchmark a dry slope will be investigated. In the second benchmark a saturated drained slope will be considered. In the third benchmark a saturated undrained slope will be considered. In the fourth benchmark a slope with 2 materials will be considered. The top material will be switched from dry to saturated to model the stress evolution during unloading by increasing the water table inside of a dyke. In the final benchmark the influence of the mesh discretization and strain softening function on the slip surface behaviour will be investigated. Material properties of each benchmark will be presented in Appendix I.

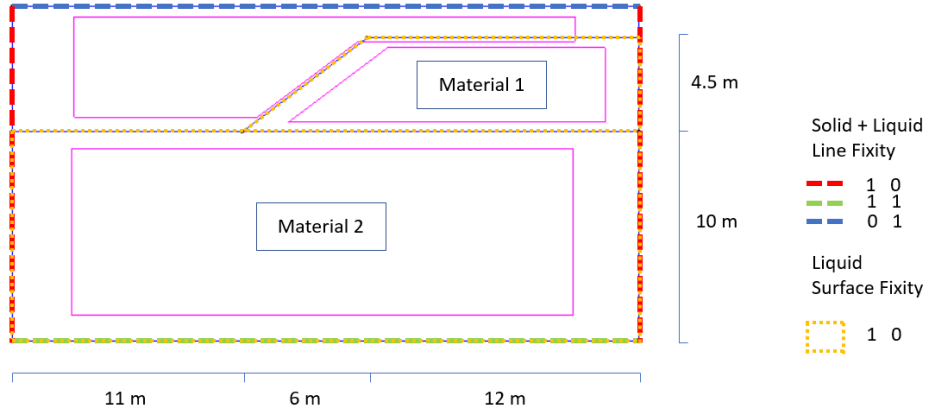


Figure 6.3: Discretization of the MPM benchmark boundary conditions

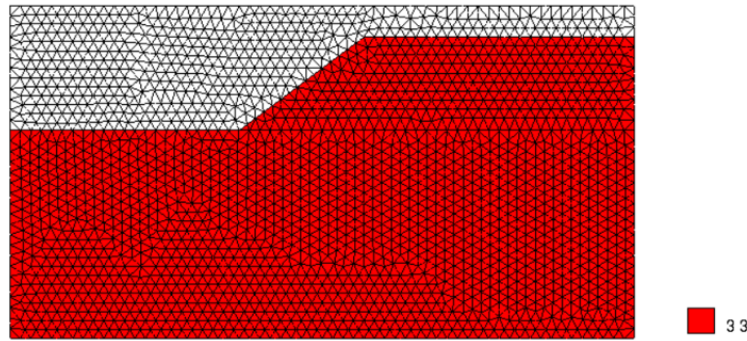


Figure 6.4: Discretization of the MPM benchmark mesh and particle specification

Soil Model: Mohr Coulomb

The soil model used to model the different benchmarks will be the Mohr-Coulomb model. This model is an elastic perfectly plastic model with two strength terms: a cohesion c and a friction angle φ' . The yield function is expressed in principle stress space with Equations 6.16, 6.17 and 6.18.

$$F_1 = \frac{|\sigma'_2 - \sigma'_3|}{2} + \frac{|\sigma'_2 + \sigma'_3|}{2} \sin(\varphi)' - c' \cos \varphi' \quad (6.16)$$

$$F_2 = \frac{|\sigma'_1 - \sigma'_3|}{2} + \frac{|\sigma'_1 + \sigma'_3|}{2} \sin(\varphi)' - c' \cos \varphi' \quad (6.17)$$

$$F_3 = \frac{|\sigma'_1 - \sigma'_2|}{2} + \frac{|\sigma'_1 + \sigma'_2|}{2} \sin(\varphi)' - c' \cos \varphi' \quad (6.18)$$

The plastic potential failure is defined with the dilatancy angle Ψ , which dictates the post failure perfectly plastic behaviour. These Plastic potential functions can be found in Equations 6.19, 6.20 and 6.21.

$$P_1 = \frac{|\sigma'_2 - \sigma'_3|}{2} + \frac{|\sigma'_2 + \sigma'_3|}{2} \sin(\psi)' \quad (6.19)$$

$$P_2 = \frac{|\sigma'_1 - \sigma'_3|}{2} + \frac{|\sigma'_1 + \sigma'_3|}{2} \sin(\psi)' \quad (6.20)$$

$$P_3 = \frac{|\sigma'_1 - \sigma'_2|}{2} + \frac{|\sigma'_1 + \sigma'_2|}{2} \sin(\psi)' \quad (6.21)$$

It can be added that the slip surface is defined based on non-associative behaviour, which means that the failure surface is independent of the dilation angle. The goal of these benchmarks is to conclude if the failure strength in MPM best match the strength defined in D-Geo Stability as associative or non-associative non-dilatative. It is therefore required to define the strength conversion used. As defined in Chapter 5 the strength parameters can be converted from associative to non associative.

The strength of undrained layers is expressed in D-Geo Stability following the Dutch norm with a SHANSEP formulation. This formulation is not available in the MPM software, therefore the strength parameters need to be converted from SHANSEP to equivalent Mohr-Coulomb parameters. Starting from the SHANSEP formulation presented in Equation 5.7. The equation of the asymptote can be found by expanding the limit of the SHANSEP equation towards infinity, as presented in Equation 6.22.

$$\lim_{x \rightarrow \infty} kx \left(\frac{x+l}{x} \right)^m = k\infty \quad (6.22)$$

Where :

- $x = \sigma'_v$
- $l = \text{PoP}$
- $m = m$ parameter from Shansep
- $k = S$ parameter from Shansep

Expanding Equation 6.22 with a Laurent series provides Equation 6.23.

$$kx + klm + \frac{kl^2(m-1)m}{2x} + \frac{kl^3(m-2)(m-1)m}{6x^2} + \frac{kl^4(m-3)(m-2)(m-1)m}{24x^3} + O\left(\frac{1}{x^4}\right) \quad (6.23)$$

In this expansion the form $Ax+b$ can be recognized, which is the form of the classic Mohr-Coulomb expression. Disregarding the terms with a higher exponential term than 1 will therefore provide a good approximation of the Mohr-Coulomb parameters, with error $O(x^2)$. The Mohr-Coulomb equation can be written down under two forms, either under associative form with $\psi = \varphi$ as given in Equation 5.5 or non associative with $\psi = 0$ in Equation 5.6. Combining these with Equations 6.23 gives us the equivalent Mohr-Coulomb parameters for both associative (Equations 6.24 and 6.25) and non-associative with $\psi = 0$ (Equations 6.26 and 6.27).

$$\varphi_{eq;a} = \arctan(S) \quad (6.24)$$

$$c_{eq;a} = S.m.PoP \quad (6.25)$$

$$\varphi_{eq;na} = \arcsin(S) \quad (6.26)$$

$$c_{eq;na} = \frac{S.m.PoP}{\cos(\varphi_{eq;na})} \quad (6.27)$$

Soil Model: Mohr-Coulomb Strain Softening

A variation to the Mohr-Coulomb model is the Mohr-Coulomb Strain Softening (MC-SS) model. Its expression is extremely close to the classic Mohr-Coulomb expression, with as only difference that a strength reduction term has been incorporated through an exponential shape factor. The reduction in strength is dependent on the accumulation of plastic strains. The expressions of the strain softening model are presented in Equations 6.28, 6.29 and 6.30. A User Defined Soil Model formulated identically as the MC-SS function in Anura 3D was used.

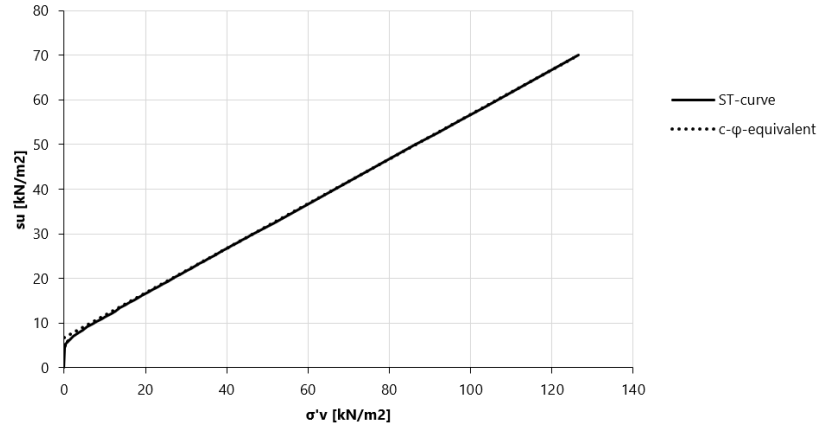


Figure 6.5: Graphic of the equivalent Mohr Coulomb line estimated from a S-T curve with SHANSEP parameters (peak parameters of peat, $S = 0.5$, $m = 0.9$, $POP = 15$ kPa)

$$c' = c'_r + (c'_p - c'_r) \exp(-\eta E_d^p) \quad (6.28)$$

$$\phi' = \phi'_r + (\phi'_p - \phi'_r) \exp(-\eta E_d^p) \quad (6.29)$$

$$\psi' = \psi'_r + (\psi'_p - \psi'_r) \exp(-\eta E_d^p) \quad (6.30)$$

In a Mohr-Coulomb elasto-plastic perfectly plastic model the elastic part of the loading will therefore result in a linear strength increase. Once failure is triggered the strength will drop exponentially, as a function of the shape factor. To illustrate the power of the exponential factor on the strength reduction the friction angle reduction has been drawn for a shape functions varying from $\eta = 0$ to $\eta = 500$ in Figure 6.6. It can be noted that for values of η above 10 the drop in strength occurs at small strains. It is therefore necessary to tune this parameter based on the magnitude of strains obtained from the MPM model. This will be done in Benchmark 5.

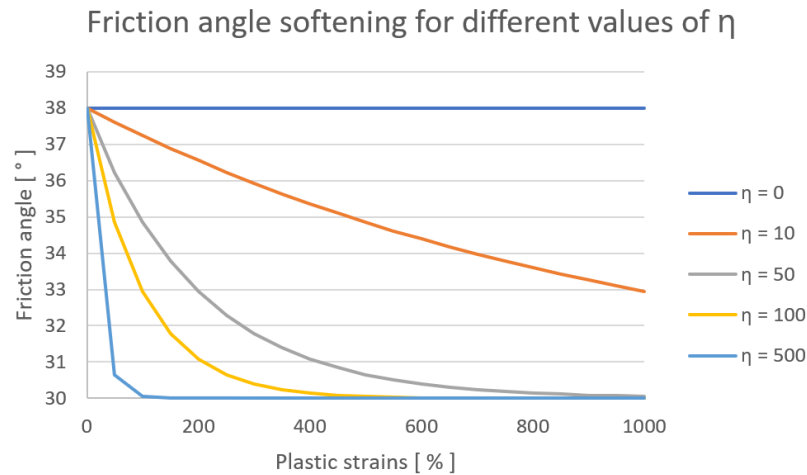


Figure 6.6: Representation of the drop in friction angle from 38 °to 30 °for values of η varying from 0 to 5.

6.2.2. Benchmark 1: Dry soil

In this benchmark a dry soil will be brought to failure. The limit strength to require failure will be used as input for D-Geo Stability, after which conclusions will be drawn regarding the difference in FOS between the D-Geo Stability and MPM model.

Stress Initialisation

The slope consists of a dry material, with unit weight 19.5 kN/m³. A very high strength was attributed to the material to prevent premature failure during gravity loading. A CPS damping of 0.75 is applied during the stress initialisation. A dry material is modelled, therefore a 1 phase formulation was used. The stress initialisation is applied over 31 steps. First, the gravity vector is increased over 30 steps, after which a Quasi-Static equilibrium phase was applied. The stresses at the end of the initialisation are shown in Figure 6.7. The target stresses at the bottom of the geometry can be calculated analytically, and compared to the MPM results. At the level of the crest the geometry is 14.5 m deep, while at the toe 10 m. The stress at the bottom of the geometry should therefore be 282.75 kPa under the crest, and 195 kPa under the toe.

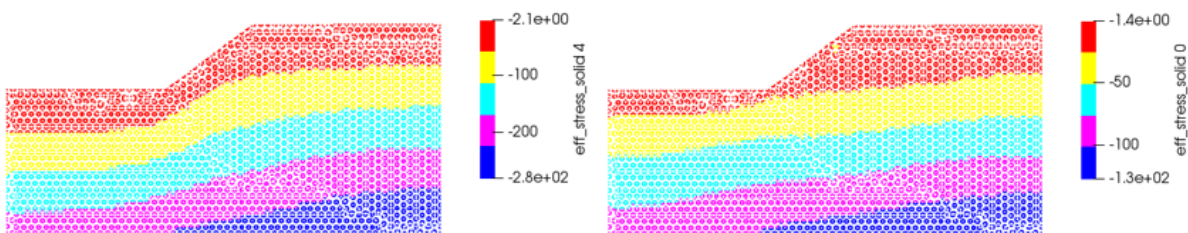


Figure 6.7: Stress initialisation results

Failure Phase

To trigger failure the strength of the material was lowered. This is equivalent to a c - ϕ' reduction.

Results

The strength at failure was determined. In this paragraph a representation of the set definition of failure will be shown. It can be seen in Figure 6.8. The failure point has been found with a friction angle of 20 ° and a cohesion of 3.6 kPa.

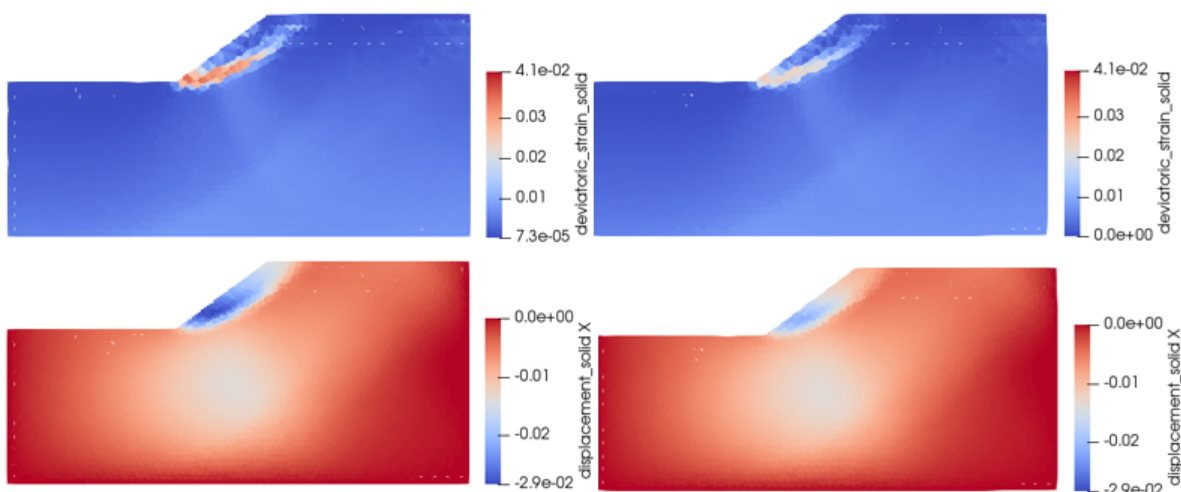


Figure 6.8: Results of Benchmark 0. On the left the deviatoric strains and x-displacements at limit strength to reach failure ($\phi = 20^\circ$, $c = 3.6$ kPa). On the right the deviatoric strains and x-displacements just above the limit strength to reach failure ($\phi = 20^\circ$, $c = 3.7$ kPa)

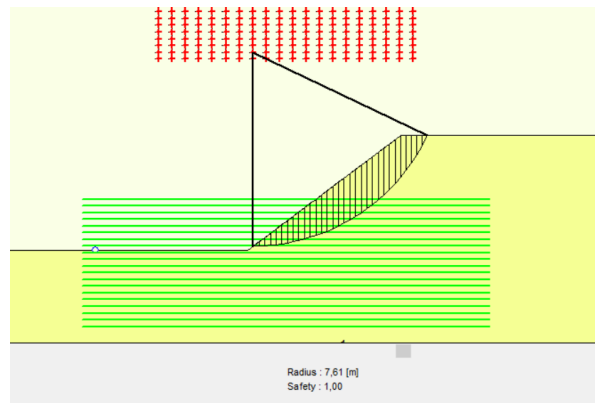


Figure 6.9: Most critical slip circle D-Geo Stability Benchmark 0

These results can be compared to the FOS one would obtain if this was used as input in D-Geo Stability. The critical slip surface found with a Bishop analysis is shown in Figure 6.9. It can first be noted that the shape of this slip circle is extremely similar to that of the slip surface found with MPM. The FOS results in D-Geo Stability for both associative and non-associative plasticity can be found below. For this case of a dry soil the associative plasticity matched the MPM results the closest.

- $c = 3.6, \varphi' = 20^\circ, \psi = 0^\circ \rightarrow \text{FOS} = 0.94,$
- $c = 3.6, \varphi' = 20^\circ, \psi = 20^\circ \rightarrow \text{FOS} = 1.00$

The difference with the D-Geo Stability FOS is therefore 6 % for the non associative non dilative parameters and 0 % for the associative parameters.

6.2.3. Benchmark 2: Saturated soil, drained

In this benchmark a saturated slope of drained material will be brought to failure. The limit strength to require failure will be used as input for D-Geo Stability, after which conclusions will be drawn regarding the difference in FOS between the D-Geo Stability and MPM model.

Stress Initialisation

This analysis now deals with a saturated slope, with total density = 19.5 kN/m³. It is important to realise that since the slope is not submerged water pressures need to be initialized. This can be done with a 2 phase analysis. The information of the liquid and solid material are now carried by different material points. A high permeability was chosen to permit pore pressures to be generated without undrained effects, and a Bulk modulus of water of 21500 kPa was chosen with a liquid density of 10 kN/m³ to generate the pore pressures under a gravity loading. These pore pressures will not be in equilibrium, therefore water movement needs to be restricted. This was done by fixing the horizontal movement of water in x-direction. 30 steps of gravity were applied, after which one step of 2 phase quasi static convergence was applied. Computation time in a coupled analysis tend to blow up, therefore the analysis was switched to a 1 phase calculation. Again, a quasi static convergence step was added to make sure the switch from 2 phase to 1 phase reached equilibrium. The stresses after stress initialisation are shown in Figure 6.10. The slope now is saturated, the vertical effective stress at the bottom of the geometry under the crest should be 137.75 kPa and 95 kPa under the toe, while the liquid pressures should be 145 and 100 kPa respectively.

Special attention can also be given to the horizontal effective stresses. Due to the fact the the pore pressures are not in equilibrium (more water right than left), a horizontal loading is created. This results in higher horizontal stresses under the toe than under the crest.

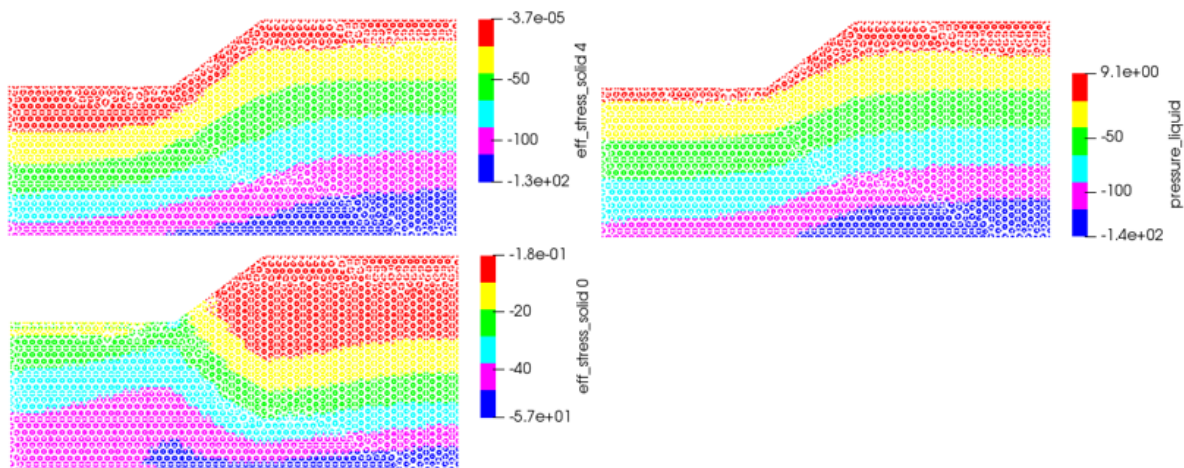


Figure 6.10: Stress initialisation results Benchmark 1. Top left: Vertical effective stress, Bottom left: horizontal effective stress, Top right: liquid pressure

Failure Phase

The failure was again triggered through a φ -c reduction. The requirement to define a soil as drained is that no pore pressures are allowed to be generated upon shearing. By changing the Bulk modulus of water to 0 this condition could be satisfied.

Results

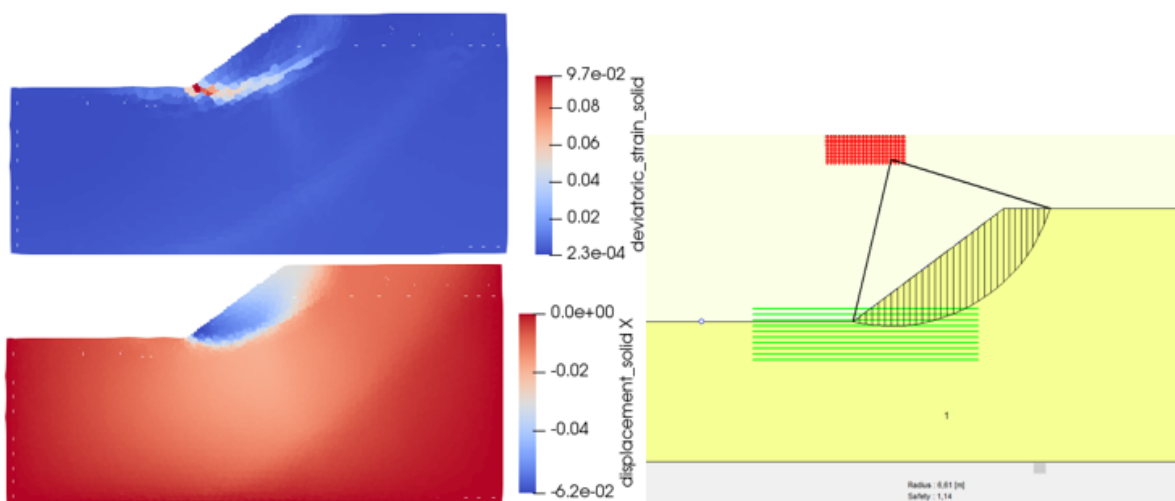


Figure 6.11: Results of Benchmark 1. On the left the deviatoric strains and x-displacements at limit strength to reach failure ($\varphi = 20^\circ$, $c = 9.5$ kPa). On the right the most critical slip surface found in D-Geo Stability (FOS corresponds to associative plasticity)

It can be noted that for a saturated slope the results are less close to the results from D-Geo Stability than in Benchmark 1. This might be due to the influence of the water pressure, resulting in a different distribution of horizontal pressures. In D-Geo Stability horizontal pressures are not computed, which creates a mismatch between the two models. For the case of a saturated drained soil the $\psi = 0$ condition resulted in the closest match with D-Geo Stability.

- $c = 9.5$, $\varphi' = 20^\circ$, $\psi = 0^\circ \rightarrow$ FOS = 1.08
- $c = 9.5$, $\varphi' = 20^\circ$, $\psi = 20^\circ \rightarrow$ FOS = 1.15

The difference with the D-Geo Stability FOS is therefore 7 % for the non associative parameters and 13 % for the associative parameters.

6.2.4. Benchmark 3: Saturated soil, undrained

In this benchmark a saturated slope of undrained material will be brought to failure. The limit strength to require failure will be used as input for D-Geo Stability, after which conclusions will be drawn regarding the difference in FOS between the D-Geo Stability and MPM model.

Stress Initialisation

The stress initialisation phase of this benchmark is identical to that of Benchmark 2.

Failure Phase

Failure was triggered again with a φ -c reduction. In order to model the undrained behaviour of the soil the Bulk modulus of water was maintained at 21500 kPa.

As described above, the undrained strength of a layer is expressed with a SHANSEP formulation. In D-Geo stability the layer was now defined as a clay with a constant Pre-Overburden Pressure of 20 kPa.

The methodology for this Benchmark is a bit different than for the previous cases. MPM does not have a SHANSEP formulation, therefore parameters of the SHANSEP formulation can be converted to equivalent associative or non-associative non-dilative c - φ' parameters following Equations 6.24, 6.25, 6.26 and 6.27. The goal of this Benchmark is to assess whether SHANSEP parameter should be converted to associative or non associative parameters. Starting from equivalent cohesion and friction angle parameters required to trigger failure, it is possible to back-calculate equivalent S-ratios and PoP depending on whether the Shansep equation would be converted to associative or non-associative non-dilative equivalent parameters. These parameters can be used as input in D-Geo Stability to conclude on the closest fit between MPM and D-Geo Stability parameters

Results

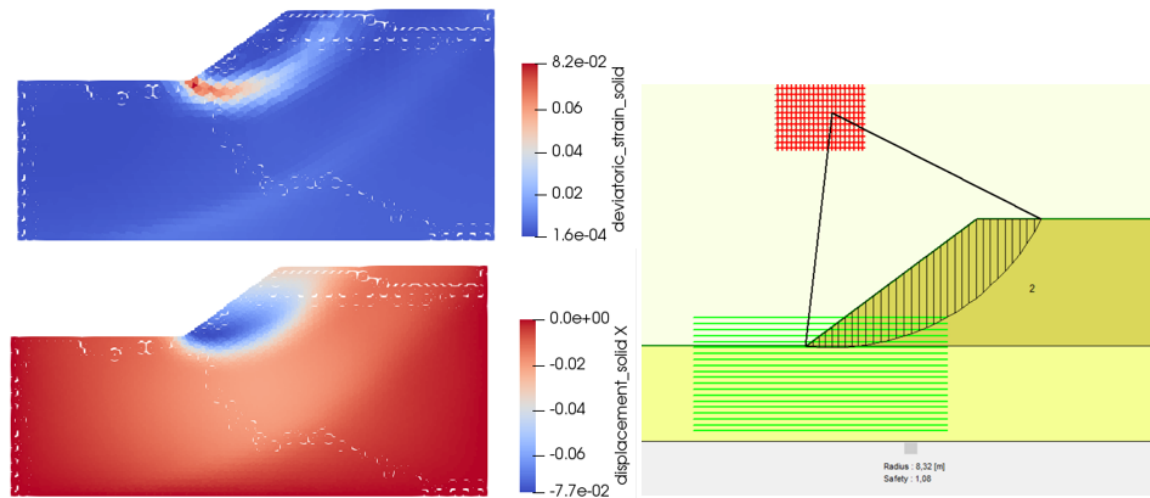


Figure 6.12: Results of Benchmark 3. On the left the deviatoric strains and x-displacements at limit strength to reach failure ($\varphi = 23.6^\circ$, $c = 7.85$ kPa). On the right the most critical slip surface found in D-Geo Stability (FOS corresponds to associative plasticity)

Failure was found to occur in MPM with $\varphi = 23.6^\circ$ and $c = 7.85$ kPa. These can be converted to the equivalent S-ratios, and used as input in D-Geo Stability. First it can be noted that the shape of the slip circle is slightly deeper in the MPM model than in the D-Geo Stability.

- $\varphi = 23.6^\circ$, $c = 7.85$ kPa, $S_{eq;a} = 0.437$, $PoP_{eq;a} = 20.2$ kPa \rightarrow FOS = 1.16
- $\varphi = 23.6^\circ$, $c = 7.85$ kPa, $S_{eq;na} = 0.4$, $PoP_{eq;na} = 20$ kPa \rightarrow FOS = 1.08

The difference with the D-Geo Stability FOS is therefore 8 % for the non associative equivalent parameters and 16 % for the associative equivalent parameters.

6.2.5. Benchmark 4: Material Switch

In this benchmark a 2 layered slope will be considered. Two goals will be checked with this benchmark. First during the stress initialisation two loading phases will be considered. In the first phase the bottom material will be saturated, why the top layer will be modelled dry. In a second loading phase the top layered will be switched to saturated, to simulate a dyke core being filled with water. The poisson ratio will be changed to simulate the loading phase. The second goal is identical as for the previous Benchmarks, to check whether associative or non associative equivalent strength parameters result in a better match.

Stress Initialisation

Stress initialisation was carried out in two phases. The goal was to initialize the stresses of a dry soil over a saturated soil, after which the material could be changed to saturated. The formulation of the code however did not permit to change the material from 1 phase dry to 2 phase saturated. It was therefore decided to model the dry soil as saturated with water with a very low density of 50 kg/m³ and Bulk modulus of 1000 kPa. A density of 0 was not possible due to the stability condition of a 2 phase formulation. The solid density was converted to a total density of 19.5 kN/m³. The bottom material was modeled with as the material from Benchmark 3. 30 Steps of Gravity loading were applied, after which a Quasi-Static convergence step was applied.

The analytical vertical stress after this stage at the bottom of the geometry under the crest can be calculated, and should be 182.75 kPa, and 95 under the toe. The liquid pressure should be 100 kPa. The results can be found in Figure 6.13. The results look good. Only the horizontal stresses show a little mismatch, as we would the isobars to follow the same shape as those of the vertical effective stress. This might be due to the water present in the top material.

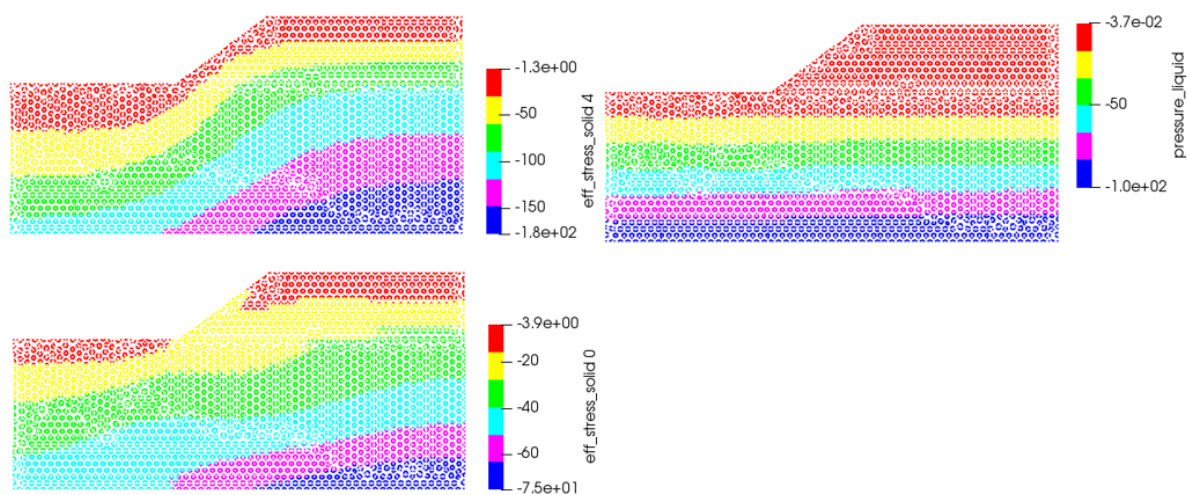


Figure 6.13: First phase stress initialisation results Benchmark 4. Top left: Vertical effective stress, Bottom left: horizontal effective stress, Top right: liquid pressure

Once the system is in equilibrium, the top material can be updated to a saturated material by changing the density of the water, the Bulk modulus of the water and the Solid density. 30 more steps are applied, after which a 2 phase quasi-static convergence step is applied, followed by a 1 phase quasi-static convergence. Special attention can be given to the poisson ratio. In Chapter 3, the active earth coefficient was presented as an underboundary for the horizontal stresses during unloading. To generate the horizontal stresses an equivalent unloading poisson ratio will be chosen, based on an active coefficient of earth pressure. Following Equation 6.31, an equivalent poisson ratio of 0.2 was found, which will also be used in the final Eemdijk experiment model.

$$Ka = \frac{\nu_{eq}}{1 - \nu_{eq}} \quad (6.31)$$

The analytical vertical stress after this stage at the bottom of the geometry under the crest can be calculated, and should be 137.75 kPa, and 95 kPa under the toe. The liquid pressure should be 145 kPa under the

crest and 100 kPa under the toe. The results can be found in Figure 6.13. The results seem to coincide with those of Benchmark 2 and 3. The excess horizontal pressures in the top material with poisson ratio 0.2 are also simulated correctly.

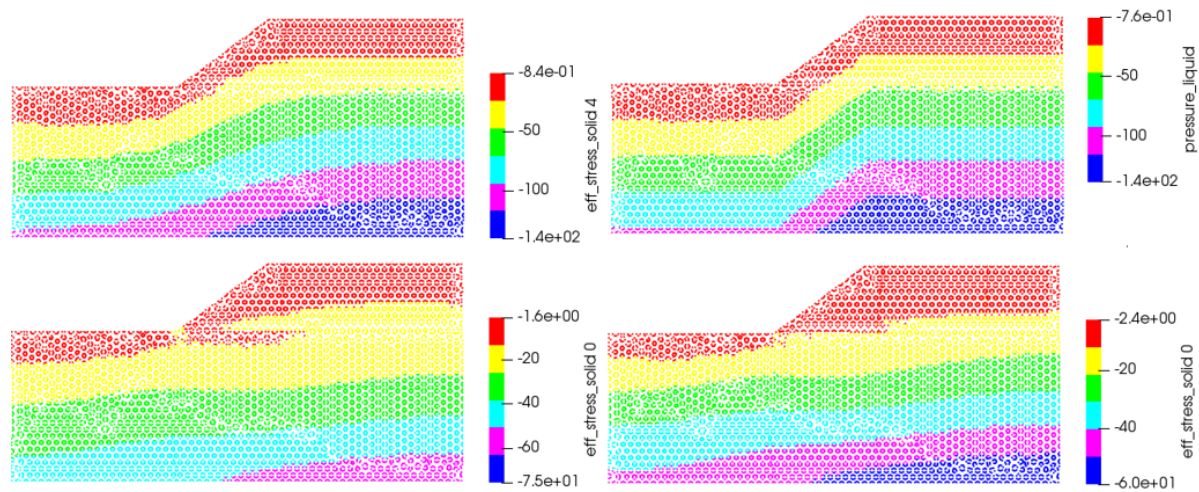


Figure 6.14: First phase stress initialisation results Benchmark 4. Top left: Vertical effective stress, Bottom left: horizontal effective stress with $\nu = 0.2$, Top right: liquid pressure, Bottom right: horizontal effective stress with $\nu = 0.3$

Failure Phase

The failure phase can now be triggered identically as for Benchmark 2 and 3. The Bulk modulus of the top material was changed to 0, and failure was triggered by effectuating a φ -c reduction. First, the strength required to trigger failure in MPM was found. The strength parameters of the undrained layer were then converted to equivalent S ratio's and cohesions. These were then used as input in D-Geo Stability.

Failure was found to occur with strength properties for the top material of $\varphi = 30^\circ$ and $c = 8$ kPa. The bottom material $\varphi = 23.6^\circ$ and $c = 7.85$ kPa were used. Parameters were converted to equivalent associative and non-associative strength parameters, and the FOS was computed in D-Geo Stability

- Material 1: $c = 8.0$, $\varphi' = 30^\circ$, $\psi = 30^\circ$
Material 2: $\varphi = 23.6^\circ$, $c = 7.85$ kPa, $S_{eq;a} = 0.437$, $PoP_{eq;a} = 20.2$ kPa \rightarrow FOS = 1.04
- Material 1: $c = 8.0$, $\varphi' = 30^\circ$, $\psi = 0^\circ$
Material 2: $\varphi = 23.6^\circ$, $c = 7.85$ kPa, $S_{eq;na} = 0.4$, $PoP_{eq;na} = 20$ kPa \rightarrow FOS = 0.92

The same procedure was applied with another strength combination. The strength properties for the top material of $\varphi = 30^\circ$ and $c = 10$ kPa. For the bottom material $\varphi = 20^\circ$ and $c = 8$ kPa were used. Parameters were converted to equivalent associative and non-associative strength parameters, and the FOS was computed in D-Geo Stability

- Material 1: $c = 10$, $\varphi' = 30^\circ$, $\psi = 30^\circ$
Material 2: $\varphi = 20^\circ$, $c = 8$ kPa, $S_{eq;a} = 0.364$, $PoP_{eq;a} = 24.42$ kPa \rightarrow FOS = 1.05
- Material 1: $c = 10$, $\varphi' = 30^\circ$, $\psi = 0^\circ$
Material 2: $\varphi = 20^\circ$, $c = 8$ kPa, $S_{eq;na} = 0.342$, $PoP_{eq;na} = 24.42$ kPa \rightarrow FOS = 0.96

Results

The results matched the D-Geo Stability for the associative conversion within 8 % while for the non-associative within 5 %. The non-associative conversion underestimated the FOS, while the associative seemed to overestimate it. For the rest of the analysis the strength modelled in the Eemdijk experiment will be based on the associative formulation with $\psi = \varphi^\circ$. It can also be added that changing the poisson ratio to model the unloading stress generation did not have a great influence on the failure point.

6.2.6. Benchmark 5: Strain softening

The goal of this Benchmark is to investigate the influence of mesh density and softening parameter η on the the strain softening behaviour. A uniform saturated slope identical as Benchmark 2 will be considered. The MC-SS function does not work with a triangular mesh. A uniform quadrilateral mesh was therefore used. At first the influence of the softening parameter η will be tested. In a second part the influence of the mesh on the result will be studied.

Stress initialisation

The stress initialisation phase of this benchmark is identical to that of Benchmark 2.

Results Eta variation

The influence of the softening parameter η on the result can be investigated. Two slopes are brought to failure with identical peak and residual friction angle and cohesion. The peak strength properties are the failure strength parameters from Benchmark 2. An arbitrary residual cohesion of 5 kPa was chosen. In the first case $\eta = 10$ was used, while for the second case $\eta = 100$. The deviatoric strains and displacements are presented in 6.15. The first thing to be noticed is the backpropagation of the slip surface with $\eta = 100$. Around the slip surface, deviatoric strains are generated. If the strain softening function is expressed too strongly, these small deviatoric strains are large enough to reduce the strength of the material. This results in secondary slip planes being formed retrogressively. It can also be noted that the magnitude of displacements is not greatly influenced by this effect (20 cm for the case tested). The difference in displacements can be explained by the fact that the driving load is larger with a back propagated slip surface.

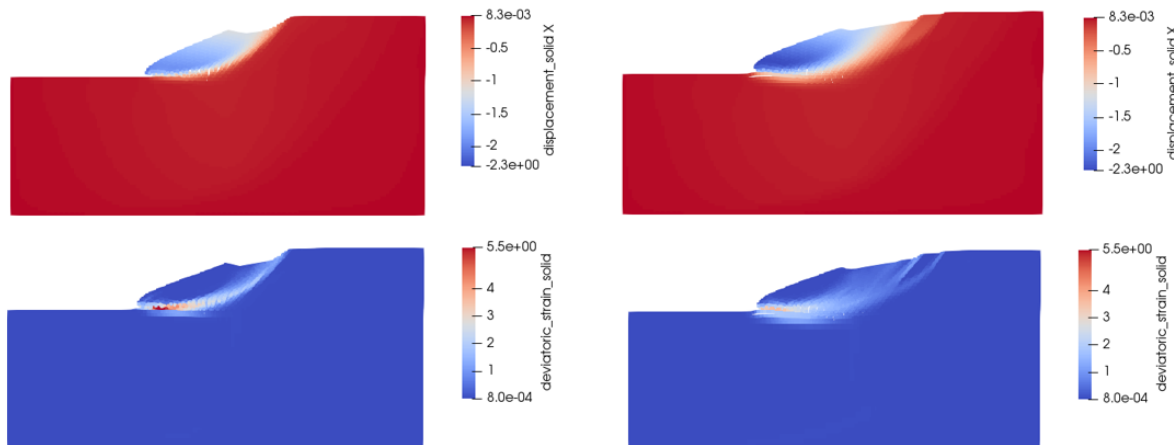


Figure 6.15: Influence of softening parameter η on displacements and deviatoric strain. Left $\eta = 10$, right $\eta = 100$

Results mesh variation

The influence of the mesh on the results of strain softening can now be investigated. The geometry was discretized in a coarse and fine mesh, with respectively 965 and 3221 elements. The η parameter was fixed at 10. The mesh discretization and displacement results are shown in Figure 6.16.

It can be noted from Figure 6.16 that the mesh had little to no influence on the displacements. The shape of the slip surface is also independent of the mesh. This indicates that in the slip surface the same softening magnitude was present in both models. Since the distance between the integration points becomes smaller with a finer mesh, the magnitude of strain becomes larger with identical displacements. This can be seen from the strain magnitude image in Figure 6.16.

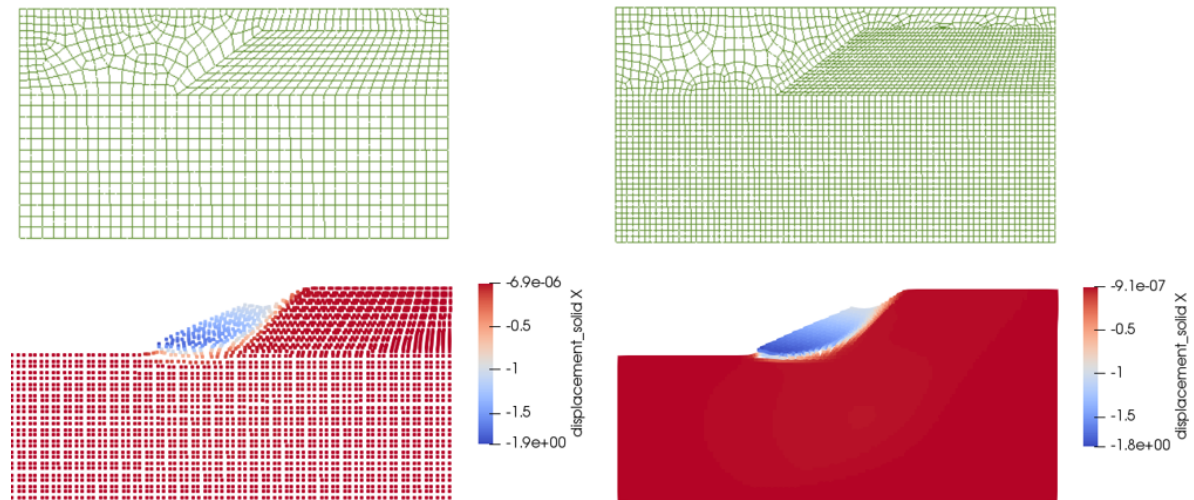


Figure 6.16: Influence of mesh density on displacements and strain softening. Left: 965 elements, right: 3221 elements

Stress oscillations

This benchmark can also be used to illustrate stress oscillations in MPM. (González Acosta et al, 2019) [23] studied stress oscillations and mitigation technique. These oscillations occur due to particles cross boundaries, and because the integrated stresses only coincide with the analytical solution at the superconvergent position. Plastic deformations are especially sensitive to these oscillations, leading in turn to more oscillations. The failure point can also be influenced by these oscillations. Figure 6.17 shows that the code used is also sensitive to these oscillations.

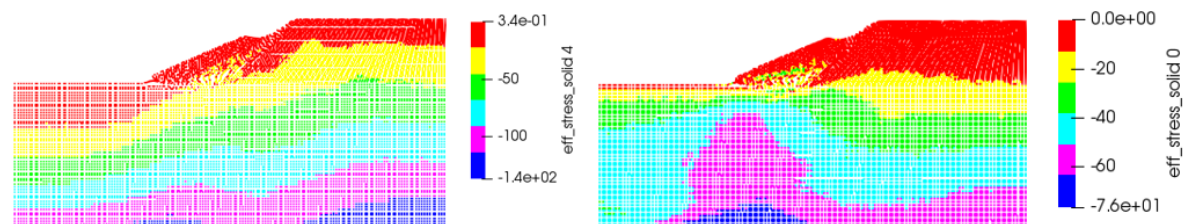


Figure 6.17: Post failure vertical stress (left) and horizontal stress (right)

6.3. Eemdijk experiment MPM discretization

Now that the influence of the strength formulation has been investigated, the Eemdijk experiment can be modelled in MPM. At first the discretization of the problem will be presented. Then, the different strength hypothesis will be converted to correct for the mismatch between MPM and LEM. Finally, the failure will be modelled after which conclusions will be drawn on the residual strength of the clay layers under the Green Eemdijk experiment.

6.3.1. Geometry

The geometry of the problem that will be used for the MPM model is based on the same coordinates as the LEM analysis, and can be seen in Figure 6.18. A quadrilateral mesh was used, as this was required by the soil model. Four material points were used inside each element. An element size of 0.5 m was used, resulting in a mesh with 5000 elements. The mesh was structured inside the material geometry. An unstructured mesh with fixed element size on the lines was used on the empty surface. A cluster of material points was also created in the toe of the geometry to overcome deformation problems occurring after large displacements. The fixities were applied on the same conditions as in Benchmark 2-4. Solid and liquid fixities were applied on the border of the geometry to prevent materials from flowing out of the mesh. A liquid surface fixity was also applied in x-direction to overcome the problem of the liquid pressures not being in equilibrium. Note can be taken that since the layers are not horizontal, a K0 stress initialisation was not possible (Communication with Mario Martinelli).

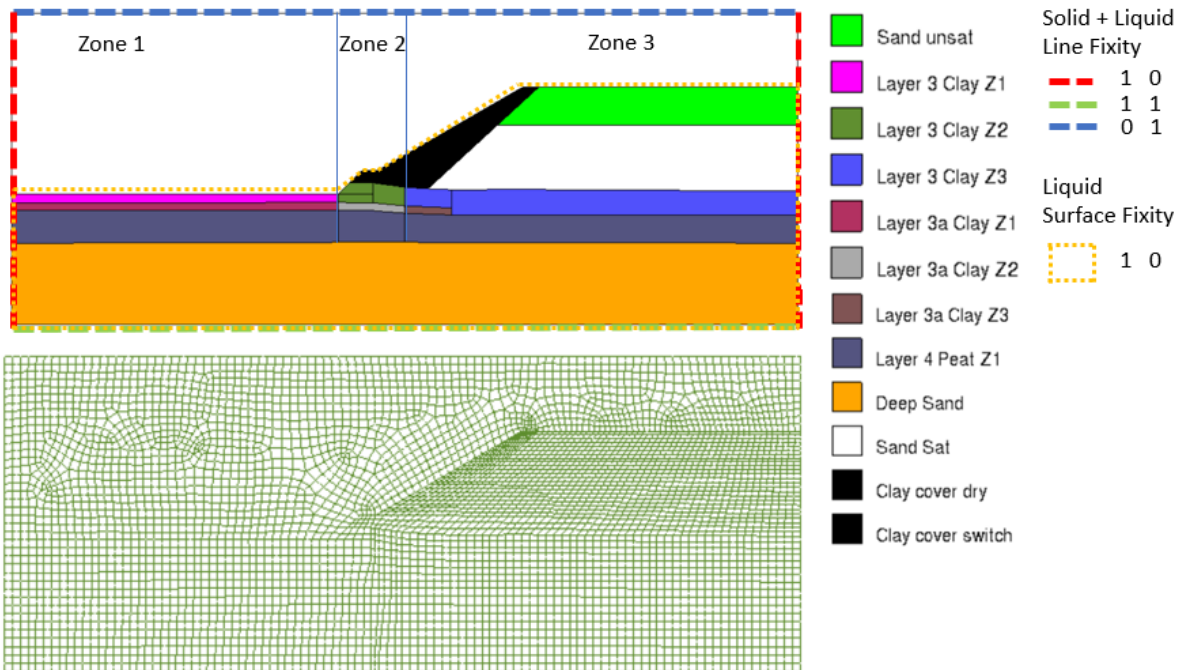


Figure 6.18: Discretization of the Eemdijk experiment in MPM. Top: The materials and boundary conditions. Bottom: the quadrilateral mesh discretization

A few geometrical differences between the LEM geometry and the MPM geometry need to be clarified. First, the crest width was extended to prevent any boundary effect from playing a role in the analysis. It was not possible to incorporate the water on the passive side excavation, therefore it was left out of the model. The strength properties were compensated in section 6.4.

The strength formulation of the clay layers in D-Geo Stability with a Shansep formulation leads to an equivalent cohesion that is dependent on the OCR of the clay. This OCR varies throughout the geometry. It is therefore necessary to create vertical subdivisions of the clay layers depending on their OCR. Three zones were created. The most left zone (Zone 1) has the highest PoP, which is the sum of the original POP with the weight of the excavated soil. The construction overpassed the highest historical stress in the zone on the right, therefore no cohesion will be attributed to Zone 3. The average PoP of Zone 2 was obtained from D-Geo Stability, and converted to an equivalent cohesion.

6.3.2. Damping

In a dynamic problem damping needs to be applied to prevent the system from vibrating. If no damping were applied, stress waves would travel throughout the geometry indefinitely. For Quasi-static problems like the stress initiation phase a high local damping value of 0.75 was considered. For the case of dynamic problems, like the failure phase, a lower local damping value should be used (around 0.05). It was however noted during the failure phase that the CPS damping resulted in same problems in combination with the Mohr-Coulomb Strain Softening model. The CPS damping was therefore removed for the failure phase.

Instead, a Bulk dynamic viscosity was applied. As discussed previously, a flowing soil mass can be considered as a Birmingham fluid, therefore the use of viscosity as replacement for local damping is appropriate. It is therefore chosen to apply a Bulk viscosity damping of 0.1 kPa.s during the failure phase.

6.4. Strength conversion

In this section the differences between the MPM and D-Geo Stability models will be tackled by determining correction factors. These will then be applied on the backcalculated strength of the different layers. Before going into the different correction factors, it is necessary to define how the correction coefficient will influence the strength parameter of the Mohr-Coulomb and SHANSEP formulations. The strength properties calculated

in LEM can be backcalculated to the strength in MPM with Equations 6.32, 6.33 and 6.34. These strength properties will then be converted to equivalent associative strength based on Equation 6.24 and 6.25.

$$S_{corr} = \gamma_{corr} \cdot S_{LEM} \quad (6.32)$$

$$c_{corr} = \gamma_{corr} \cdot c_{LEM} \quad (6.33)$$

$$\varphi_{corr} = atan[tan(\varphi_{LEM}) \cdot \gamma_{corr}] \quad (6.34)$$

6.4.1. Factor of safety

In the LEM analysis the FOS was determined taking into account the 3D effect. The MPM analysis is a 2D plane strain analysis. This means that the strength parameters need to be converted back to a 2D case FOS of 1. The FOS correction factor γ_{FOS} can be determined simply with Equation 6.35.

$$\gamma_{FOS} = \frac{1}{FOS_{LEM}} \quad (6.35)$$

For the case of the Green dyke, the target FOS was 0.79. This means that a factor of $\gamma_{FOS} = 1.266$ needs to be applied on the strength properties.

6.4.2. Water on passive side of excavation

It is to this day not yet possible to add a free water surface in the MPM code used. It is therefore necessary to assess the contribution of the water in the passive side excavation on the FOS. To assess what the influence of the water is, the water on the passive side of the excavation has been removed from the Green peak LEM model.

$$\gamma_{wat} = \frac{FOS_{LEM}}{FOS_{LEM;nowater}} \quad (6.36)$$

The new factor of safety obtained is now 0.68. For the case of the Green dyke a correction factor of $0.79/0.68 = 1.16$ needs to be applied on the strength properties of the different layers in the MPM model to correct for the inability of Anura 3D to model the water on the passive side, and trigger failure at identical strength.

The same was done for the residual profile LEM model. A FOS of 0.74 was obtained. Correcting the residual strength values based on the peak strength water on passive side can therefore influence the residual strength conversion by around 9 %. (Strength converted used) in MPM is actually slightly too large, displacements could be underestimated.

$$\gamma_{corr} = \gamma_{FOS} + \gamma_{wat} = 1.46 \quad (6.37)$$

The final correction factor that needs to be applied on the different strength properties back calculated in the LEM analysis part to match the MPM model can therefore be found with Equation 6.37 to be 1.46. This factor will be applied on both peak and residual parameters.

6.5. Strength summary

6.5.1. Peak strength

Now that the different correction factors have been calculated, the peak strength properties to be used as input for the MPM model can be presented. It was concluded from the Benchmarks that an associative formulation resulted in the closest match between the D-Geo Stability and MPM model. The strength properties of the layer were determined in Chapter 5. A full conversion of the parameters is presented in Appendix I. A summary of the equivalent peak strength properties of the clay layers and sand core can be found in Tables 6.1 and 6.2 respectively.

Table 6.1: Equivalent peak strength properties of clay layers used in the MPM analysis

	$S_{p,LEM}$	$S_{p,corr}$	POP	m	$\varphi_{eq;a,corr}$	$c_{corr,eq;a}$
Layer 3 Z1	0.45	0.66	28	0.9	33	16.7
Layer 3 Z2	0.45	0.66	15.7	0.9	33	9.3
Layer 3 Z3	0.45	0.66	0	0.9	33	0.0
Layer 3a Z1	0.35	0.51	20	0.9	27	9.3
Layer 3a Z2	0.35	0.51	9.2	0.9	27	4.3
Layer 3a Z3	0.35	0.51	0	0.9	27	0.0

Table 6.2: Equivalent peak strength properties of sand core used in the MPM analysis

	φ	c	ψ	$\varphi_{eq;a}$	$c_{eq;a}$	$\varphi_{eq;a,corr}$	$c_{eq;a,corr}$
Sand sat	38	0	10	34	0	45	0
Sand unsat	38	4	10	34	3.5	45	5.1

6.5.2. Residual strength Hypothesis 1

The same procedure can be applied on the residual strength properties following Hypothesis 1. Starting from the backcalculated strength presented in Chapter 5 and converting according to Appendix J, Table 6.3 summarises the converted residual strength properties following Hypothesis 1.

Table 6.3: Summary of the conversion of Hypothesis 1 residual strength parameters

Residual Hyp 1	φ_r	$\varphi_{eq;a}$	$\varphi_{eq;a,corr}$
Layer 3	11	10.8	15.6
Layer 3a	8.7	8.6	12.7
Sand core	30	27	36.8

6.5.3. Residual strength Hypothesis 2

The same procedure can be applied on the residual strength properties following Hypothesis 2. Starting from the backcalculated strength presented in Chapter 5 and converting according to J. Table 6.4 summarises the converted residual strength properties following Hypothesis 2.

Table 6.4: Summary of the conversion of Hypothesis 2 residual strength parameters

Residual Hyp 2	$S_{r,LEM}$	$S_{r,corr}$	m	$\varphi_{eq;a,corr}$	$c_{eq;a,corr}$
Layer 3	0.31	0.46	0	24	0.0
Layer 3a	0.24	0.35	0	19	0.0

6.5.4. Residual strength Hypothesis 3

The same was done for the strength properties from Hypothesis 3. The corrected values presented in Section 6.4 should be used as input for the MPM model as these values are formulated based on the deformed geometry stress. Table 6.5 summarises the converted residual strength properties following Hypothesis 3.

Table 6.5: Summary of the conversion of Hypothesis 3 residual strength parameters

Residual Hyp 3	$S_{r,LEM}$	$S_{r,corr}$	m	$\varphi_{eq;a,corr}$	$c_{eq;a,corr}$
Layer 3	0.43	0.63	0	32	0.0
Layer 3a	0.34	0.50	0	27	0.0

6.6. Modeling steps

In this section the modelling steps will be explained. A 2-phase coupled stress initialisation will be considered, after which a 1-phase failure is triggered.

6.6.1. Stress initialisation

The goal of the stress initialisation phase was to model the loading of the dyke core by increasing the water table to +2.9 m. Two Loading stages will therefore be considered. In the first stage the stresses in the geometry will be generated based on the sand core being dry. In the second stage the loading will be considered. In this phase the bottom part of the sand core will be saturated, and the poisson ratio will be changed to model the unloading behaviour as described in Benchmark 4.

Stress initialisation was performed in a similar fashion as Benchmark 4. A 2 phase (coupled) formulation was used with a high permeability to prevent excess pore pressures from being generated. The soil model during stress initialisation was simplified to a Mohr-Coulomb expression by using a softening parameter $\eta = 0$. The layers were given a high strength to prevent premature failure.

As in Benchmark 4 it was chosen to first model the sand core part that would get saturated (Sand sat and Clay switch in Figure 6.18 as a saturated material with a water density of 50 g/m³ and a bulk modulus of 1000 kPa. This should result in a total density of 18 kN/m³ for the sand core and 17 kN/m³ for the clay cover. The rest of the materials were considered saturated. Gravity was applied over 30 steps. A Quasi-static convergence step was applied. A CPS damping of 0.75 was used. The horizontal and vertical stresses and the liquid pressures after the 31st steps can be found in Figure 6.19.

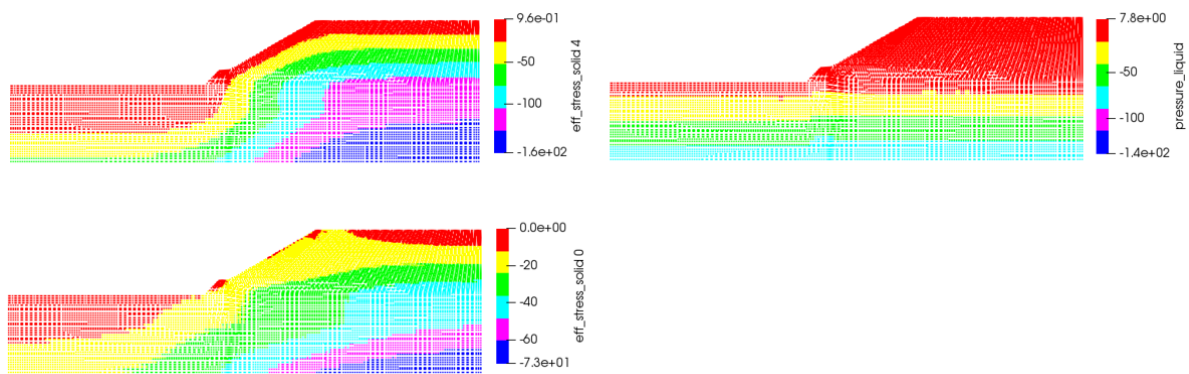


Figure 6.19: First phase stress initialisation results of the Eemdijk. Top left: Vertical effective stress, Bottom left: horizontal effective stress, Top right: liquid pressure

The material properties of the clay and sand layers were then changed to model the filling of the dyke core with water. Water density was increased to 10 kN/m³, Bulk modulus to 21500 kPa and the solid density changed to reach a total density of 19.5 kN/m³. The same was done for the clay cover. Thirty more steps were added after the material switch. Again, a quasi static convergence was applied after which the analysis was changed to a 1 point formulation with another quasi static convergence step. The horizontal and vertical stresses and the liquid pressures after the 63 steps can be found in Figure 6.20.

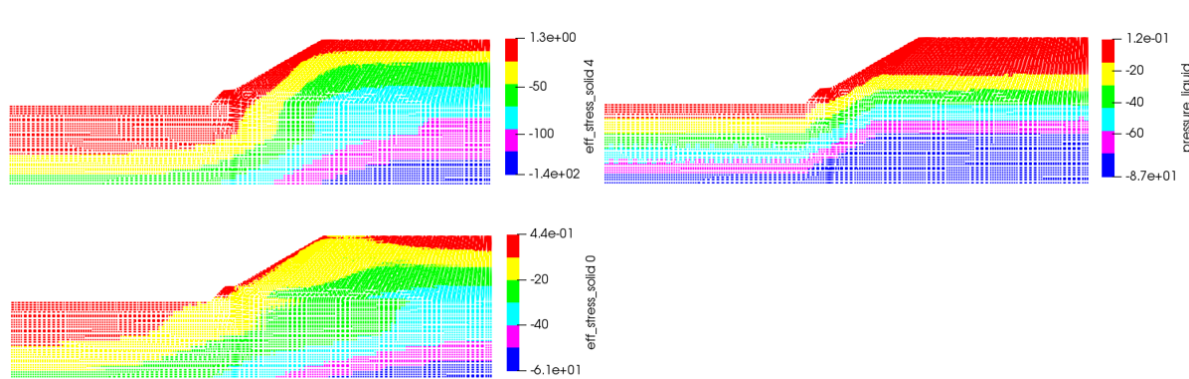


Figure 6.20: First phase stress initialisation results Benchmark 4. Top left: Vertical effective stress, Bottom left: horizontal effective stress, Top right: liquid pressure

A few words need to be added on the generation of (excess) pore pressure generated from the construction. It was evaluated that for each individual layer these could be generated by changing the hydraulic conductivity of the layers, or by changing the Bulk modulus of water in the layers. It was however concluded by running a LEM without excess pore pressures, and with water table at +2.9m (as if the core had been saturated for a long time, which is what was modelled in this MPM model) that the excess pore pressures almost did not influence the FOS. The FOS without excess pore pressures was 0.76, ie 3 % lower than the target FOS. In the context of the other uncertainties it was therefore chosen to ignore these. If the reader wished to undertake an MPM analysis of a slope stability problem in which excess pore pressures still play a role, it is recommended to subdivide the different region with liquid fixities to generate different pore pressures in each zone.

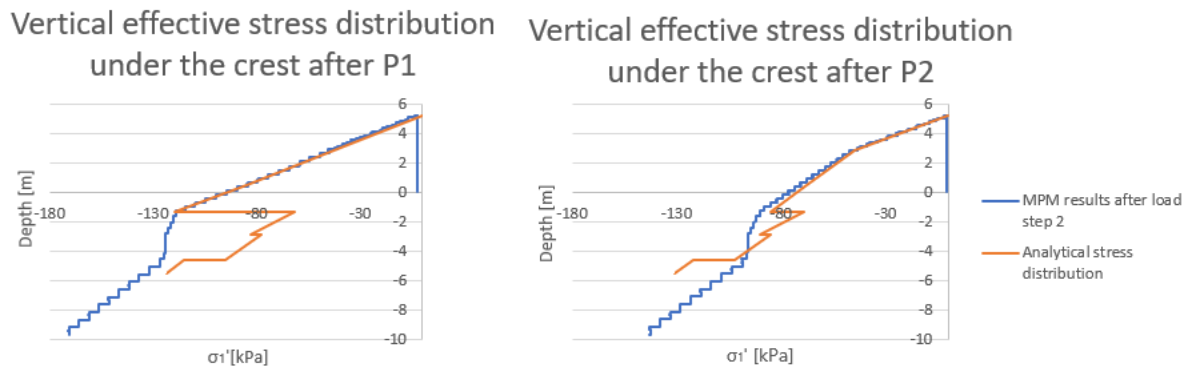


Figure 6.21: Vertical stress results under the crest after the first and second loading stage

The stresses obtained under the crest can be compared to the analytical solution. The results can be found in Figure 6.21. The first thing that can be noticed is that the stresses in the sand core match the analytical solution very well. The solution diverges from the analytical solution in the peat and clay layers due to the fact that excess pore pressure generation was neglected in this analysis. The jump in stress in the deep sand layer originates from the second water table governing the water pressures in that layer. Since the failure surface passed through the clay layers, it was decided not to try to incorporate this in the model.

6.6.2. Failure triggering

To trigger failure the strength of the layers was reduced to the back calculated peak strength. The bulk modulus of water was changed to 0 for the sand layers to model the drained behaviour. Fifteen steps were added to the analysis to model the failure initiation.

The strength properties were converted to both equivalent associative and non-associative non-dilative parameters in Appendix J. The values obtained were used as input for the MPM model. The goal is to verify that the back calculated values actually lead to failure. The results are presented in Figure 6.22. First of all it can be noted that the equivalent associative parameters lead to failure, while the equivalent non-associative non-dilative parameters do not (following the failure definition in the Benchmarks). It can also be noted from the magnitude of the displacements that the FOS with equivalent associative parameters is actually quite smaller than 1. A slight underestimation of the strength of one or more layers therefore probably happened. However the fact that for non-associative equivalent parameters failure did not occur shows that the results are not so far off.

Comparing the shape of the slip surface with what was measured post failure shows a close match. The slip surface passed through the clay layer 3a, and emerged 2.3 m from the crest edge in the MPM model. In reality the slip surface emerge 1.5 m from the crest edge. This is deemed close enough to the MPM results.

The η parameter was changed to non-0 values to model the softening behaviour of the different materials. The peak and residual strength were used as input. The bulk modulus of water was changed depending on whether the soil layers should be modelled as drained or undrained. The failure phase was carried out for 100 steps.

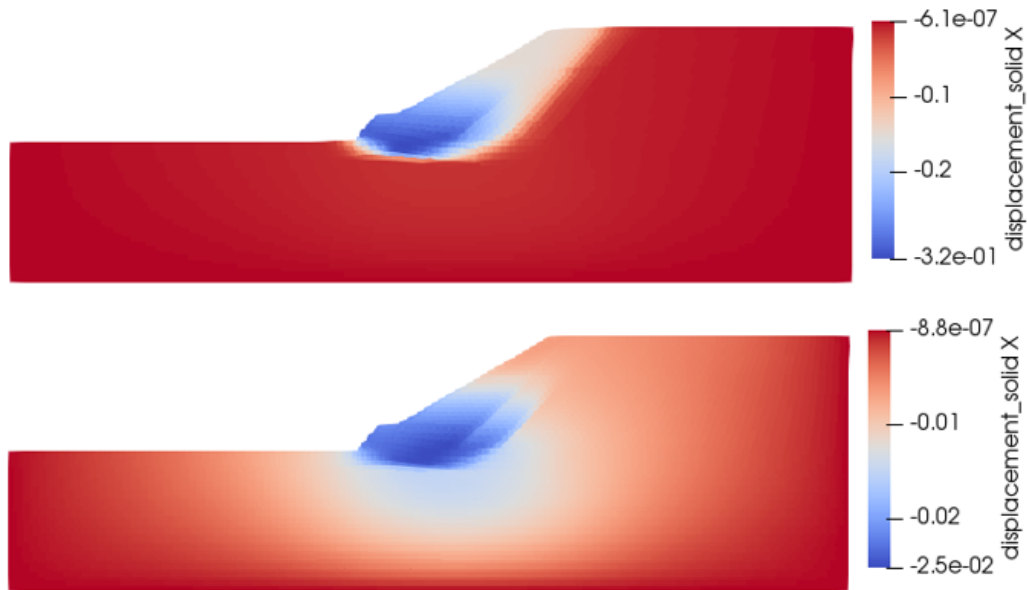


Figure 6.22: Failure triggering results for equivalent associative parameters (Top) and equivalent non-associative non-dilative parameters (Bottom)

6.7. Failure phase results

In this section the results of the failure phase with strain softening will be presented. The three hypothesis strength were translated to equivalent strength for the MPM model. The final geometry will be presented in each case, and the magnitude of the displacements will be compared to the experiment results to conclude. The full failure phase for each different run is presented in Appendix K. A fixed point needs to be recognized in both the peak and deformed geometry. As discussed in Chapter 3, the bottom of the clay cover moved 6 to 8 m horizontally, and the top of the clay layer moved around 3.5m vertically. This point is easily recognisable in both peak and deformed geometry, both in the MPM model and in the real experiment. The displacement measurements will be compared to that point. The undeformed mesh will also be presented in the background of the deformed geometry to serve as reference.

6.7.1. Results Hypothesis 1

The final position of the failed dyke with residual parameters following Hypothesis 1 can be found in Figure 6.23. The first thing that can be noted is that the displacements in horizontal direction of the dyke toe are almost twice the measured displacements, around 14 m. The vertical displacements of the crest were found to be around 3.6 m. The back propagation of the slip surface was also notably large. This seems to indicate that the backcalculated drained residual strength is too low, or that a drained analysis is not suitable to model the path from peak to residual strength of clay.

An interesting side note can be made on the shape of the slip surface. In all the models the slip surface shape passed through the soft clay layer 3a, like in the experiment. In the LEM calculations of the residual models attention was payed to the trajectory of the slip surface at the location of the excavation. It was unclear whether the slip surface passed through clay layer 3a, pushing it forward, or whether the slip surface emerged and slid over the bottom of the excavation, on clay layer 3. In the LEM analysis the most critical circle was always found to be passing through clay layer 3a. The results of this Hypothesis show the slip surface passing over Layer 3. More than being able to conclude on the real behaviour of the slip surface, it indicates the influence of the drainage type on the failing behaviour of the soil, and the shortcomings of a LEM to model this complex behaviour.

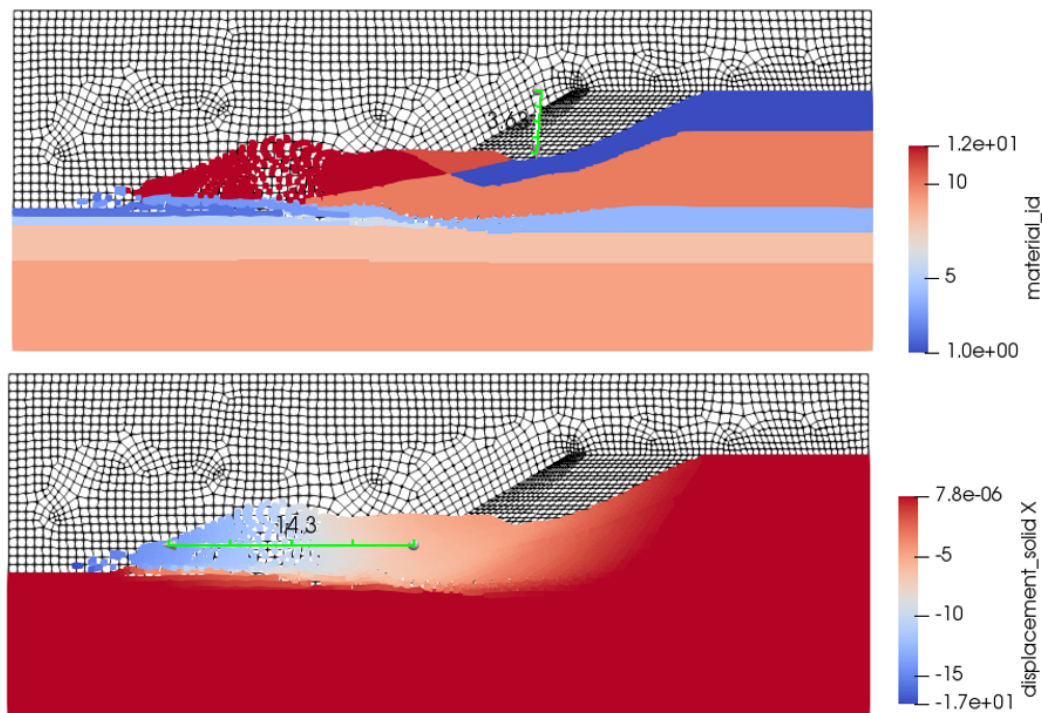


Figure 6.23: MPM results of deformation with residual strength parameters according to Hypothesis 1

6.7.2. Results Hypothesis 2

The final geometry of MPM model with strength reduction Hypothesis 2 is presented in Figure 6.24. The horizontal displacements of the dyke toe are now around 7.5 m. The vertical displacements of the crest were found to be around 3.3 m. The residual profile obtained is very close to the residual profile found in the experiment, presented in Figure 3.7, with displacements slightly larger than what was measured during the experiment. The residual strength properties calculated with Hypothesis 2 can therefore be seen as an under boundary of the residual strength of the clay layers.

A point of difference between the results of this model and the slip surface found during the experiment is the back propagation of the slip surface during failure. Due to the strain softening function, the deformation in the sand core induced by the moving soil mass generate strains in the sand core, which, due to the strain softening function, looses strength. This in turn results in the slip surface moving backwards. The back propagation of the slip surface results in a larger amount of soil loading the passive side. This might overestimate the load, and therefore overestimate the displacements. A different discretization will be presented later to test the influence of this slipsurface backpropagation on the residual profile.

6.7.3. Results Hypothesis 3

The final geometry of MPM model with strength reduction Hypothesis 3 is presented in Figure 6.25. The horizontal displacements of the dyke toe are now around 5 m. The vertical displacements of the crest were found to be around 2.6 m. These displacements are slightly lower than what was found during the experiment. The overall shape of the residual profile is as expected close to Hypothesis 2. The strength properties backcalculated with Hypothesis 3 can therefore be seen as an upperboundary of the residual strength of the clay layers.

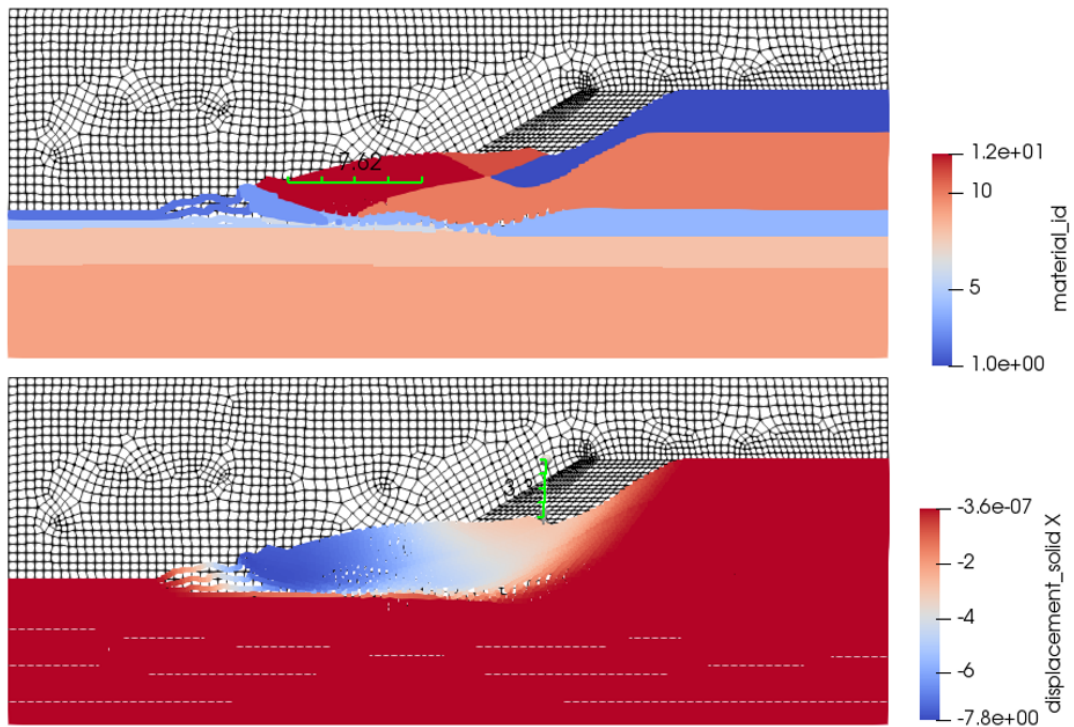


Figure 6.24: MPM results of deformation with residual strength parameters according to Hypothesis 2

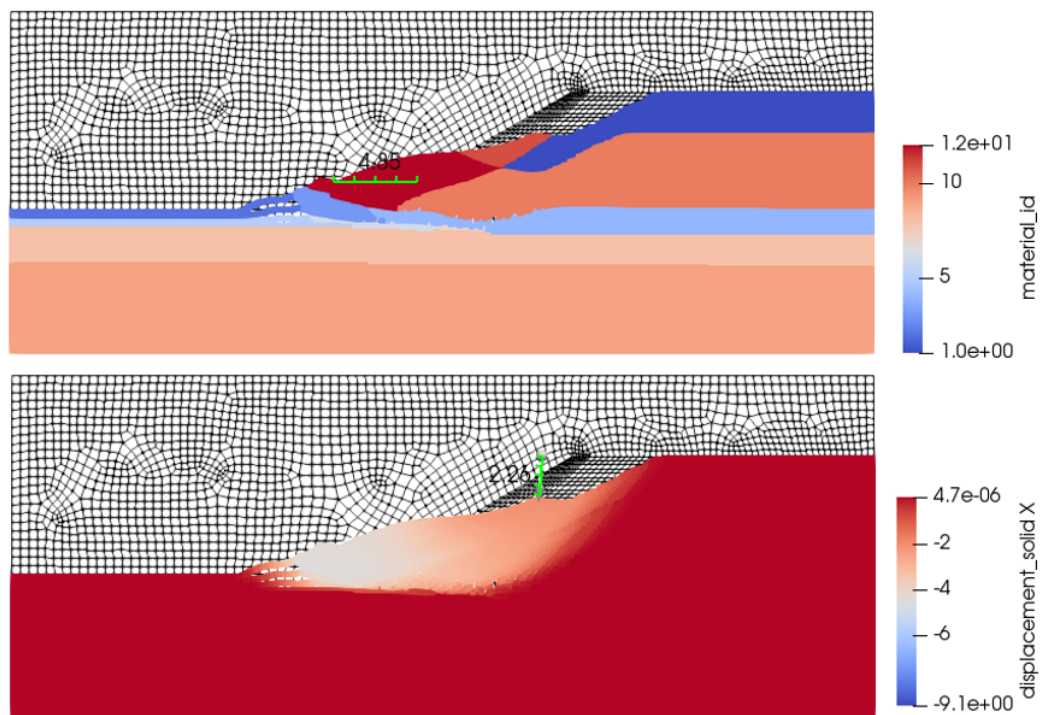


Figure 6.25: MPM results of deformation with residual strength parameters according to Hypothesis 3

6.8. Variation: Mohr-Coulomb sand core

It was noted from the results of the hypothesis with strain-softening that the sand core shows a strong tendency to back propagate the slip circle. This enhances the driving force, and might therefore influence the total displacements. It is thought that this slip surface back propagation is due to the sensitiveness of the softening parameter Eta in the sand core.

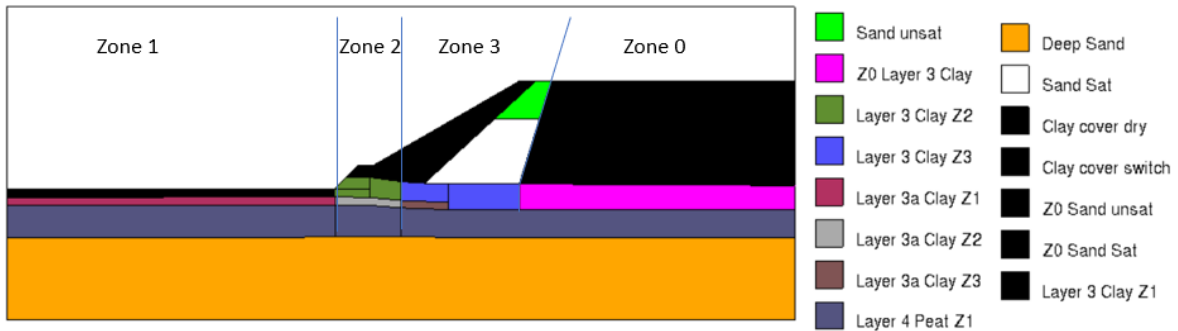


Figure 6.26: Discretization of the Eemdijk experiment with Mohr-Coulomb model in the dyke core

In an effort to reduce the slip surface backpropagation a geometry was created without the strain softening function in the soil layers under the crest. The discretization of this geometry is shown in Figure 6.26. A new zone Z0 was added compared to 6.18. In this zone, the material properties are given the peak strength properties of Zone 3, without strain softening function. For the rest of the layers the residual strength parameters of Hypothesis 2 are used as input.

The deformation results are provided in Figure 6.26. The first thing that can be noticed is that the magnitude of the displacements is similar to that of Hypothesis 2.

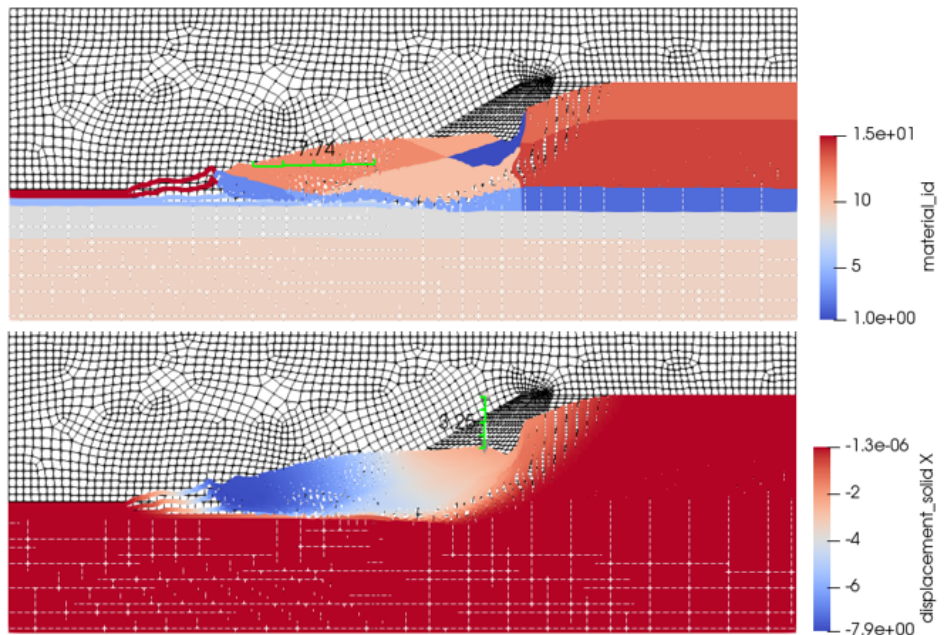


Figure 6.27: Deformation results without strain softening in the dyke core

It can also be noted that at step 110 a secondary slip surface forms in the top of the slope, as can be seen in Appendix K. This contradicts the results from the LEM analysis on the strength of the dyke core. Indeed, the back analysis was carried out such that the apparent cohesion induced by suction would be large enough to prevent failure from happening. The secondary slip surface resulted in a soil wedge pushing on the main slip

surface. This in turn increased the driving force again, which explains why the obtained displacements are so close to the displacements obtained in the main model on Hypothesis 2. A final run was therefore carried out with increased cohesion in the unsaturated sand Z0. To prevent the slip surface from expanding, a cohesion of 6 kPa was also added to the saturated sand layer Z0. The results in the displacements presented in Figure 6.28. The magnitude of the displacements is again very close to the results of Hypothesis 2. The influence of the backpropagation of slip surface on the results therefore seems restricted, and the conclusions drawn previously still hold.

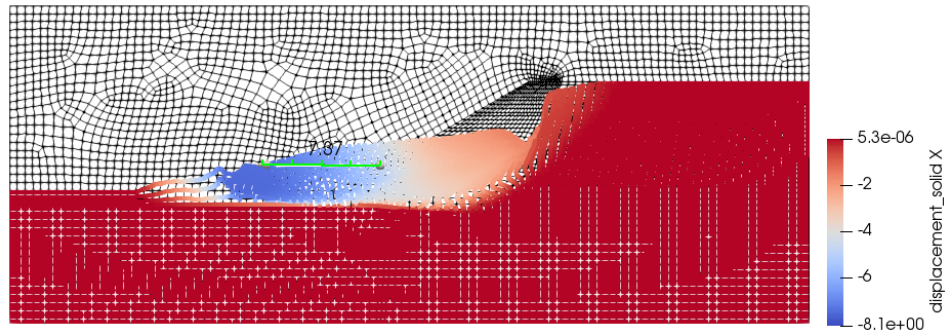


Figure 6.28: Deformation results without strain softening in the dyke core, and added cohesion in Z0 sand layers

7

Discussion

The first thing that was concluded from this thesis is that the failure of a dyke without sheet pile wall could be modelled accurately with MPM. The process of determining the 3D-effect and strength of layers at the same time with a LEM analysis was deemed successful. The application of strength factors to correct for differences in models between MPM and LEM was also successful. Two corrections were applied: a factor of 1.23 on the strength properties of the soil layers to correct for the 3D effect, and a factor of 1.16 to account for the absence of water on the passive side excavation in the MPM model. It should be added that this factor was based on the peak geometry. For the peak geometry the conversion resulted in a good match between the failure point in MPM and the results from the LEM analysis. In the residual geometry the water on the passive side had less influence on the overall FOS. This effect was not taken into account, and could result in the underestimation of displacements obtained from the MPM model.

The back-calculated peak and residual strength with LEM proved to be strongly dependent on the calculated 3D effect, which in turn was related to the chosen slipplane width. It was shown that assuming a 30 m wide slip surface instead of 20 m resulted in a target FOS around of 0.85 instead of 0.78. This would result in a difference in backcalculated strength around 10%. It can also be noted that this only influenced the absolute value of back-calculated strength. The back calculated peak and residual strength are equally dependent on the discretized slip surface width, the percentual strength drop therefore remains unaffected.

Best match between the measured displacements from the Green dyke full-scale test and the obtained displacements from the MPM model was found using an Undrained formulation for the clay layer, with loss of cohesion and a reduction of S- ratio by 0 to 30%. This resulted in horizontal displacements of the toe of 4.5 m to 7.5 m (around 6 m to 8 m in reality), and vertical displacements of 2.5 m to 3.5 m (around 3.5 m in reality). The OCR was concluded to not play a role anymore in the residual strength of the clay. Most of the mobilized strength originated from the cohesion of the clay. Leaving cohesion in the residual strength through the OCR in the SHANSEP formulation resulted in displacements that were too small in comparison to the full-scale test measurements. Stress oscillations were shown to take place during failure in the MPM model. It is unknown how this influenced the results.

The Mohr-Coulomb Strain Softening model used in MPM was shown to be a relatively easy way to investigate the relation between strength loss and displacements. This resulted however in shortcomings to model the undrained behaviour of shearing soils. Indeed, the MC-SS model does not account for the generation of shear induced pore pressures. The only difference between drained and undrained model is therefore the 0 volume change upon shearing restriction for the undrained case. Literature shows that the strength loss measured in clays might be induced by the generation of pore pressures due to undrained shearing. It is therefore possible that a part of the calculated 30% S-ratio reduction was actually induced by the generation of pore pressures. This could not be tested.

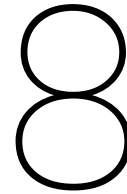
Pore pressures induced by the shifting weight from the failed geometry were shown to have a large influence on the back-calculated residual strength. These pore pressures were estimated based on the primary loading response of the soil during construction. They were incorporated through a Consolidation term

in D-Geo Stability (40% of the primary load generating pore pressure). No experimental data was available about the post-failure pore pressures, which could therefore have influenced the accuracy of the result.

Based on this analysis, conclusions can be formulated on the ability to test the residual strength of Dutch clays with LDSS or cyDSS apparatus. These tests showed a strength drop around 17%. Empirical correlations based on clay fraction and liquid limit showed residual friction angles around 30°. Results from this analysis indicate values that are much lower, with only the loss of OCR resulting in a strength loss of 50%. The conclusions drawn by Deltares that these tests are not suited for the Dutch clays therefore seem to be validated. Reversal of the shearing orientation in the cyDSS test probably prevented the particles from aligning face to face. Torsional ring apparatus need to be investigated as option to measure the residual strength instead.

The LEM analysis of the Blue dyke proved unsuccessful. In the analysis of the Blue dyke a single rotational slip circle was assumed. It is unproven whether this was the real failure behaviour of the Blue dyke. Strain localization as measured by the SAAF's indicate that the failure mode of a dyke with sheet pile wall is different from the classic rotational slip surface. The failing soil behaviour resembles a DSS test, where the sheet pile wall can be seen as a boundary of the shear box. This supports conclusions from previous full-scale tests back analysis, which indicate that the most representative laboratory test for the strength measurement is a DSS test. These conclusions need to be confirmed with a FEM to include soil-structure interactions.

To this day, soil-structure interactions are scarcely incorporated in the MPM code used. An MPM analysis of a dyke with sheet pile wall was therefore not yet possible. Further conclusions on the failing behaviour of a dyke with sheet pile wall should be carried out once an MPM code has been developed capable of capturing soil-structure interactions.



Conclusions

Do the clay and peat layers behave drained or undrained when subjected to large shear strain?

The results showed a best match between the backcalculated strength in LEM and the displacements from the MPM model with the behaviour of clay under the Green dyke modelled as undrained, like the current national standard recommends. The question whether the softening behaviour of clays is drained or undrained could however not be answered properly. Indeed, even though the backcalculated strength with a drained model resulted in displacements that were too large, it is still possible to find a drained friction angle for which the displacements obtained from the model match the experiment results. Constitutive models based on the Critical State theory including shear induced pore pressures should be used in the future to further investigate the behaviour of clays subjected to large strains.

The Blue dyke analysis could not be carried out properly, therefore conclusions on the residual strength of peat could not be formulated from this analysis. Literature study of previous historical case studies showed that when subjected to large shear strain, the behaviour of peat was dominated by formation of cracks.

Does the Overconsolidation Ratio still play a role in the slip plane strength after remoulding due large shear strain?

It was further proven that the Overconsolidation ratio did not play a role anymore in the residual strength. Indeed, discarding the cohesion from the equivalent Mohr-Coulomb parameters resulted in horizontal displacements of the toe of magnitude around 4.5 m, and vertical displacement of the crest of 2.2 m in the MPM model (6 to 8 m horizontal displacements in the experiment, and around 2.5 m vertical drop of crest height). This magnitude of displacements could not be obtained with a sole reduction of S-ratio, which proves that the OCR (through an equivalent cohesion with a Mohr-Coulomb formulation) can be discarded from the residual strength expression. Rearrangement of particle orientation therefore leads to a strength only dependent on interparticle friction.

What is the magnitude of the strain softening of different soil layers?

When expressing the strength of clay with a SHANSEP formulation, a peak S-ratio of layer 3 of 0.45 was found, and a residual S-ratio of 0.31. This reduction of S-ratio up to 30 % lead to horizontal displacement of the dyke toe of 7.6 m, and vertical displacement of the crest of 3.3 m. These displacements are slightly larger than what was measured from the full- scale test. In light of the uncertainties brought with this analysis this value can be seen as an upper bound of the S-ratio reduction, where the peak S-ratio is the under bound of the reduction.

The sand core was modelled according to literature to soften until a Constant Volume friction angle of 30°, identical for most quartz sands.

How is the failure mode of a dyke influenced by the presence of a sheet pile wall?

The sheet pile wall was shown to influence the failure behaviour of the soil on the passive side slope. Strain localization measured by the SAAF's indicated that the soil was "pushed" by the sheet pile wall, which would explain why a slip surface was not found post-failure. The resemblance of the failure mode with the strain localization in a DSS test needs to be noted.

This pushing behaviour induced by horizontal loading from the soil-structure interaction led to the inability to back-calculate the strength of the dyke with sheet pile wall with a LEM analysis. The failure mode seemed to be different from a classic rotational slip surface. The pushing by the sheet pile wall might have favored the formation of a slip surface at the interface of 2 layers, in this case of peat and sand. A more advanced model like FEM needs to be used to validate this behaviour.

Can MPM be used in practice to predict the post failure geometry?

The MPM analysis showed a good coupling with the experiment results. Both the peak strength at failure and the residual strength of the soil layers under the dyke without sheet pile wall were found with satisfying accuracy with LEM. The back-calculated strength in LEM matched the failure point in MPM. The use of a strain softening function with residual strength parameters in MPM resulted in a residual profile close to what was found from the full-scale test.

An answer to the question whether MPM can be used *in practice* to predict the post failure geometry of a dyke is more difficult to formulate. A high amount of effort was required to obtain stable results. Completion of this project would not have been possible without the help of software developers at Deltares. It is therefore advisable to restrict the use of MPM to specific analysis, in cooperation with Deltares.

9

Recommendations

Reflections on the current Dutch standard (WBI) about the design of dykes with sheet pile wall can be formulated. The current design advises to design a sheet pile wall based on a deformed soil profile on the passive side with 1/3 of the original height, without strength loss attributed to the soil. The deformed profile of the Blue dyke was approximately half the height of the original profile, which seems in line with the WBI recommendations.

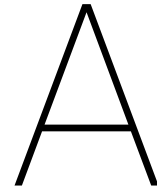
This thesis however showed that clay layers can show significant strain softening due to large displacements the soil mass can undergo during failure. It is therefore advised to model clayey layers as undrained with a SHANSEP formulation, reduce the cohesion of clayey layers to 0 (through the removal of OCR), and further reduce the S-ratio up to 70 % of its peak strength. DSS tests were furthermore shown to provide results close to the back-calculated value of peak strength. Empirical correlations based on index properties of clays with the residual strength did not show a good match with the back-calculated residual strength, and should be used with care.

Better conclusions could have been drawn if post failure measurements of in situ pore pressures would have been carried out. These could be compared to results of more advanced soil models taking into account shear induced pore pressures. This lack of information limited the conclusions that could be drawn regarding the drained or undrained behaviour of a clays when exposed to large levels of strain, or on the origin of the softening behaviour.

It is advised not to use LEM to backcalculate the strength of a dyke with sheet pile wall. A more advanced model like FEM is necessary to obtain satisfactory results.

The 3D effect was assessed based on a LEM analysis, and a discretized geometry. The magnitude of this effect should be investigated by carrying out a 3D FEM analysis. It is not required to perform this in MPM, as the magnitude of the 3D effect can already be determined from the small strain deformed geometry. The method used to determine the 3D effect provided good results, but was quite time consuming. It is therefore advised to automate this process with a computer code if this method is to be used repetitively.

To anyone willing to use a MPM software for a case in practice: go speak to the software developers in an early stage of your problem analysis! Some implemented functions can prove to malfunction for specific cases. A heads on approach will spare a lot of trouble later in the analysis. It must be emphasized that this thesis would not have been possible without the help of Mario Martinelli at Deltares



Pore pressure development

A.1. Green dyke subsurface pore pressure development

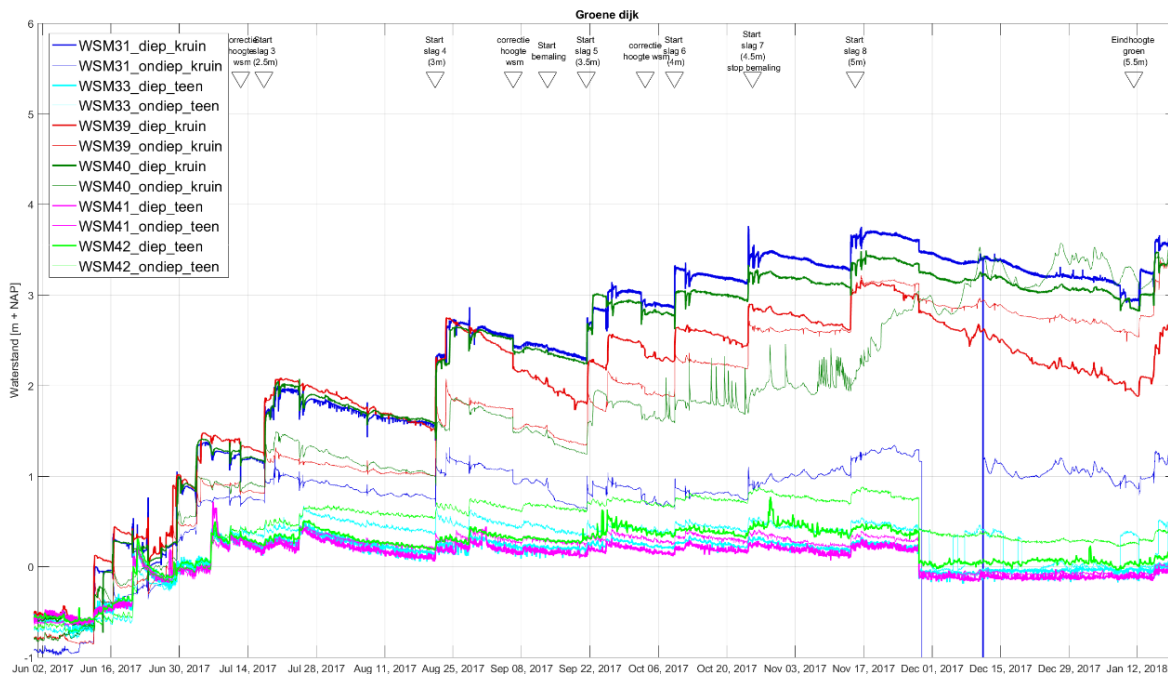


Figure A.1: Development of pore pressures under the green dyke during construction and loading

Table A.1: Pore pressure measurements under Green dyke toe and crest before failure

Green dyke toe	33o (toe)	41o (toe)	42o (toe)	33d (toe)	41d (toe)	42d (toe)
Pressure day 232 [kPa]	15.91	16.50	17.09	30.61	30.97	32.25
Pressure day 232 [m]	0.11	-0.32	-0.12	-0.14	-0.20	-0.06
Green dyke toe	31o (crest)	39o (crest)	40o (crest)	31d (crest)	39d (crest)	40d (crest)
Pressure day 232 [kPa]	47.07	58.24	54.29	63.85	59.54	65.76
Pressure day 232 [m]	2.94	3.93	3.68	3.20	2.64	3.42

In Figure A.1 the pore pressure development in the different layers under the Green dyke during construction and loading phase can be observed. The subscript "o" refers to shallow, and transducers are placed

in the clay layer. The subscript "d" refers to deep, and transducers are placed in the clay layers. It can be noted that pore pressure 31o and 40o showed faulty measurements. Table A.1 summarize the pore pressures measurements before failure, and that were therefore use in the LEM back analysis.

A.2. Blue dyke subsurface pore pressure development

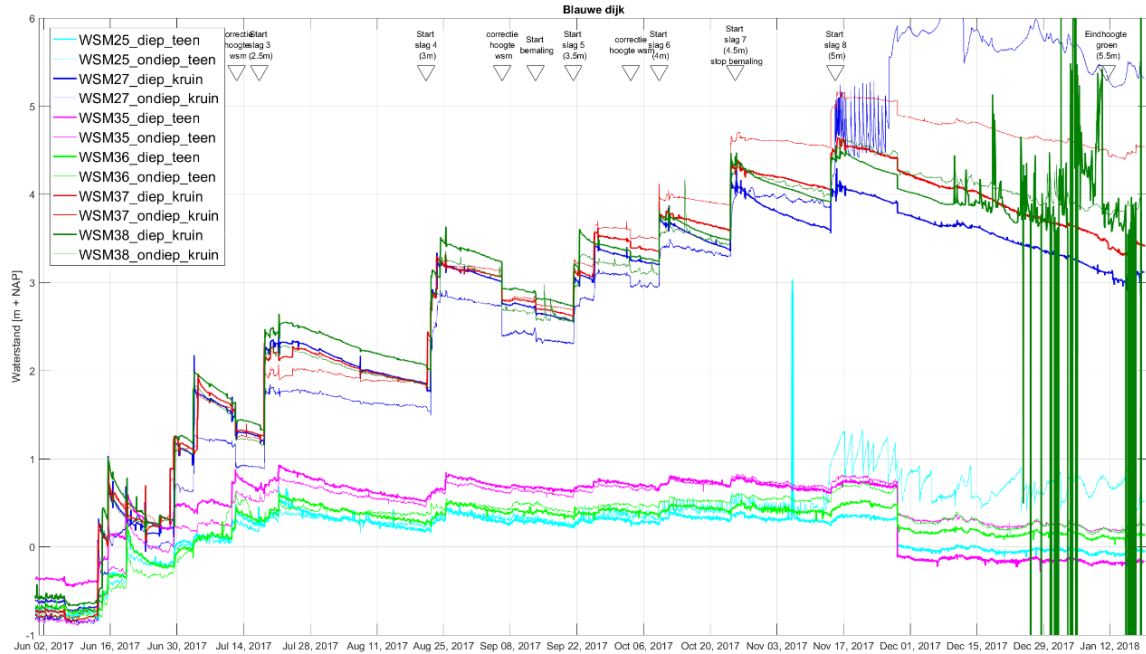


Figure A.2: Development of pore pressures under the blue dyke during construction and loading

Table A.2: Pore pressure measurements under Blue dyke toe and crest before failure

Blue dyke toe	36o (toe)	25o (toe)	35o (toe)	36d (toe)	25d (toe)	35d (toe)
Pressure day 278 15h00 [kPa]	12.84	17.11	16.20	31.06	32.57	36.18
Pressure day 278 15h00 [m]	-0.49	-0.06	-0.23	-0.08	0.00	-0.15
Blue dyke crest	38o (crest)	27o (crest)	37o (crest)	38d (crest)	27d (crest)	37d (crest)
Pressure day 278 15h00 [kPa]	70.76	75.00	72.54	82.51	73.89	74.05
Pressure day 278 15h00 [m]	4.90	5.31	5.07	4.70	3.68	3.83

In Figure A.2 the pore pressure development in the different layers under the Green dyke during construction and loading phase can be observed. It can be noted that pore pressure 27d, 27o and 38d showed faulty measurements. Table A.2 summarizes the pore pressures measurements before failure, and that were therefore use in the LEM back analysis.

B

Staggered sheet pile wall schematization

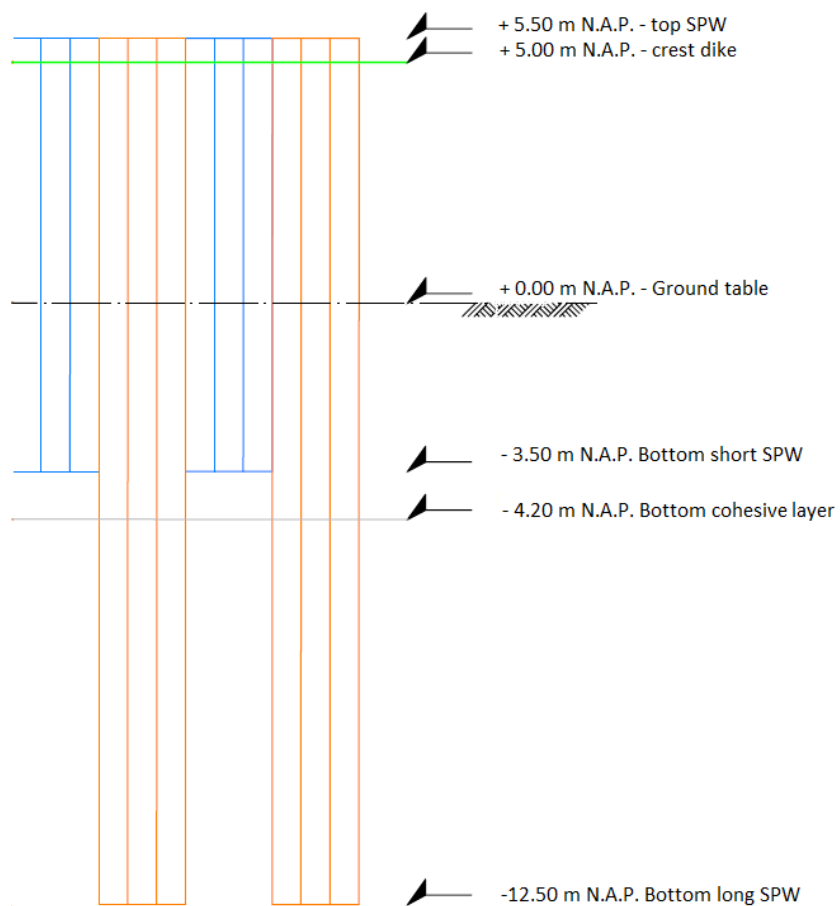


Figure B.1: Sheet pile wall staggered embedment schematization

D

Experiment Phasing

Table D.1: Green dyke construction phasing

Phase	Date	Description	Start day	End day	Crest heightening [m]	Basin heightening [m]
1	12-06-17	Heightening	0	1	1.2	1.2
		Consolidation	1	16		
2	28-06-17	Heightening	16	17	1	1
		Consolidation	17	35		
3	17-07-17	Heightening	35	36	0.5	1
		Consolidation	36	70		
4	21-08-17	Heightening	70	71	0.5	0.5
		Consolidation	71	101		
5	21-09-17	Heightening	101	102	0.5	0.5
		Consolidation	102	119		
6	09-10-17	Heightening	119	120	0.5	0
		Consolidation	120	135		
7	25-10-17	Heightening	135	136	0.6	0
		Consolidation	136	155		
8	15-11-17	Heightening	155	156	0.6	0
		Consolidation	156	214		
9	12-01-18	Heightening	214	215	0.8	0
		Consolidation	215	226		
		Start Experiment phase	226	233		

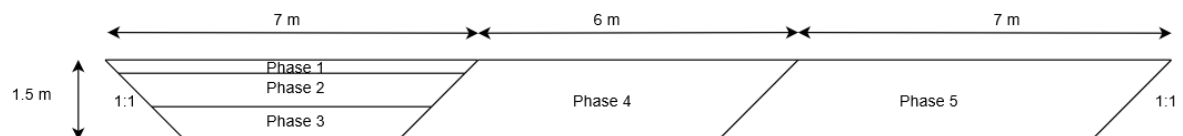


Figure D.1: Overview of the passive side excavation phases on the Green dyke

Table D.2: Blue dyke construction phasing

Phase	Date	Description	Start day	End day	Crest heightening [m]	Basin heightening [m]
1	12-06-17	Heightening	0	1	1.1	1.1
		Consolidation	1	16		
2	28-06-17	Heightening	16	17	1.1	1.1
		Consolidation	17	35		
3	17-07-17	Heightening	35	36	0.6	1.1
		Consolidation	36	70		
4	21-08-17	Heightening	70	71	0.6	0.6
		Consolidation	71	101		
5	21-09-17	Heightening	101	102	0.6	0.6
		Consolidation	102	119		
6	09-10-17	Heightening	119	120	0.6	0
		Consolidation	120	135		
7	25-10-17	Heightening	135	136	0.6	0
		Consolidation	136	156		
8	15-11-17	Heightening	156	157	0.6	0
		Consolidation	157	266		
9	23-02-18	SPW driving	256	257	0	0
10	05-03-18	Heightening	266	267	0	0
		Consolidation	267	273		
		Start Experiment phase	273	279		

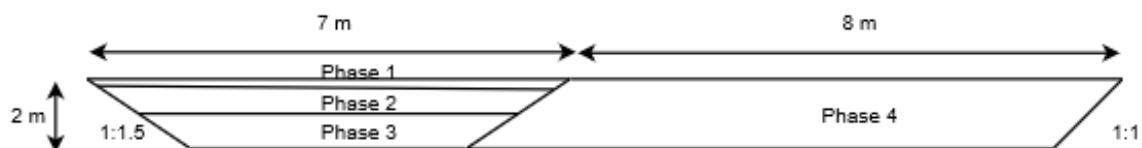


Figure D.2: Overview of the passive side excavation phases on the Blue dyke

Table D.3: Green dyke experiment phasing

Phase	Start	End	Time [days]	Water level core [m]	Water level excavation [m]
Wet excavation passive side 1 (removal top layer)	24-01 08:00	24-01 10:00	0.1	0.5	-
Wet excavation passive side 2 (to -0.9 m N.A.P.)	24-01 10:00	24-01 13:00	0.1	0.5	-0.4
Wet excavation passive side 3 (to -1.5 m N.A.P.)	24-01 13:00	24-01 16:00	0.1	0.5	-0.2
Night/ no work	24-01 16:00	25-01 08:00	0.7	0.5	-0.2
Wet excavation passive side 4 (to -1.5 m N.A.P.)	25-01 08:00	25-01 16:00	0.3	0.5	-0.2
Night/ no work	25-01 16:00	26-01 08:00	0.7	0.5	-0.2
Wet excavation passive side 5 (to -1.5 m N.A.P.)	26-01 08:00	26-01 15:45	0.3	0.5	-0.2
Lowering water table passive side (GT - 0.5 m)	26-01 15:45	26-01 21:50	0.2	0.5	-0.5
Night/ no work	26-01 21:50	27-01 01:45	0.25	0.5	-0.5
Elevation water table core (to + 1 m N.A.P.)	27-01 01:45	27-01 13:52	0.5	1.0	-0.5
Elevation water table core (to + 2 m N.A.P.)	27-01 13:52	28-01 20:05	1.25	2.0	-0.5
Elevation water table core (to + 2.9 m N.A.P.)	28-01 20:05	30-01 09:25	1.5 to 1.6	2.9	-0.5
Failure of green dyke	30-01 11:15				

Table D.4: Blue dyke experiment phasing

Phase	Start	End	Water level excavation [m]	Water level slope [m]	Behind Sheet Pile wall	Water level basin [m]	Water level containers [m]
Wet excavation passive side 1 (to -2 m)	12-03 07:41	12-03 15:58	-0.4	0.4	0.4	0.4	0
Wet excavation passive side 2 (to -2 m N.A.P)	13-03 6:59	13-03 16:45	-0.4	0.4	0.4	0.4	0
Infiltration water core (to +2 m N.A.P)	13-03 16:45	14-03 17:21	-0.4	0.4	1.6	2.0	0
Infiltration water core (to +3 m N.A.P)	14-03 17:21	15-03 9:18	-0.4	0.4	2.6	3.0	0
Infiltration water core (to +4.2 m N.A.P)	15-03 9:18	16-03 8:24	-0.4	0.4	3.8	4.2	0
Filling containers with water (to +1 m)	16-03 8:24	16-03 16:00	-0.4	0.4	3.8	4.2	1.0
Filling containers with water (to +2 m) Infiltration water slope (to +1.0 m N.A.P)	16-03 16:00	17-03 02:45	-0.4	1.0	3.8	4.2	2.0
Filling basin water (to +4.5 m N.A.P)	17-03 02:45	17-03 10:14	-0.4	1.0	4.5	4.5	2.0
Filling basin water (to +5.0 m N.A.P)	17-03 10:14	17-03 13:38	-0.4	1.0	5.0	5.0	2.0
Infiltration water slope (to +1.5 m N.A.P)	17-03 13:38	17-03 15:25	-0.4	1.5	5.0	5.0	2.0
Lowering water table excavation (-0.9 m N.A.P)	17-03 15:25	17-03 16:00	-0.9	1.5	5.0	5.0	2.0
Failure Blue dyke	17-03 16:00	17-03 16:10					

E

As failed pictures



Figure E.1: Photographic report of the Green dyke failure



Figure E.2: Photographic report of the Blue dyke failure

F

Limit Equilibrium Method discretizations

F.1. Settlement analysis

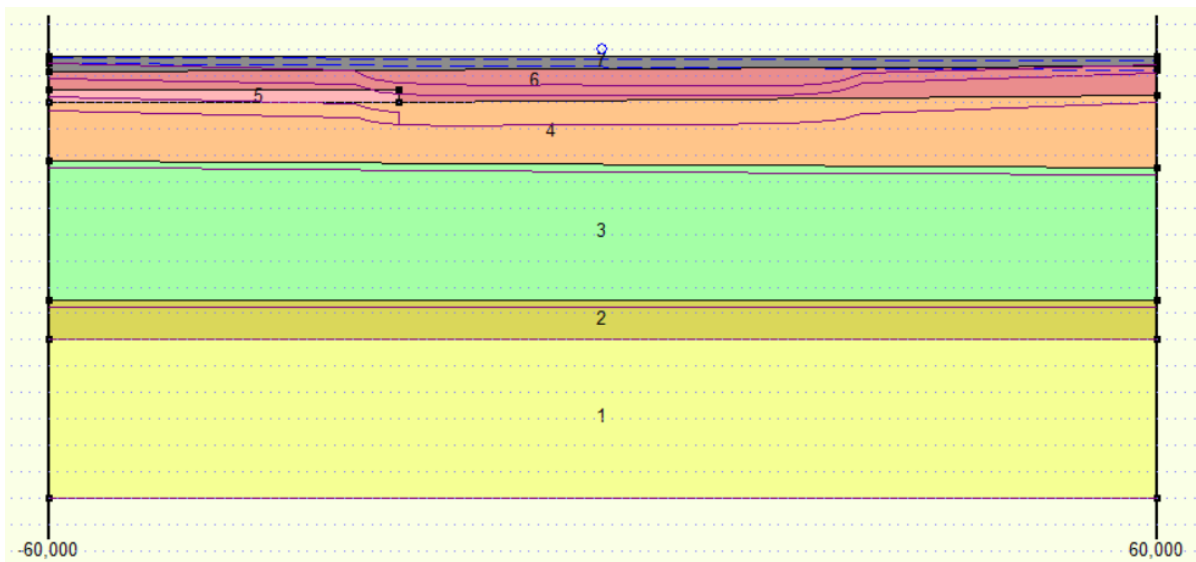


Figure F.1: Graphical representation of the settled profile exported in the LEM analysis

Figure F.1 shows the results of the settlement analysis used as basis for the LEM analysis and MPM geometry.

F.2. Green dyke LEM models

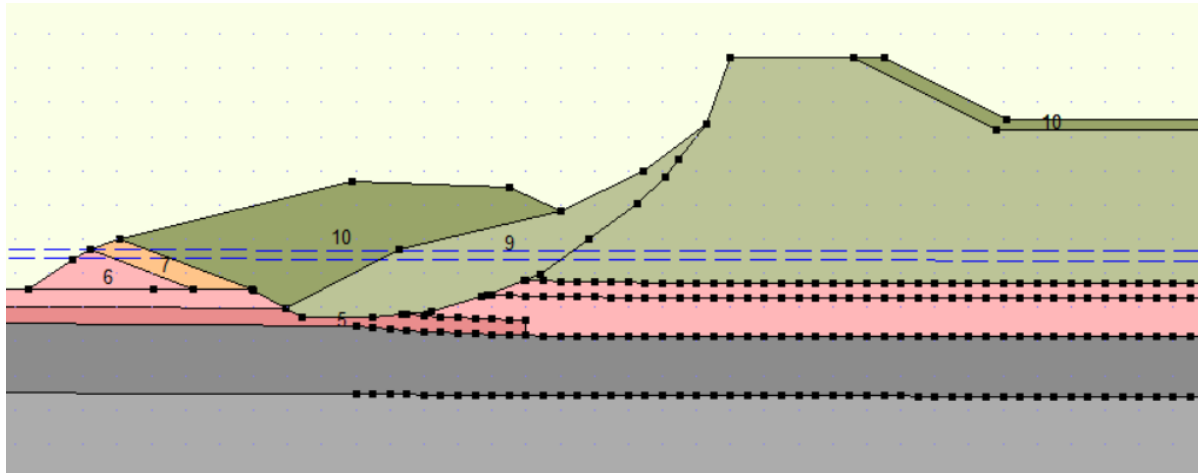


Figure E2: D-Geo Stability model used for the peak strength properties of the unsaturated sand

Figure E2 shows the discretization of the top of the failed dyke core. The slope of the top part was made slightly steeper than the discretization used in E3.

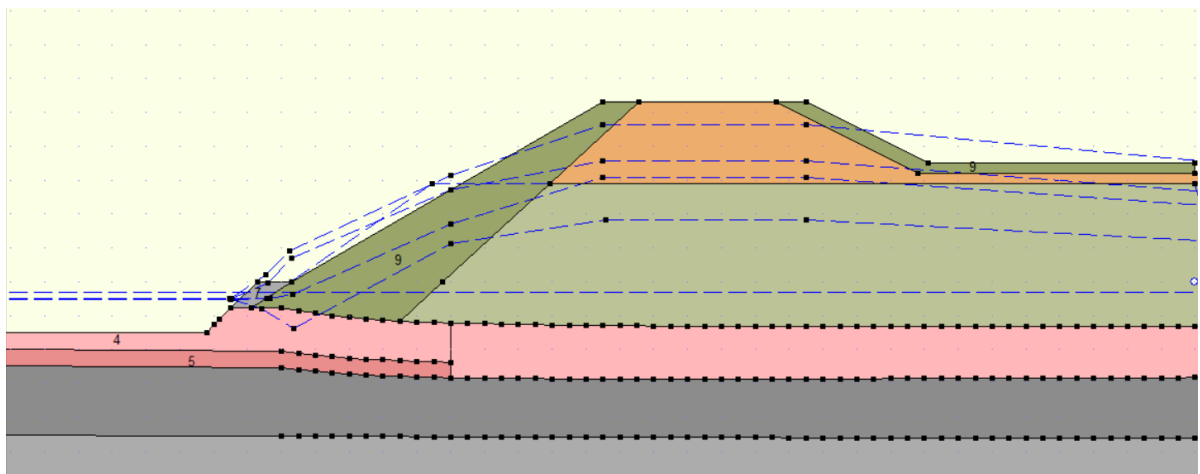


Figure E3: Final model used to determine the peak strength properties of clay layers in the green dyke

Figure E3 shows the final model of the pre-failure Green dyke used to backcalculate the peak strength properties of the clay layers 3 and 3a.

Figure E4 shows the final model of the post-failure Green dyke used to backcalculate the residual strength properties of the clay layers 3 and 3a, following hypothesis 1. Note that the PI lines used to model the pore pressures inside the clay layers are removed. The red circle shows the point of the Spencer analysis with two slip surfaces. It was unknown whether the slip circle was passed through the clay layer or emerged over the passive excavation. The results of this analysis showed that the critical slip surface passed through the clay layer.

Figure E5 shows the final model of the post-failure Green dyke used to backcalculate the residual strength properties of the clay layers 3 and 3a, following hypothesis 2 and 3. The excess pore pressures are maintained at the same location as the peak model.

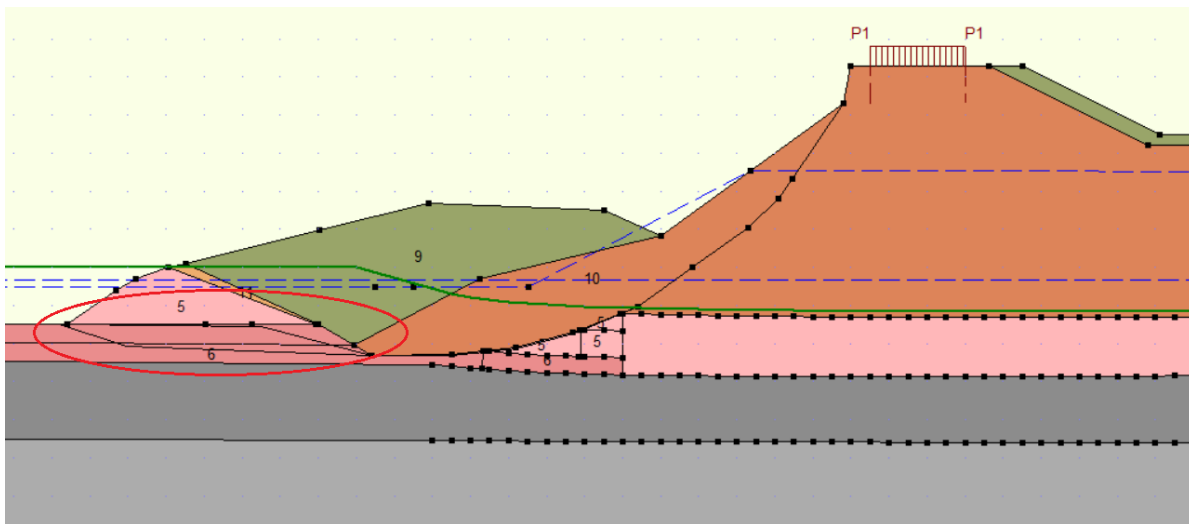


Figure E4: Final model used to determine the residual strength properties of clay layers in the green dyke following Hypothesis 1

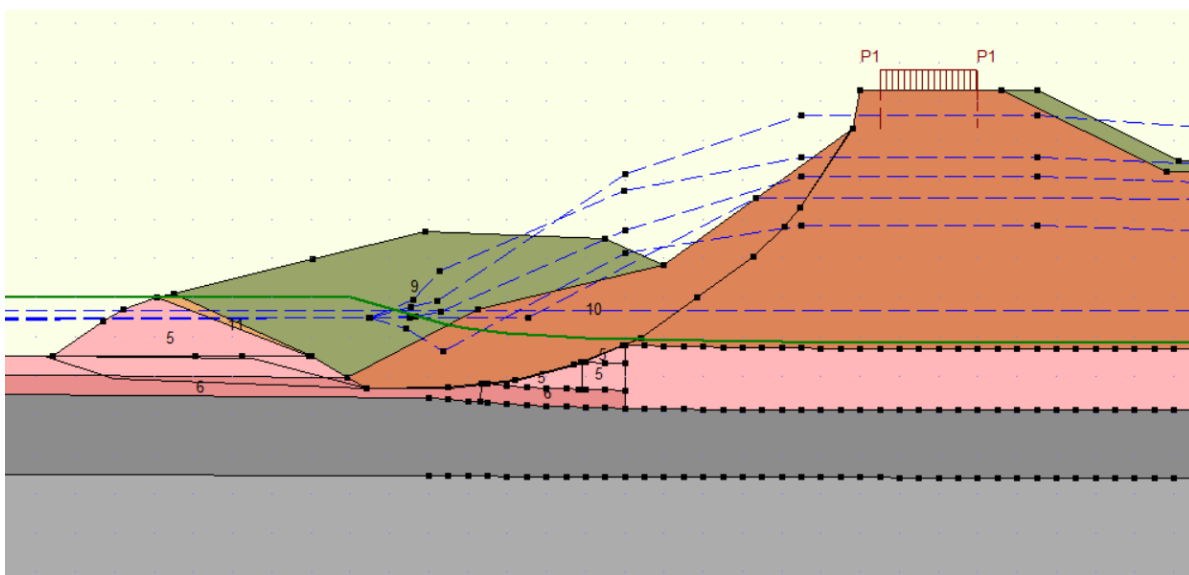


Figure E5: Final model used to determine the residual strength properties of clay layers in the green dyke following Hypothesis 2 and 3

E.3. Blue dyke LEM model

Figure F.6 shows the final model of the pre failure Blue dyke used to backcalculate the equivalent water height resulting in a moment equivalent to the added force induced in reality by the sheetpile wall. A Bishop analysis was used here since it outputs the resultant water moment induced by a high water table. Note that the dyke core left of the sheetpile wall location was removed, and that the water table was heightened to find the equivalent load.

Figure E.7 shows the final model used to determine the strength reduction of the peat layer. The water table left of the sheetpile wall was lowered to induce the same moment as for the peak strength model.

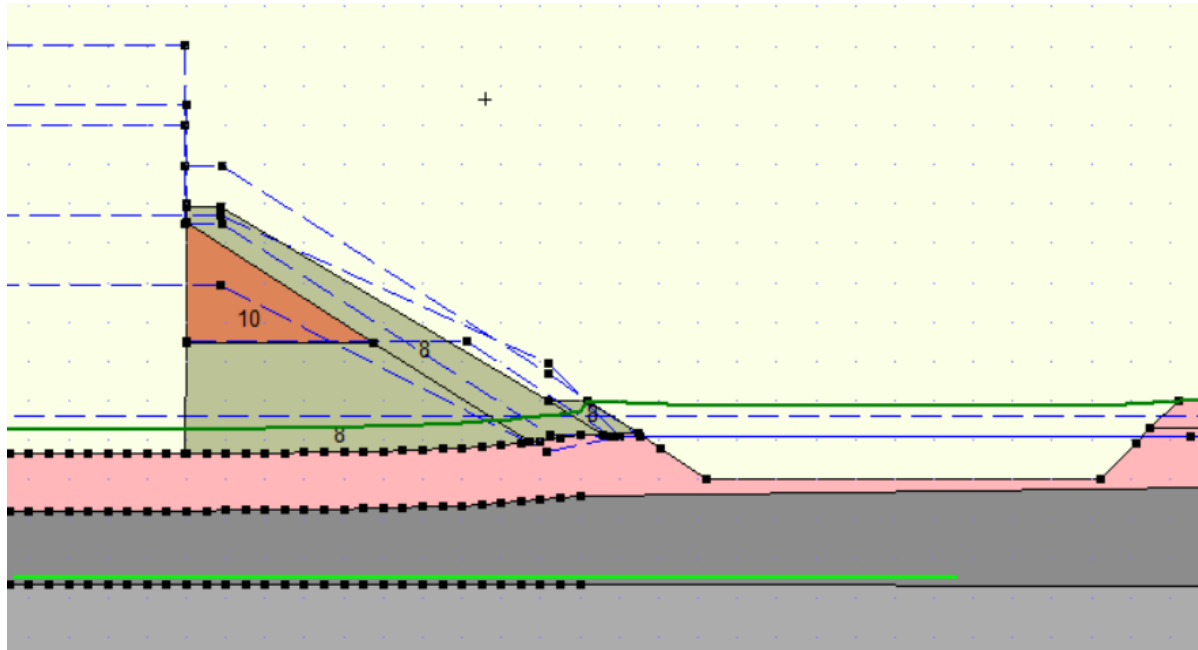


Figure E6: Final model used to determine the peak strength properties of peat layer in the blue dyke

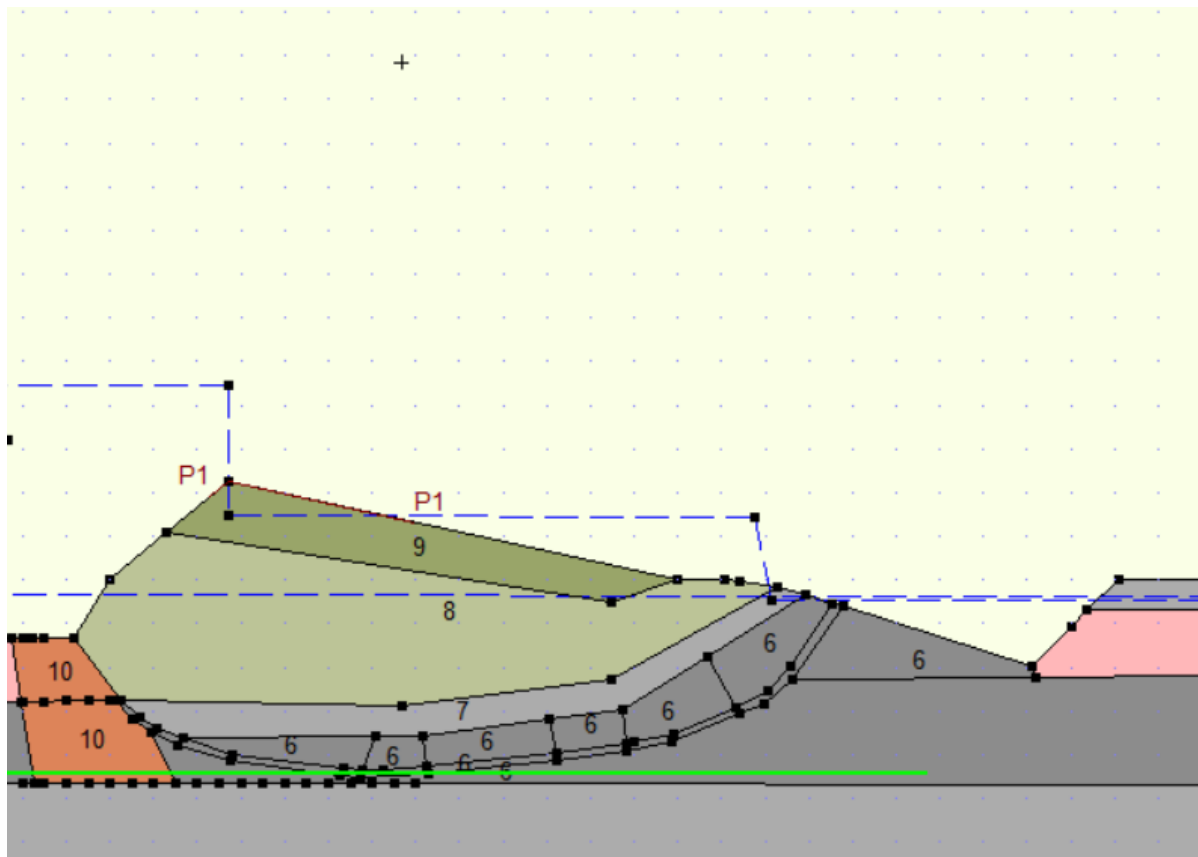


Figure E7: Final model used to determine the residual strength properties of peat layer in the blue dyke

G

3D Effect calculation

In this Appendix an example calculation of the 3D effect and strength backcalculation is provided. The radius of the "bottom", or real slip surface is reduced in steps of 1m until the whole dyke profile is covered. With these slip circles an estimation can be made of the mobilized strength at the sides of the failure envelope. By comparing this to the mobilized strength at the bottom slip surface the 3D effect can be found.

- 1. Start with a first target Factor of Safety (in this example already 0.78)
- 2. Determine strength of layer 3 and 3a
- 3. Change model to a Bishop model
- 4. Report the arc length, and mobilized shear strength (Output of D-Geo Stability)
- 5. Reduce circle radius by 1m, report Step 4., repeat until whole profile covered
- 6. For each slice, determine mobilized strength $F_{mob,slice}$ (Equation G.1)
- 7. For each radius, determine sum of slice mobilized strength (Equation 5.1)
- 8. Calculate 3D effect → Update target Factor of safety if necessary and iterate step 1 to 8

$$F_{mob,slice} = arc.len_i \times Sshear_i \quad (G.1)$$

In this example the real slip surface, or bottom slip surface, is found with a radius of 13.05 m. The mobilized strength over each whole slip circle can now be computed for each circle radius with Equation 5.1. The results are presented below.

- $F_{mob.R=13.05} = 260kN/m$
- $F_{mob.R=12.05} = 173kN/m$
- $F_{mob.R=11.05} = 112kN/m$
- $F_{mob.R=10.05} = 46kN/m$

$$F_{side} = (F_{mob.R=12.05} + F_{mob.R=11.05} + F_{mob.R=10.05}) = 568kN$$

$$F_{bot} = B \cdot F_{mob.R=13.05} = 20 \times 260 = 5202kN$$

$$3D-effect = \frac{2 \cdot F_{sides}}{F_{bot}} = \frac{1136}{5202} = 0.22$$

The mobilized force on the sides and bottom of the slip surface can now be determined. The mobilized strength of a single side needs to be multiplied by 2, and 3D effect can be determined. The factor of safety

obtained is identical to the original target FOS, the 3D effect and the strength of the clay layers is therefore found.

The influence of the slipplane width B on the 3D effect can now be computed easily, and is presented in Figure G.1. This Figure illustrates the importance of taking the 3D effect magnitude in account when back analysing a slip surface. It should also be specified that for less wide slip surfaces the simple slip cone assumption might have a larger influence on the target FOS, and should therefore be used with caution. Another conclusion that can be drawn is that assuming a 30 m wide slip surface would have influenced the target FOS by 10 %, which is significant

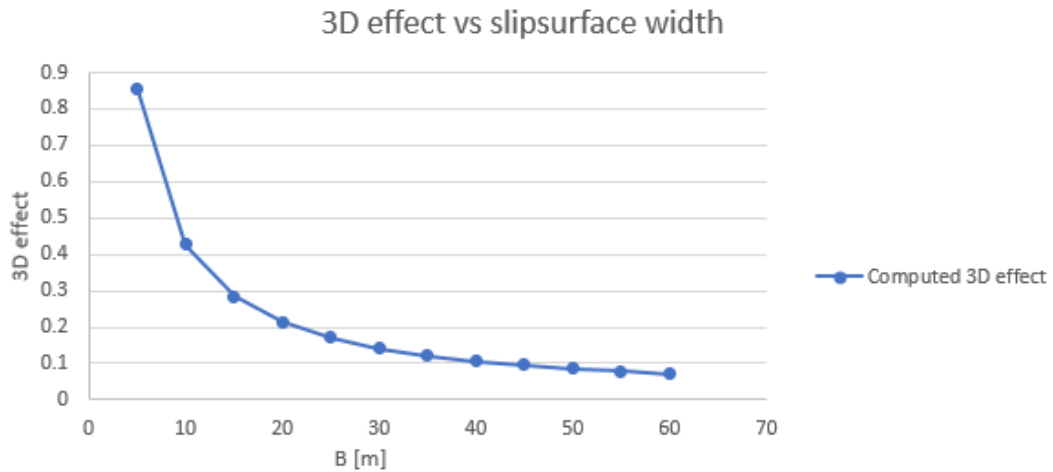


Figure G.1: Magnitude of 3D effect for varying slip surface width

R =13.05			
Slice	Arc.len. [m]	S shear [kN/m ²]	F_mob,slice [kN/m]
1	0.57	7.05	4.0185
2	0.56	8	4.48
3	0.56	8.5	4.76
4	0.51	5.3	2.703
5	0.51	5.44	2.7744
6	0.5	5.54	2.77
7	0.22	5.71	1.2562
8	0.15	5.89	0.8835
9	0.3	6.07	1.821
10	0.04	6.2	8.91
11	0	6.21	8.53
12	0	6.21	0
13	0.01	6.23	0.0623
14	0.26	6.59	1.7134
15	0.34	7.44	2.5296
16	0.17	8.09	1.3753
17	0.13	8.12	1.0556
18	0.08	7.88	0.6304
19	0.03	7.75	0.2325
20	0.01	7.71	0.0771
21	0.02	7.69	0.1538
22	0.06	7.6	0.456
23	0.05	7.49	0.3745
24	0.28	7.05	1.974

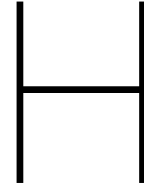
R =12.05			
Slice	Arc.len. [m]	S shear [kN/m ²]	F_mob, slice [kN/m]
1	0.06	6.19	0.3714
2	0.15	7.23	1.0845
3	0.3	8.04	2.412
4	0.04	8.41	0.3364
5	0	8.44	0
6	0	8.43	0
7	0.01	8.46	0.0846
8	0.26	8.84	2.2984
9	0.34	9.81	3.3354
10	0.17	10.44	8.91
11	0.13	10.3	8.53
12	0.08	9.85	0.788
13	0.03	9.6	0.288
14	0.01	9.53	0.0953
15	0.02	9.47	0.1894
16	0.06	9.28	0.5568
17	0.05	9.02	0.451
18	0.28	8.16	2.2848
19	0.07	7.22	0.5054
20	0.23	6.9	1.587
21	0.05	6.62	0.331
22	0.02	6.61	0.1322
23	0	6.61	0
24	0.03	6.64	0.1992

25	0.07	6.58	0.4606
26	0.23	6.63	1.5249
27	0.05	6.72	0.336
28	0.02	6.74	0.1348
29	0	6.75	0
30	0.03	6.77	0.2031
31	0.05	6.8	0.34
32	0.13	6.85	0.8905
33	0.5	6.97	3.485
34	0.5	7.11	3.555
35	0.25	7.17	1.7925
36	0.26	11.75	3.055
37	0.51	11.72	5.9772
38	0.52	11.62	6.0424
39	0.52	11.43	5.9436
40	0.53	11.37	6.0261
41	0.47	11.54	5.4238
42	0.07	11.83	0.8281
43	0.28	11.63	3.2564
44	0.23	11.31	2.6013
45	0.02	17.47	0.3494
46	0.01	17.47	0.1747
47	0.01	17.47	0.1747
48	0	17.47	0
49	0.36	17.44	6.2784
50	0.19	17.64	3.3516
51	0.57	18.45	10.5165
52	0.58	19.46	11.2868
53	0.6	20.2	12.12
54	0.62	20.67	12.8154
55	0.55	20.87	11.4785
56	0.1	20.88	2.088
57	0.67	20.76	13.9092
58	0.71	20.34	14.4414
59	0.75	19.6	14.7
60	0.81	17.59	14.2479
61	0.02	16.06	0.3212
62	0.86	14.99	12.8914
63	0.08	12.08	0.9664
64	0.91	8.94	8.1354
65	0.93	4.77	4.4361

25	0.05	6.69	0.3345
26	0.13	6.8	0.884
27	0.25	6.96	1.74
28	0.25	7.11	1.7775
29	0.25	7.2	1.8
30	0.25	7.25	1.8125
31	0.25	7.27	1.8175
32	0.26	7.26	1.8876
33	0.35	7.21	2.5235
34	0.16	11.78	1.8848
35	0.26	11.89	3.0914
36	0.26	12	3.12
37	0.26	12.09	3.1434
38	0.26	12.15	3.159
39	0.27	12.18	3.2886
40	0.27	12.18	3.2886
41	0.32	12.16	3.8912
42	0.15	11.17	1.6755
43	0.07	11.21	0.7847
44	0.29	11.26	3.2654
45	0.25	11.3	2.825
46	0.01	11.31	0.1131
47	0.01	11.31	0.1131
48	0	11.31	0
49	0.37	11.29	4.1773
50	0.2	11.49	2.298
51	0.29	12.02	3.4858
52	0.29	12.58	3.6482
53	0.3	13.06	3.918
54	0.3	13.48	4.044
55	0.31	13.82	4.2842
56	0.32	14.08	4.5056
57	0.32	14.27	4.5664
58	0.33	14.38	4.7454
59	0.58	14.39	8.3462
60	0.11	14.34	1.5774
61	0.36	14.23	5.1228
62	0.37	14.01	5.1837
63	0.37	13.7	5.069
64	0.41	14.63	5.9983
65	0.42	12.91	5.4222
66	0.44	11.11	4.8884
67	0.46	8.79	4.0434
68	0.49	6.03	2.9547
69	0.2	4.15	0.83
70	0.46	2.7	1.242

R=11.05			
Slice	Arc.len.	S shear	F_mob
	[m]	[kN/m ²]	[kN/m]
1	0.21	4.58	0.9618
2	0.21	6.61	1.3881
3	0.21	7.58	1.5918
4	0.03	7.55	0.2265
5	0.08	7.54	0.6032

R=10.05			
Slice	Arc.len.	S shear	F_mob
	[m]	[kN/m ²]	[kN/m]
1	0.17	3.92	0.6664
2	0.17	4.13	0.7021
3	0.18	4.32	0.7776
4	0.18	4.49	0.8082
5	0.18	4.65	0.837



Blue dyke LEM analysis

In this Appendix the LEM analysis of the Blue dyke is carried out. The results were deemed unsatisfactory due to the inability of LEM to account for horizontal loading induced the SPW on the slipsurface. The method presented here shows the assumptions made to try and assess the peak and residual strength of the peat layer under the Blue dyke.

H.0.1. Peak strength sand core

The sand core has been attributed the same strength as in the Green dyke of $\varphi = 38^\circ$. The possibility of the slip surface passing at the interface of the SPW and the sand was also investigated. The strength attributed in that case should be an interface friction angle δ instead of an internal friction angle φ . (Aksoy, 2016) [2], and (Rinne, 1989) [41] showed that the friction angle of cohesionless materials on steel is strongly dependent on the composition of the sand, namely the size of particles (through a d50 term) and their rounding. Another factor of influence is the roughness of the interface. In this study no data is available on the d50 of the sand. The Eurocode states that an interface friction of sand on steel for sheet pile wall can be taken as Equation H.1.

$$\delta = 2/3 \cdot \varphi_{peak} \quad (\text{H.1})$$

In the numerical models a sheetpile wall is represented as an infinitely small line. In reality the profile of the Z-shape of the sheetpile wall creates more contact area, therefore a geometrical correction factor needs to be applied on Equation H.1. The final expression for friction alongside a sheetpile wall is presented in Equation H.2.

$$\delta = 2/3 \cdot A_{3d} = 2/3 \cdot (1 + 1/5) \cdot \varphi = 0.8 \times 38 = 30 \quad (\text{H.2})$$

The influence of this change in friction angle was neglectable, since the slipsurface was close to vertical in the sand core. The peak friction angle of the sand core was fixed at 38° .

H.0.2. Peak strength of peat

The peak strength of the peat layer under the Blue dyke needs to be determined. Following the flowchart presented in Figure 5.4, the 3D effect was found to be around 22 %, with a peat S-ratio $S_{p,peat} = 0.29$. It can quickly be concluded that these values are too low. The analysis of the green dyke showed that the peak strength of clay was $S_{p,clay3} = 0.45$. If the strength of the peat really was $S_{p,peat} = 0.29$, the slip surface would have passed through the peat instead of the clay. This shows that further investigations into the peat strength are required, as the conclusions obtained do not match the observed behaviour in the full-scale test.

The underestimation of the strength of peat can be attributed to an underestimation of driving force on the slip surface. The SPW is modelled in LEM as a boundary, through which no horizontal loading is transferred. In reality the SPW is pushed by the soil on the active side, resulting in a horizontal load acting as driving force on the slip surface. A more advanced model, for example a FEM, is therefore required to back-calculate the strength of the peat layer.

Literature study showed that the strength of peat can best be described with a DSS test. The DSS laboratory tests [14] on peat showed a S-ratio $S_{p,peat} = 0.5$. This value will therefore be used in the rest of the analysis.

H.0.3. Residual strength of peat

A new method is proposed to try and assess the driving force on the slipplane. This driving force is required to make an estimation of the residual strength of peat. The SPW was removed from the peak model, and a fictional water table was applied at the crest location, behind the crest location. In reality the water table at that location was +5.0 m NAP. The flowchart presented in Figure H.1 is a variation on Figure 5.4. This method was used to estimate the missing horizontal load, and 3D effect in the pre-failure geometry, and then to transfer this load in the residual model to estimate the residual strength of peat.

A Bishop method was used in the model to find the fictional water table required to create an unstable situation. Based on these conditions the required fictional water height behind the SPW was assessed to be 7.5 m, with a 3D effect of 0.19 (target FOS = 0.81). The effect of the fictional water height on the water driven moment was assessed by comparing the moment with high water table to the moment without high water table. At low water level a moment of 192 kNm/m was active on the slip surface. With a high fictional water table a moment of 2395 kNm/m was found. The fictional moment to be added on the slip surface in the residual model is therefore 2200 kNm/m.

This load was transferred on the post-failure geometry discretization in LEM, presented in Appendix F. The water level on the outer slope side was set at the same level as the inner slope (1.5m NAP). This resulted in a water driven moment of 624 kNm/m. The water level in the residual model was heightened until moment of 2824 kNm/m was obtained. This was found for a water level on the active side of 4.45 m NAP.

Based on this model the resultant residual strength of peat was found to be $S_{peat,residual} = 0.20$. This value should however be presented with great care. A high number of assumptions were made to obtain it, and it still only represents an average strength of the slipplane through peat. It might also be more representative of an interface strength between peat and sand. To obtain a value with more certitude, it is necessary to perform a FEM analysis.

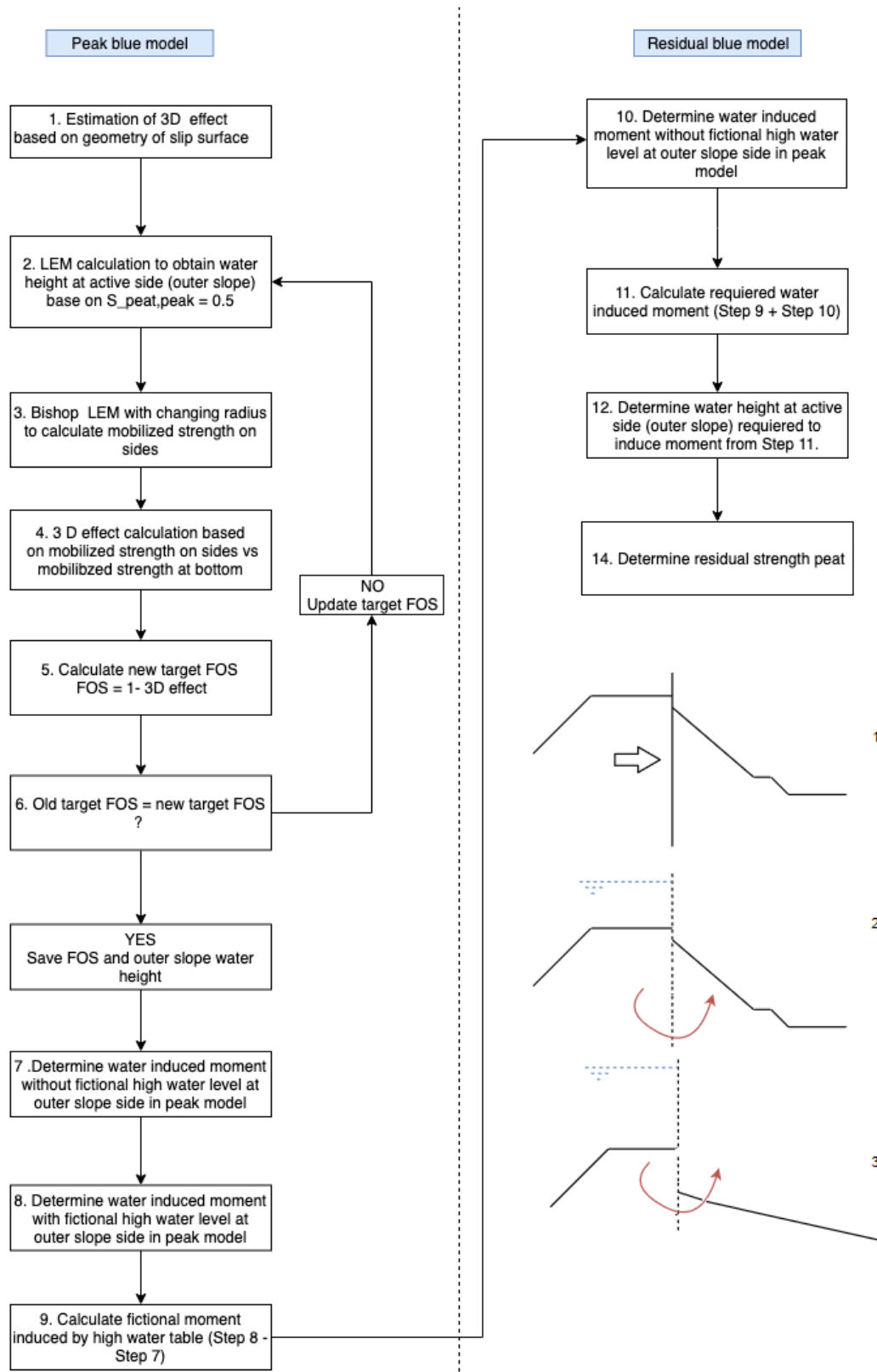


Figure H.1: Flowchart to determine the residual strength of peat based on a fictional water load moment. Visual representation of new methodology to estimate strength reduction of peat. 1: original situation with unknown horizontal force by SPW. 2: Fictional water table to create a moment on the slipsurface. 3: Apply same moment as in Step 2 to backcalculate the residual strength of peat

Benchmark material properties

In this Appendix the density conversions for each Benchmark will be presented.

I.1. Benchmark 1

A dry soil was considered, with a total unit weight of 19.5 kN/m³, equivalent to a density of 1988 kg/m³. A porosity $n_0 = 0.3968$ was used. The solid density can now be computed as:

$$\rho_{tot} = \frac{\gamma}{g} \quad (I.1)$$

$$\rho_{solid,mpm} = \frac{\rho}{1 - n_0} \quad (I.2)$$

$$\rho_{solid,mpm} = 3295$$

kg/m³

I.2. Benchmark 2 and 3

Again starting from a total unit weight of 19.5 kN/m³, equivalent to a density of 1988 kg/m³ following Equation I.1. The soil is now saturated. A solid density of 2650 kg/m³ was used. The total weight can be converted to find the porosity of the soil according to equation I.4. A porosity $n_0 = 0.3968$ was found.

$$\gamma = \gamma_s \cdot (1 - n_0) + \gamma_w \cdot n_0 \quad (I.3)$$

$$n_0 = \frac{\rho_{tot} - \rho_{solid}}{\rho_w - \rho_{solid}} \quad (I.4)$$

I.3. Benchmark 4

In this Benchmark two loading phases were considered with two materials. In the first phase the bottom material was given the same properties as the material in Benchmark 2 and 3. The top material was initialized with the same material properties as the Benchmark 1 material. The only difference being that water in the top material was given a density of 50kg/m³ to permit the saturation in the second phase to be modelled.

In the second phase the top material properties were changed to match the bottom material.



MPM strength conversion

In this Appendix the strength parameter conversion of the different layers will be presented. For each case the "real" parameters will be recapitulated, after which these will be converted to Equivalent associative or non-associative non-dilative material parameters. These will then be corrected based the factors presented in section 6.4.

J.1. Peak

J.1.1. Real

The real parameters were determined based on a LEM analysis and described in Chapter 5

- Sand, unsat: $\varphi_p = 38$ $\psi = 10$ $c = 4$ kPa
- Clay Layer 3: $S_{p,3} = 0.45$
- Clay Layer 3a: $S_{p,3a} = 0.35$

J.1.2. Equivalent, Associative

The Equivalent Associative parameters for the sand layer can now be found.

Mohr-Coulomb expression in general terms is given in Equation J.1.

$$\tau = c * \frac{\cos\psi \cdot \cos\varphi_i}{1 - \sin\psi \cdot \sin\varphi} + \sigma'_n * \frac{\cos\psi \cdot \sin\varphi}{1 - \sin\psi \cdot \sin\varphi} \quad (J.1)$$

Associative formulation

$$\begin{aligned} \tau &= c + \sigma'_n * \tan\varphi \\ \tau &= c + \sigma'_n * \tan\varphi \end{aligned} \quad (J.2)$$

$$c_{eq,a} + \sigma'_n * \tan\varphi_{eq,a} = c * \frac{\cos\psi \cdot \cos\varphi}{1 - \sin\psi \cdot \sin\varphi} + \sigma'_n * \frac{\cos\psi \cdot \sin\varphi}{1 - \sin\psi \cdot \sin\varphi}$$

$$c_{eq,a} = c * \frac{\cos\psi \cdot \cos\varphi}{1 - \sin\psi \cdot \sin\varphi}$$

$$\varphi_{eq,a} = \tan^{-1}\left(\frac{\cos\psi \cdot \sin\varphi}{1 - \sin\psi \cdot \sin\varphi}\right)$$

Sand Unsat

$$c_{eq,a} = 4 * \frac{\cos(10) \cdot \cos(38)}{1 - \sin(10) \cdot \sin(38)}$$

$$c_{eq,a} = 3.5 \text{ kPa}$$

$$\varphi_{eq,a} = \tan^{-1}\left(\frac{\cos(10) \cdot \sin(38)}{1 - \sin(10) \cdot \sin(38)}\right)$$

$$\varphi_{eq,a} = 34^\circ$$

Clay layer 3

$$\varphi_{eq,a} = \tan^{-1}(S_{p,3})$$

$$c_{eq,a} = S_{p,3} \cdot m \cdot PoP$$

$$\varphi_{eq,a} = 24^\circ$$

Note: the cohesions are dependent on the PoP, and is therefore dependent on the horizontal layering created.

Clay layer 3a

$$\varphi_{eq,a} = \tan^{-1}(S_{p,3a})$$

$$c_{eq,a} = S_{p,3a} \cdot m \cdot PoP$$

$$\varphi_{eq,a} = 19^\circ$$

J.1.3. Equivalent, Non-associative, non-dilative

Non-associative non-dilative formulation

$$\tau = c * \cos\varphi + \sigma'_n * \sin\varphi$$

$$c_{eq,na} * \cos\varphi_{eq,na} + \sigma'_n * \sin\varphi_{eq,na} = c * \frac{\cos\psi \cdot \cos\varphi}{1 - \sin\psi \cdot \sin\varphi} + \sigma'_n * \frac{\cos\psi \cdot \sin\varphi}{1 - \sin\psi \cdot \sin\varphi}$$

$$\varphi_{eq,na} = \sin^{-1}\left(\frac{\cos\psi \cdot \sin\varphi}{1 - \sin\psi \cdot \sin\varphi}\right)$$

Sand unsat

$$\varphi_{eq,na} = 43^\circ$$

$$c_{eq,na} = c * \frac{\cos\psi \cdot \cos\varphi}{(1 - \sin\psi \cdot \sin\varphi) * \cos\varphi_{eq,na}}$$

$$c_{eq,na} = 4.75 \text{ kPa}$$

Clay layer 3

$$\varphi_{eq,na} = \sin^{-1}(S_{p,3})$$

$$c_{eq,a} = \frac{S_{p,3} \cdot m \cdot PoP}{\cos(\varphi_{eq,na})}$$

$$\varphi_{eq,a} = 27^\circ$$

Cohesion dependent on zoning.

Clay layer 3a

$$\varphi_{eq,na} = \sin^{-1}(S_{p,3a})$$

$$c_{eq,a} = \frac{S_{p,3a} \cdot m \cdot PoP}{\cos(\varphi_{eq,na})}$$

$$\varphi_{eq,a} = 20^\circ$$

J.2. Residual: Hypothesis 1

J.2.1. Real

The real parameters were determined based on a LEM analysis and described in Chapter 5. The residual strength is here expressed as a drained friction angle. As explained, all the dilation angles are set to 0. This is already a non-associative, non-dilative formulation and will therefore only be converted to equivalent associative parameters.

- Sand: $\varphi_{cs} = 30$ $\psi = 0$ $c = 0$ kPa
- Clay Layer 3: $\varphi_r = 11$ $\psi = 0$ $c = 0$ kPa
- Clay Layer 3a: $\varphi_r = 8.7$ $\psi = 0$ $c = 0$ kPa

J.2.2. Equivalent Associative

Conversion can be done easily, as the expression is already in non-associative, non-dilative form.

$$\varphi_{eq,a} = \tan^{-1}(\sin(\varphi_r))$$

- Sand: $\varphi_{eq,a} = 27$
- Clay layer 3: $\varphi_{eq,a} = 10.8$
- Clay layer 3a: $\varphi_{eq,a} = 8.6$

J.3. Residual: Hypothesis 2

J.3.1. Real

As explained, the residual strength of cohesive layers is here expressed as an undrained S-ratio

- Sand: $\varphi_{cv} = 30$ $\psi = 0$ $c = 0$ kPa
- Clay Layer 3: $S_{r,3} = 0.31$
- Clay Layer 3a: $S_{r,3a} = 0.24$

J.3.2. Equivalent Associative

- Sand: $\varphi_{eq,a} = \tan^{-1}(\sin(\varphi_{cv})) = 27^\circ$
- Clay Layer 3: $\varphi_{eq,a} = \tan^{-1}(S_{p,3}) = 17^\circ$
- Clay Layer 3a: $\varphi_{eq,a} = \tan^{-1}(S_{p,3a}) = 13.5^\circ$

J.3.3. Equivalent, Non-associative, non-dilative

- Clay Layer 3: $\varphi_{eq,a} = \sin^{-1}(S_{p,3}) = 18^\circ$
- Clay Layer 3a: $\varphi_{eq,a} = \sin^{-1}(S_{p,3a}) = 14^\circ$



MPM failure phase snapshots

Figure K.1: **Click on image to animate** Strain development in MPM model of Green dyke failure with residual strength parameters following Hypothesis 1

Figure K.2: **Click on image to animate** Strain development in MPM model of Green dyke failure with residual strength parameters following Hypothesis 2

Figure K.3: **Click on image to animate** Strain development in MPM model of Green dyke failure with residual strength parameters following Hypothesis 3

Figure K.4: **Click on image to animate** Strain development in MPM model of Green dyke failure with residual strength parameters following Hypothesis 2, and Mohr-Coulomb model under the crest

Bibliography

- [1] M.W. Agam, M.H.M. Hashim, M.I. Murand, and H. Zabidi. Slope sensitivity analysis using spencer's method in comparison with general limit equilibrium method. *Elsevier ,Procedia Chemistry*, 19:651–658, 2016.
- [2] H. Aksoy, E. İnal, and M. Gör. Skin friction between soil and pile materials. In *ACE 2016 12th international congress on advances in civil engineering*, 09 2016.
- [3] J. Atkinson. *An Introduction to the Mechanics of Soils and Foundations*. Mc Graw Hill Book Company, 1993.
- [4] M. Baligh and S. Azzouz. End effects on stability of cohesive slopes. *Journal of the Geotechnical Engineering Division*, 101:1105–1117, 11 1975.
- [5] C.M. Bauduin, M De Vos, and P A. Vermeer. *Back analysis of staged embankment failure: The case study Streefkerk*, pages 79–90. Balkema, 01 1999.
- [6] K. Been and M. Jefferies. A state parameter for sands. *Geotechnique*, 35:99–112, 12 1985. doi: 10.1680/geot.1985.35.2.99.
- [7] K. Been, M. G. Jefferies, and J. Hachey. The critical state of sands. *Géotechnique*, 41(3):365–381, 1991.
- [8] L. Beuth, Z. Wieckowski, and P.A. Vermeer. Solution of quasi-static large-strain problems by the material point method. *International Journal for Numerical and Analytical Methods in Geomechanics*, 35:1451–1465, 10 2011. doi: 10.1002/nag.965.
- [9] T. Biryaltseva, T. Mörz, S. Brandt, S. Kreiter, U. Gerdes, and B. Ossig. Relative densities and void ratios derived from cpt data using in site field calibration. *Geotechnical and Geophysical Site Characterisation* 5, 136, 2016.
- [10] L. Bjerrum. The effective shear strength parameters of sensitive clays. In *Proc. 5th International Conference Soil Mechanics Foundation Engineering Paris*, pages 23–28, 1961.
- [11] M. Bolton. Strength and dilatancy of sands. *Geotechnique*, 36:65–78, 01 1986.
- [12] N. Boylan. *The Shear Strength of Peat*. Ph. D. Thesis. University College Dublin, 2008.
- [13] J. Bredevelde. Eindrapport proefprogramma, product v. Technical report, Deltares, 11 2018.
- [14] J. Bredevelde. Geotechnisch basisrapport, product f. Technical report, Deltares, 08 2018.
- [15] B.B. Broms and A.O. Casbarian. Effects of rotation of the principal stress axes and of the intermediate principal stress on the shear strength. *Proceedings of the 6th ICSMFE, Montreal*, 1:179–183, 1965.
- [16] M. Budhu. *Soil Mechanics and Foundation*. John Wiley & Sons, Inc, Hoboken, 3rd edition, 2011.
- [17] RC. Chaney, K. Demars, T. Stark, and IA Contreras. Constant volume ring shear apparatus. *Geotechnical Testing Journal - GEOTECH TESTING J*, 19, 03 1996. doi: 10.1520/GTJ11402J.
- [18] H. De Bruin. Factual report opbouw fsp-groen/blauw product t. Technical report, Deltares, 06 2018.
- [19] T. M. P. de Campos and M. S. V. Galindo. Evaluation of the viscosity of tropical soils for debris flow analysis: a new approach. *Géotechnique*, 66(7):533–545, 2016. doi: 10.1680/jgeot.15.P.080.
- [20] *D-Geo Stability User Manual*. Deltares, 2016.
- [21] *Anura3D Scientific Manual*. Deltares, 2019.

- [22] E. Den Haan and G.A.M. Kruse. Characterisation and engineering properties of dutch peats. *Characterisation and Engineering Properties of Natural Soils*, 3:2101–2133, 01 2007.
- [23] J.L.G González Acosta, P.J. Vardon, G. Remmerswaal, and M.A. Hicks. An investigation of stress inaccuracies and proposed solution in the material point method. *Computational Mechanics*, 11 2019. doi: 10.1007/s00466-019-01783-3.
- [24] A. Gylland, H. Jostad, and S. Nordal. Failure geometry around a shear vane in sensitive clay. In *NGM 2012 proceedings*, pages 103–110, 01 2012.
- [25] D. Hight, M.J.P.R. Symes, and A. Gens. Undrained anisotropy and principal stress rotation in saturated sand. *Geotechnique*, 34:11–27, 01 1984.
- [26] M. Jamiolkowski, D. Lo Presti, and M. Manassero. Evaluation of relative density and shear strength of sands from cpt and dmt. *Geotechnical Special Publication*, pages 201–238, 01 2003.
- [27] N. Janbu. Soil models in offshore engineering. *Géotechnique*, 35(3):241–281, 1985.
- [28] H. Jostad, L. Andresen, and V. Thakur. Calculation of shear band thickness in sensitive clays. In *Conference: 6th Numerical Methods in Geotechnical Engineering*, 06 2006.
- [29] F.H. Kulhawy and P.W. Mayne. *Manual on Estimating Soil Properties for Foundation Design*. Electric Power Research Institute EL-6800, Project 1493-6, Electric Power Research Institute, Palo Alto, Calif., 1990.
- [30] A. O. Landva. Vane testing in peat. *Canadian Geotechnical Journal*, 17(1):1–19, 1980. doi: 10.1139/t80-001.
- [31] A.O Landva and P. La Rochelle. Compressibility and shear characteristics of radforth peats. In *GIN: P.M. Jarett (ed.), Testing of Peats and Organic Soils, ASTM STP 820*, pages 157–191. ASTM International, 1983.
- [32] J. Lindenberg, M.A. Van, A.R. Koelewijn, J.W.M. Lambert, C. Zwanenburg, M.T. Van der Meer, P.A.A Teunissen, and E.C.C Loos. Dijken op veen. Technical report, Deltares, 06 2012.
- [33] T. Lunne and H.P. Christoffersen. Interpretation of cone penetrometer data for offshore sands. In *Offshore Technology Conference, 2-5 May, Houston, Texas*. Offshore Technology Conference, 01 1983.
- [34] J. F. Lupini, A. E. Skinner, and P. R. Vaughan. The drained residual strength of cohesive soils. *Géotechnique*, 31(2):181–213, 1981. doi: 10.1680/geot.1981.31.2.181.
- [35] J.F. Lupini. *The residual strength of soils*. PhD thesis, Imperial College London, 1980.
- [36] G. Mesri and E.M. Abdel-Ghaffar. Cohesion intercept in effective stress-stability analysis. *Journal of Geotechnical Engineering*, 119, 08 1993.
- [37] G. Mesri and M. Shahien. Residual shear strength mobilized in first-time slope failures. *Journal of Geotechnical and Geoenvironmental Engineering - J GEOTECH GEOENVIRON ENG*, 129, 01 2003. doi: 10.1061/(ASCE)1090-0241(2003)129:1(12).
- [38] R. Michalowski. Limit analysis and stability charts for 3d slope failures. *Journal of Geotechnical and Geoenvironmental Engineering - J GEOTECH GEOENVIRON ENG*, 136, 04 2010.
- [39] F. Mirada. The material point method in slope stability analysis. Master's thesis, Universitat Politècnica de Catalunya, 06 2015.
- [40] S. Murano. *The deviatoric behaviour of peat: a route between past empiricism and future perspectives*. PhD thesis, TU Delft, 2019.
- [41] N.F Rinne. Evaluation of interface friction between cohesionless soil and common construction materials. Master's thesis, University of Waterloo, 1985.
- [42] K. H. Roscoe and C. P. Schofield, A. N. and Wroth. On the yielding of soils. *Géotechnique*, 8, no1:22–53, 1958.

- [43] A. Schofield and P. Wroth. *Critical State Soil Mechanics*. McGraw-Hill, Cambridge, 01 1968.
- [44] S.R. Sinclair and E.W. Brooker. On shear strength properties of natural soils and rocks: The shear strength of edmonton shale. In *Proceedings of the Geotechnical Conference Oslo 1967*, 1967.
- [45] A. W. Skempton. Long-term stability of clay slopes. *Géotechnique*, 14(2):77–102, 1964.
- [46] A.W. Skempton. First-time slides in over-consolidated clays. *Géotechnique*, 20, no3:320–324, 1970.
- [47] A.W. Skempton. Residual strength of clays in landslides, folded strata and the laboratory. *Géotechnique*, 35, no1:3–18, 1985.
- [48] K. Sorensen. Influence of shearing rate on residual strength of clays. In *Conference: 6th International Symposium on Deformation Characteristics of Geomaterials*, 01 2015.
- [49] T. Stark and H. Eid. Drained residual strength of cohesive soils. *Journal of Geotechnical Engineering*, 120: 856–871, 05 1994. doi: 10.1061/(ASCE)0733-9410(1994)120:5(856).
- [50] T. Stark and H. Eid. Drained residual strength of cohesive soils. *Journal of Geotechnical Engineering*, 120: 856–871, 05 1994. doi: 10.1061/(ASCE)0733-9410(1994)120:5(856).
- [51] T. Stark and H. Eid. Slope stability analyses in stiff fissured clays. *Journal of Geotechnical and Geoenvironmental Engineering - J GEOTECH GEOENVIRON ENG*, 123, 04 1997.
- [52] T. Stark, H. Choi, and S. McCone. Drained shear strength parameters for analysis of landslides. *Journal of Geotechnical and Geoenvironmental Engineering*, 131(5):575–588, 2005.
- [53] D. Sulsky, Z. Chen, and H.L. Schreyer. A particle method for history-dependent materials. *Computer Methods in Applied Mechanics and Engineering*, 118(1-2):179–196, 09 1994. doi: [https://doi.org/10.1016/0045-7825\(94\)90112-0](https://doi.org/10.1016/0045-7825(94)90112-0).
- [54] K. Terzaghi and Peck R.B. *Soil mechanics in engineering practice*. John Wiley & Sons, Inc, New-York, 3rd edition, 1996.
- [55] V. Thakur. *Strain Localization in sensitive SOFT CLAYS*. PhD thesis, Norwegian University of Science and Technology, 2007.
- [56] V. Thakur, H. Jostad, H.A. Amundsen, and S. Degago. How well do we understand the undrained strain softening response in soft sensitive clays? *Advances in Natural and Technological Hazards Research*, page 14, 03 2014.
- [57] B. Wang, M. Hicks, and P. Vardon. Slope failure analysis using the random material point method. *Géotechnique Letters*, 6:1–6, 06 2016. doi: 10.1680/jgele.16.00019.
- [58] H. Yamaguchi, Y. Ohira, K. Kogure, and S. Mori. Undrained shear characteristics of normally consolidated peat under triaxial compression and extension conditions. *Soils and Foundations*, 25(3):1–18, 1985.
- [59] C. Zwanenburg and H.T.J. De Bruijn. Dijken op veen. Technical report, Deltares, 2012.
- [60] C Zwanenburg, E.J. Den Haan, G.A.M. Kruse, and A.R. Koelewijn. Failure of a trial embankment on peat in booneschans, the netherlands. *Géotechnique*, 62(6):479–490, 2012.